Technische Universität München
Lehrstuhl für Biotechnologie der Nutztiere

Downstream Signaling of Oncogenic Kras in Pancreatic Ductal Adenocarcinoma: *In Vivo* and *Ex Vivo* Imaging of Tumor Cell Proliferation as a Tool for the Identification of Therapeutic Targets

Sandra Baumann

Vollständiger Abdruck der von der Fakultät Wissenschaftszentrum Weihenstephan für Ernährung, Landnutzung und Umwelt der Technischen Universität München zur Erlangung des akademischen Grades eines

Doktors der Naturwissenschaften

genehmigten Dissertation.

Vorsitzender:		Univ.-Prof. Dr. M. Schemann
Prüfer der Dissertation:	1.	Univ.-Prof. A. Schnieke, Ph.D.
	2.	Priv.-Doz. Dr. D. K. M. Saur

Die Dissertation wurde am 03.05.2011 bei der Technischen Universität München eingereicht und durch die Fakultät Wissenschaftszentrum Weihenstephan für Ernährung, Landnutzung und Umwelt am 17.08.2011 angenommen.

Table of Abbreviations

°C	degree Celsius
4-OHT	4-hydroxytamoxifen
ADP	adenosine diphosphate
AFN	atipamezole, flumazenil, naloxone
ATP	adenosine triphosphate
BLI	bioluminescence imaging
Bp	base pairs
BrdU	5-bromo-2´-deoxyuridine
BSA	bovine serum albumin
CCD	charge coupled device
CDK	cyclin-dependent kinase
CDNA	complementary desoxyribonucleic acid
Cm	centimeter
CMV	cytomegalovirus
CO_2	carbondioxid
DCTP	2'-deoxycytidine 5'-triphosphate
DMEM	Dulbecco's Modified Eagle Medium
DMSO	dimethylsulfoxide
DNA	desoxyribonucleic acid
DTT	1,4-dithiothreitol
E	embryonic development day
EDTA	ethylenediaminetetraacetic acid
EGFP	enhanced green fluorescent protein
ES	embryonic stem
et al.	et alii
EtBr	ethidium bromide
EtOH	ethanol
FCS	fetal calf serum
fLuc	Firefly luciferase
g	G force

g	gram
GAP	GTPase activating protein
GDP	guanine diphosphate
GTP	guanine triphosphate
GTPγS	guanosine 5'-O-[γ-thio]triphosphate
h	hours
H_2O	water
HE	haematoxylin eosin
Hsp	heat shock protein
i.p.	intraperitoneal
kb	kilo base pairs
kg	kilogram
Kras	V-Ki-Ras2
LBD	ligand binding domain
LIF	leukemia inhibitory factor
LOH	loss of heterozygositiy
LSL	LoxP-stop-LoxP
mbar	millibar
MEF	murine embryonic fibroblasts
min	minutes
mL	milliliter
MMF	midazolam, medetomidine, fentanyl
MTT	3-(4,5-dimethylthiazol-2-yl)-2,5-diphenyltetrazoliumbromide
mut	mutated
ng	nanogram
nm	nanometer
OD	optical densitiy
o/n	over night
p	phospho
PanIN	pancreatic intraepithelial neoplasia
PBS	phosphate buffered saline
PCNA	proliferating cell nuclear antigen

PCR	polymerase chain reaction
PDAC	pancreatic ductal adenocarcinoma
Pdx1	pancreas duodenum homeobox 1
PI3-kinase	phosphoinositid-3-kinase
PLB	passive lysis buffer
PPT	pancreatic primary tumor
Prm1	protamine 1
Ptf1a	pancreas transcription factor subunit alpha
Rb	retinoblastoma
RBD	ras binding domain
RNA	ribonucleic acid
rpm	rounds per minute
RT	room temperature
SDS	sodium dodecyl sulfate
sec	second
TGF-β	transforming growth factor β
U	units
UV	ultra violet
V	volt
w/	with
w/o	without
WT	wild type
µF	microfarad
µg	microgram
µL	microliter

List of Figures

List of Tables

1 Introduction

1.1. Pancreatic Ductal Adenocarcinoma (PDAC)

The annual statistics of cancer incidence and mortality in the United States report pancreatic cancer as one of the four leading causes of cancer related death. The estimation of 43.000 new cases and 37.000 deaths in 2010 shows the high mortality of this disease (Jemal et al., 2010). Due to the lack of early diagnostic tools, the absence of specific symptoms and the retroperitoneal location of the pancreas as well as the small size of precursor lesions, in fact only 10-15% of pancreatic cancer cases are being diagnosed at an early stage which allows pancreatic resection (Bardeesy and DePinho, 2002; Hingorani et al., 2003; Jemal et al., 2010). Aggravating to late diagnosis, pancreatic cancer is resistant to most conventional chemotherapies and radiation therapies (Hingorani et al., 2005). Until now, treatment is mostly restricted to palliative care with gemcitabine as a standard first-line treatment which results in a marginal improvement of median survival (Chames et al., 2010). Even after surgical resection and adjuvant chemotherapy the survival rate is around 20-25% (Neoptolemos et al., 2004). This shows the tremendous need for further improvement in understanding pancreatic cancer progression and for the development of early diagnosis methods and new therapy strategies.

1.1.1 Carcinogenesis and the Role of Oncogenic Kras in PDAC

The most common pancreatic neoplasm (>85%) is the pancreatic ductal adenocarcinoma (PDAC) which usually arises in the head of the pancreas (Hezel et al., 2006). It typically infiltrates surrounding tissues, e.g. lymph nodes, spleen and peritoneal cavity, and metastasizes to liver and lungs. PDAC is accompanied by a strong desmoplastic reaction in the stroma (Hezel et al., 2006; Ghaneh et al., 2007).
PDAC development is understood as a stepwise process of defined histological and genetic changes, which in the end lead to invasive carcinoma. The histological changes are staged in so called pancreatic intraepithelial neoplasias (PanINs). While the normal ductal structure consists of cuboidal to low-columnar epithelium without cytoplasmatic mucin, the earliest lesions, PanIN-1A, display tall-columnar cells with abundant mucin, which acquire a papillary, micropapillary or basally pseudostratified

architecture when progressing to PanIN-1B (see Figure 1-1). In both PanIN-1A and PanIN-1B, nuclei are located at the basal membrane. PanINs are classified as PanIN-2 when nuclear abnormalities occur, e.g. enlargement of nuclei, loss of polarity or hyperchromatism. Architecture may be flat or papillary. PanIN-3 are characterized by papillary or micropapillary structures, loss of polarity, abnormal mitosis, nuclear abnormalities, dystrophic globet cells and budding into the lumen (Hruban et al., 2001). PanIN-3 are considered as so called carcinoma *in situ* which is immediately preceding stromal invasion (Feldmann and McNamara, 2000). PanIN-3 lesions are the last precursors before PDAC.

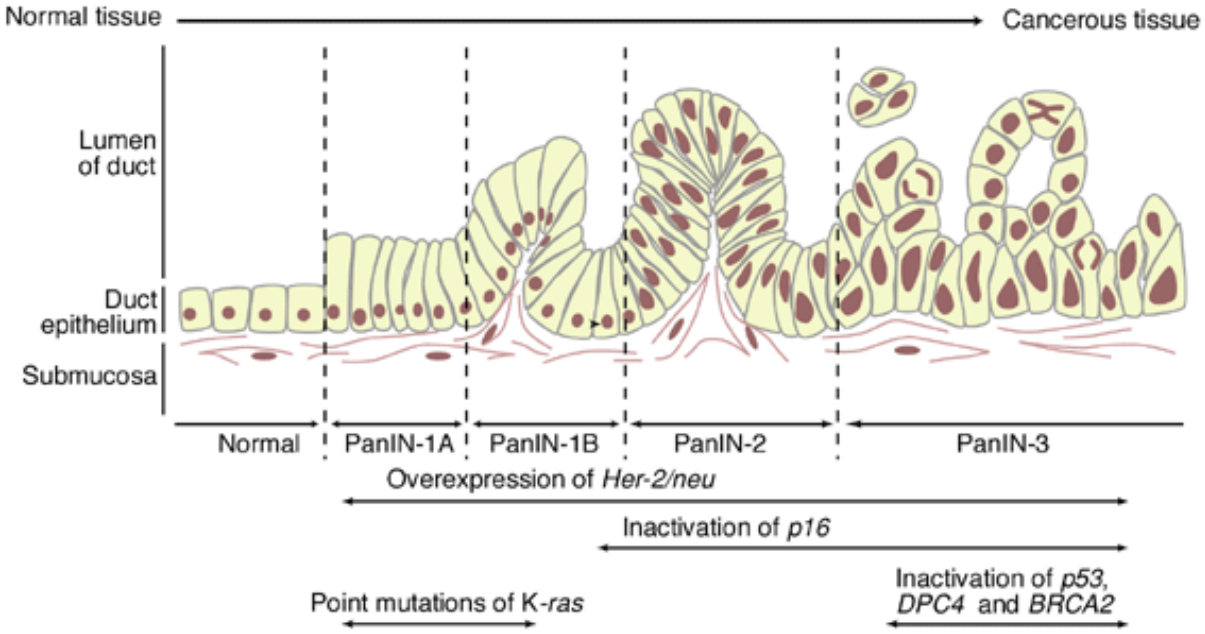

Figure 1-1: Progression model of pancreatic cancer: Progression from normal ductal epithelium to invasive carcinoma comes along with a series of histologically defined lesions, called pancreatic intraepithelial neoplasias (PanINs). In parallel, distinct genetic mutations, such as activating point mutations in the Kras gene or inactivation of the tumor suppressor geneTrp53, occur (Hruban et al., 2000; Arnold and Goggins, 2001)(Figure from Arnold and Goggins, 2001).

Next to morphological changes an increasing number of genetic alterations of known oncogenes and tumor suppressor genes occurs (Hruban et al., 2000; Hezel et al., 2006). Rozenblum et al. report mutations of somatic origin in the oncogene *V-Ki-RAS2* (*KRAS)* and in the tumor suppressor genes *TP53*, $p16^{INK4A}$, *SMAD4* and *BRCA2* with a vast majority of tumors displaying three or four of these mutations. Loss of heterozygosity (LOH) was observed in all of these tumor suppressor genes (Rozenblum et al., 1997).

One of the earliest mutations in PDAC carcinogenesis is the most frequent one. An activating mutation of the *KRAS* oncogene, mostly at codon 12, 13 or 61, can be observed in approximately 90% of all PDACs. It also occurs with increasing frequencies in PanIN-1A (36%), PanIN-1B (44%) as well as PanIN-2 and -3 (78%) (Feldmann and McNamara, 2000). Kras is a farnesylated, monomeric G-protein, which is located at the cell membrane. Being part of the family of small GTPases it is involved in a multitude of cellular processes such as proliferation, apoptosis and survival. The activating mutation at codon 12 (glycine to aspartic acid; G12D) leads to a conformational change resulting in the loss of intrinsic GTPase activity and insensitivity to GTPase activating proteins (GAPs). Thus, Kras is constitutively active and independent of external growth stimuli (Hezel et al., 2006).

80-95% of spontaneous PDACs are associated with mutations, deletions or promoter hypermethylation at the *CDKN2A* locus (9q21), which encodes two tumor suppressor genes, namely $p16^{INK4A}$ and $p19^{ARF}$, via distinct first exons and alternative reading frames in shared downstream exons. Of those two, $p16^{INK4A}$ seems to be the more important tumor suppressor as mutations have been identified predominantly in $p16^{INK4A}$ and rarely in $p19^{ARF}$ (Bardeesy and DePinho, 2002; Leipner et al., 2004). Mutations at the *CDKN2A* locus affect two different pathways: the retinoblastoma (Rb) pathway and the Trp53 pathway. While $p16^{Ink4A}$ inhibits CDK4/6-mediated phosphorylation of Rb and therefore blocks entry into S-phase, $p19^{Arf}$ inhibits Mdm2-mediated tagging of Trp53 for proteasomal degradation (Bardeesy and DePinho, 2002; Hezel et al., 2006).

A rather late event in PanIN progression is the appearance of missense alterations in the DNA binding domain of the tumor suppressor gene *TP53*. Mutations of *TP53* occur in 50-75% of PDACs and 57% of PanIN-3 lesions, but not in PanIN-1 and -2 lesions (Maitra et al., 2003). Wild type TP53 plays an important role in cell cycle regulation, induction of apoptosis and maintenance of genomic stability. As *TP53* mutation is commonly accompanied by loss of wild type allele, protection against genetic rearrangements and accumulation of DNA damage is impaired and cell cycle regulation is lost, resulting in uncontrolled proliferation and aneuploidy (Boschman et al., 1994, Leipner et al., 2004).

Another tumor suppressor gene worth mentioning is the transcription factor *SMAD4*, also known as *DPC4*, which is an important regulator of the transforming growth

factor β (TGF-β) signaling pathway. With a frequency of approximately 55% this is a rather late event in tumorigenesis as homozygous deletions or a combination of intragenic point mutations and loss of heterozygosity are found in PanIN-3 and PDAC, but not in PanIN-1 and -2 lesions (Wilentz et al., 2000; Maitra et al., 2003). The impact of SMAD4 in PDAC development is most probably a result of its central role in TGF-β signaling, but, herein, rather due to modulation of tumor microenvironment than growth control via TGF- β signaling (Bardeesy et al., 2006; Hezel et al., 2006).
Besides those major genetic alterations, mutations with a lower frequency can be observed, e.g. in *BRCA2, LKB1/STK11, AKT2* or DNA mismatch repair genes (Leipner et al., 2004). Furthermore, increased growth factor receptor signaling, activation of developmental signaling pathways, telomere dysfunction and epigenetic silencing are characteristics of invasive PDAC (Hezel et al., 2006; Maitra and Hruban, 2008).

1.1.2 Oncogenic Kras in Mouse Models of Pancreatic Cancer

The murine pancreas was one of the first organs in which tissue-specific transgene expression and transgenic tumor induction could be achieved. Nevertheless, it took almost 20 years from the earliest studies until David Tuveson and colleagues evolved a model that resembles human PDAC development (Hingorani et al., 2003; Leach, 2004).
Within those first experiments, transgenic mice were generated which expressed *Hras* (Quaife et al., 1987), *SV40 T-antigen* (Ornitz et al., 1987), *c-myc* (Sandgren et al., 1991) or *TGF-α* (Wagner et al., 2001) under the control of the pancreas-specific *elastase* promoter. Expression from the *elastase* promoter was mostly seen in the acinar compartment of the pancreas, thus leading to development of acinar cell carcinoma or mixed acinar-ductal tumor histology. No characteristics of PDAC were observed. As it became clear that activated Kras plays a key-role in PDAC development, mouse models were generated expressing *Kras* with the activating G12D mutation ($Kras^{G12D}$). Expression of $Kras^{G12D}$ under the control of the *Cytokeratin 19* promoter in pancreatic ductal cells resulted in lymphatic infiltration and hyperplasia of gastric mucous neck cells, but not in PDAC (Brembeck et al., 2003). In another approach $Kras^{G12D}$ was expressed under the control of the *elastase* promoter in acinar cells. This lead to acinar hyperplasia, tubular complexes and preinvasive

ductal neoplasia in the exocrine pancreas (Grippo et al., 2003). Nevertheless, both models failed to recapitulate the major hallmarks of human PanINs and PDAC.

The major problem was targeting *Kras*^{G12D} to the pancreatic ductal epithelium. Thus, a breakthrough was achieved when two transcription factors, the homeodomain protein Pdx1 and the basic helix-loop-helix protein Pancreas transcription factor subunit alpha Ptf1a (also known as Ptf1-p48), were recognized as regulators of the pancreatic development (Offield et al., 1996; Kawaguchi et al., 2002). Pdx1 can first be detected at embryonic development day E8.5 and is restricted to the dorsal gut endoderm, later to dorsal and ventral pancreatic buds and the duodenal epithelium (Ohlsson et al., 1993; Guz et al., 1995; Milewski et al., 1998). In adult animals *Pdx1* expression is found in insulin producing and somatostatin producing cells and the duodenal epithelium (Ohlsson et al., 1993; Miller et al., 1994; Offield et al., 1996). *Ptf1a* is expressed shortly afterwards (E9.5) and is required for pancreatic development (Kawaguchi et al., 2002; Lin et al., 2004). In adult animals *Ptf1a* expression is restricted to pancreatic acinar cells (Lin et al., 2004). As both transcription factors are active in precursor cells which give rise to all mature pancreatic cells, this gives the opportunity to specifically target the pancreas, including the ductal cells.

To specifically target *Kras*^{G12D} to the murine pancreas, a conditionally expressed allele was applied. A transcriptional stop element which is floxed by two functional *loxP* sites (*lox-Stop-lox; LSL*) was inserted upstream of the murine *Kras* locus. The locus itself was modified by introduction of the activating G12D mutation (Jackson et al., 2001). To express the mutant allele, *LSL-Kras*^{G12D} mice were interbred with mouse strains that express *Cre* from the *Pdx1* or *Ptf1a* promoter. *Cre* is stochastically expressed in the pancreas of transgenically derived *Pdx1-Cre* mice, whereas it is uniformly expressed in the whole organ when knocked into the *Ptf1a* locus (Kawaguchi et al., 2002; Hingorani et al., 2003). Until recombination, the *LSL-Kras*^{G12D} animals are heterozygous for wild type *Kras* (*Kras*$^{+/-}$) as the mutant allele is silenced by *LSL*. Upon excision of the stop element and recombination, activated *Kras*^{G12D} is expressed from its locus at endogenous levels, resulting in a heterozygous mutant condition (*Kras*$^{G12D/+}$) (Jackson et al., 2001; Hingorani et al., 2003). In 100% *of Pdx1-Cre;LSL-Kras*$^{G12D/+}$ and *Ptf1a*$^{Cre/+}$*;LSL-Kras*$^{G12D/+}$ mice PanIN lesions were observed which recapitulate, for the first time, all different stages of the human

PanINs. The incidence of higher graded PanINs increased with age, but PDAC development and metastasis were seen rarely, even after longitudinal follow-up (Hingorani et al., 2003). To analyze whether additional alterations in tumor suppressor genes affect the course and onset of the disease, *Pdx1-Cre;LSL-Kras$^{G12D/+}$* or *Ptf1a$^{Cre/+}$;LSL-Kras$^{G12D/+}$* mice were interbred with *LSL-Trp53^{R172H}* mice. This *Trp53* mutation equals the most common *TP53* mutation in human PDAC and, when expressed concomitantly with *Kras^{G12D}* in murine pancreatic progenitor cells, Trp53^{R172H} promotes development of invasive and widely metastatic PDAC initiated by Kras^{G12D}. By introduction of *Trp53^{R172H}*, tumor development was also accelerated from 15 months in *Pdx1-Cre;LSL-Kras$^{G12D/+}$* mice to five months in *Pdx1-Cre;LSL-Kras$^{G12D/+}$;LSL-Trp53$^{R712H/+}$* mice (Hingorani et al., 2005). Mice display clinical symptoms, histopathology and metastatic profile as observed in the human disease. Therefore, this model became widely accepted as genetically defined mouse model of human PDAC.

1.2. Controlling Gene Activity: a Tamoxifen Inducible System

One major drawback of the genetically defined Kras^{G12D}-dependent model is the lack of temporal control of *Kras^{G12D}* expression as, once activated, Kras^{G12D} remains active. It is not possible to determine the role of Kras^{G12D} in tumor maintenance.
Thus, a model which allows time- and tissue-specific control of Kras^{G12D} activity would be of advantage. Feil et al. created a model in which the Cre/loxP system was modified in a way, which allows shuttling of Cre recombinase into the nucleus where it is active. In this model, the estrogen receptor was employed as it is actively translocated into the nucleus in the presence of 17 β-estradiol. To circumvent effects of endogenous 17 β-estradiol, a mutated DNA ligand binding domain (LBD) of the human estrogen receptor (G521R), which cannot bind 17 β-estradiol, but the synthetic ligands tamoxifen and 4-hydroxytamoxifen (4-OHT), was used. By fusing *Cre recombinase* to the mutated *LBD* it was possible to generate an inducible system of gene expression. The resulting fusion protein Cre-ER^{T} is independent of endogenous 17 β-estradiol, but by addition of tamoxifen or 4-OHT it can be shuttled into the nucleus (Feil et al., 1996). To optimize binding properties and enhance sensitivity to synthetic ligands, additional mutations were introduced into the LBD.

The triple mutant G400V/M543A/L544A, called *Cre-ER*^{T2}, is highly sensitive to nanomolar concentrations of 4-OHT.

To allow modulation of Kras^{G12D} activity at defined time points during carcinogenesis, this model can be adopted by creating a fusion protein of Kras^{G12D} and the triple mutant LBD ER^{T2}. Thus, it can be analyzed whether Kras is solely necessary for tumor initiation or as well for tumor promotion. It is also possible to suppress Kras^{G12D} activity until adulthood by treating pregnant females and offspring with tamoxifen until Kras^{G12D} activity is requested. To monitor effects of Kras^{G12D} de-activation in the growing tumor *in vivo* a mouse model was generated in our lab. In this model proliferation is visualized via bioluminescence imaging and will be further described in the following section.

1.3. Bioluminescence Imaging in Tumor Development

1.3.1 Mechanism of Bioluminescence Imaging

Standard mouse models apply caliper measurement of palpable tumors to monitor tumor growth and animals are sacrificed at multiple and predetermined end points. Therefore, large animal cohorts are needed and the number of end points for evaluation is limited. Furthermore, no real-time measurement of tumor development or monitoring of therapy response can be conducted within the same animal (Jenkins et al., 2003; Gross and Piwnica-Worms, 2005). To overcome this drawback extensive research on *in vivo* imaging was performed over the last decades.

Currently various molecular imaging techniques using reporter genes are applied for non-invasive longitudinal studies of biological processes in intact cells or living animals (Dothager et al., 2009). Well characterized and commonly used reporters are green fluorescent protein (fluorescent imaging), transferrin receptor (magnetic resonance imaging), herpes simplex virus-1 thymidine kinase (positron emission tomography) and luciferase (bioluminescence imaging) (Dothager et al., 2009).

Bioluminescence imaging (BLI) takes advantage of a naturally occurring process observed in several non-mammalian species (Sato et al., 2004). An oxygenase catalyzes the oxidation of a substrate which is accompanied by the emission of light (Sato et al., 2004). The most common bioluminescence reporter gene is *luciferase* from the North American firefly (*Photinus pyralis*) with D-luciferin as its substrate and

an emission peak at 562 nm. Despite the broad emission spectrum (530 to 640 nm) one might argue that an emission peak at 562 nm would be absorbed by hemoglobin which absorbs wavelengths below 600 nm (Contag and Ross, 2002; Sadikot and Blackwell, 2005). But by examination of temperature dependency of emission, Zhao et al. could show that emission peak of firefly luciferase (fLuc) is shifted from 560 nm at 22 °C to 612 nm at 37 °C (Zhao et al., 2005; Contag, 2007). Coupled with optical properties of tissue, this allows light to penetrate through several millimeters to centimeters of tissue, even though photon intensity decreases 10-fold with each centimeter of tissue depth (Contag and Bachmann, 2002; Sato et al., 2004; Sadikot and Blackwell, 2005).

For detection of photons and conversion into an electrical charge pattern, corresponding to the intensity of incoming photons, a cooled charge coupled device (CCD) camera is used (Spibey et al., 2001; Sadikot and Blackwell, 2005). Besides the properties of the CCD, several other factors determine the sensitivity of detection, e.g. the expression level of luciferase, the tissue depth (i.e. the distance photons must travel through tissue), the availability of cofactors, the time after D-luciferin injection and the presence of fur (Sato et al., 2004; Sadikot and Blackwell, 2005).

Since BLI is a robust, sensitive and relatively cheap method of molecular imaging it is used in a variety of applications, e.g. monitoring of tumor development after subcutaneous or orthotopic transplantation of tumor cells and responsiveness to hormon treatment or to control target gene delivery (Lemmen et al., 2004; Hsieh et al., 2005; Mayr et al., 2008; Kim et al., 2010; Tao et al., 2010). Mouse models using BLI offer the unique opportunity to follow biological processes in real-time and within their natural context (Prescher and Contag, 2010).

1.3.2 Mouse Models Applying Bioluminescence Imaging

Over the years a variety of mouse models applying BLI has been published. These models include transplantation models as well as endogenous models and are very diverse in design depending on the question addressed.

Subcutaneous or orthotopic transplantation models of tumor cells that stably express *fLuc* are commonly used. Alternatively, tumor cells can be injected into the tail vein or heart. BLI then allows monitoring of tumor growth, distribution of tumor cells via circulation and development of metastasis (Edinger et al., 1999; Mayr et al., 2008;

Miretti et al., 2008; Jenkins et al., 2005). Kim et al. could show the high sensitivity of BLI by detecting small numbers of cells, e.g. five or ten cells, shortly after subcutaneous transplantation. Over the time course they could monitor an increase of the clearly visible BLI signal (Kim et al., 2010). In an orthotopic transplantation model of pancreatic cancer Angst et al. demonstrate the feasibility of longitudinal monitoring of angiogenesis by placing *fLuc* under the control of the *vascular endothelial growth factor receptor 2* promoter (Angst et al., 2010). Limitations of these systems are high background levels induced by activation of the promoter due to endogenous hormones and stimuli or by constitutively high promoter activity in some tissues (Lemmen et al., 2004; Hsieh et al., 2005; Angst et al., 2010).

Besides transplantation models, endogenous mouse models employing BLI are published. These models either express *fLuc* under the control of a promoter which is activated upon a stimulus, e.g. hormones or growth factors, or *fLuc* is silenced by a transcriptional stop element flanked by *loxP* sites which allows a tissue-specific expression of *fLuc*. For example, Hsieh et al. developed a model in which *fLuc* is expressed under the control of a highly active *supra prostate specific antigen* (*sPSA*) promoter. A similar approach was performed by Lemmen et al. who established an endogenous model to detect activation of the estrogen receptor by positioning *fLuc* under the control of three consensus estrogen-responsive elements coupled to a minimal TATA-box. Both models enable monitoring of developmental processes as well as response to hormone treatment (Lemmen et al., 2004; Hsieh et al., 2005).

To circumvent background expression of *fLuc* in other than the targeted tissue, the *Cre/loxP* system is used in endogenous mouse models. Lyons et al. generated a transgenic mouse model with an ubiquitously expressed conditional *fLuc* transgene driven by the *β-actin* promoter. This reporter mouse was then crossed into the pre-existing *Cre/loxP*-based tumor models of non-small cell lung cancer (Lyons et al., 2003). A similar approach was followed by placing *fLuc* under control of the ubiquitously expressed and constitutively active *CAG* promoter in a transgenic mouse model to monitor development of glioblastoma (Woolfenden et al., 2009). Safran et al. generated a knock-in mouse model wherein *fLuc* is driven by the *Rosa26* promoter (Safran et al., 2003). These models all use a transcriptional stop element to silence *fLuc* expression unless recombination takes place by Cre

recombinase which is expressed from a tissue-specific promoter or by using Adeno-Cre (Lyons et al., 2003; Woolfenden et al., 2009; Tao et al., 2010).

All of these models allowed monitoring of tumor development as the BLI signal increases with tumor size (Mayr et al., 2008; Woolfenden et al., 2009). Still, these models are not capable of direct monitoring of proliferation as BLI signal is solely depending on tumor size, but not on proliferation rate. An approach to monitor loss of Rb pathway function and, as a consequence, proliferation of tumor cells was done by the group around Eric Holland. In a transgenic mouse model *fLuc* is driven by the human *E2F1* promoter which shows tumor-selective transgene expression. Still, this model requires loss of Rb pathway control and showed background light production (Uhrbom et al., 2004).

Therefore, we set out to develop a more general model, the *LSL-PCNA*$^{fLuc/+}$ mouse model, which allows spatio-temporal visualization of cell proliferation *in vivo*. Furthermore, as there is an urgent need for development of novel drugs for PDAC treatment, the model is aimed towards a high-troughput screening approach to analyze therapy response *in vitro* and *in vivo* by bioluminescence imaging.

1.4. Aims of this Work

To overcome limitations of the existing and well-established Kras^{G12D}-dependent mouse model of PDAC, I set out to generate a tamoxifen inducible, Kras^{G12D}-driven mouse model of PDAC. This model, on the one hand, offers the opportunity to initiate carcinogenesis at different stages, i.e. embryonic development, postnatally as well as in adult animals. On the other hand, it enables the analysis of the effects of switching oncogenic Kras^{G12D} off in an already initiated tumor. Thus, the role of Kras signaling in tumor maintenance can be investigated. One of the aims of this thesis was to generate and analyze this new *LSL-Rosa26*^{KE} mouse model.

Furthermore, I set out to characterize and establish the *LSL-PCNA*$^{fLuc/+}$ mouse model, which was designed and generated in our lab, to monitor tumor cell proliferation *in vivo* via bioluminescence imaging. Moreover, I set out to generate and validate an *in vitro* screening platform which enables evaluation of novel drug candidates for the treatment of PDAC in a high-throughput approach. Potential drug candidates can then be tested for treatment response in orthotopic transplantation models and in the endogenous PDAC mouse model *in vivo*.

2 Materials

2.1. Technical Equipment

Technical equipment	Source
Analytical balance Kern AGB	Gottlieb Kern & Sohn GmbH, Balingen-Frommern
ASP300 Tissue Protector	Leica Mikrosysteme Vertrieb GmbH, Wetzlar
Avanti® J25 centrifuge	Beckman Coulter Inc., Brea, CA, USA
AxioCam MRc	Carl Zeiss AG, Oberkochen
Biometra WT 18	Biometra GmbH, Göttingen
Centrifuge 5417R	Eppendorf AG, Hamburg
CO_2 incubator HERAcell®	Heraeus Instruments GmbH, Osterode
Dewar Carrying Flask, type B	KGW-Isotherm, Karlsruhe
Digital CCD camera ORCA II-ER-1394	Hamamatsu, Herrsching
Duo Therm hybridization oven OV5	Biometra GmbH, Göttingen
Elektrophoresis-power supply Power Pac 200	Bio-Rad Laboratories GmbH, München
Elisa Plate reader Anthos 2001	Anthos Mikrosysteme GmbH, Krefeld
Eppendorf 5432 mixer	Eppendorf AG, Hamburg
FluoSTAR optima	BMG Labtech GmbH, Offenburg
Gel doc XR+ documentation system	Bio-Rad Laboratories GmbH, München
Gene Amp PCR system 9700	Applied Biosystems Inc., Foster City, CA
Gene Pulser II	Bio-Rad Laboratories GmbH, München
Genequant Pro	Biochrom Ltd., Cambrige, UK
Hemocytometer (Neubauer improved)	LO-Laboroptik GmbH, Bad Homburg

Technical equipment	Source
Hera Safe biological safety cabinet	Thermo Fisher Scientific Inc.Waltham, MA, USA
Homogenizer Silent Crusher M with tool 6F	Heidolph Instruments GmbH, Schwabach
Horizontal gel electrophoresis system	Biozym Scientific GmbH, Hessisch Oldenburg
Hyper Processor	GE Healthcare Europe GmbH, Freiburg
Leica EG 1150 H embedding system	Leica Mikrosysteme Vertrieb GmbH, Wetzlar
Luminometer Lumat LB 9501	Berthold Technologies GmbH, Bad Wildbad
Magnetic stirrer COMBIMAG	IKA-Werke GmbH, Staufen
Microliter syringe	Hamilton Bonaduz AG, Bonaduz, Switzerland
Microscope Axiovert 25	Carl Zeiss AG, Oberkochen
Microscope DM LB	Leica Mikrosysteme Vertrieb GmbH, Wetzlar
Microtome Microm HM355S	Thermo Scientific, Walldorf
Microwave	Siemens, München
Mighty Small II Western blot system	Hoefer Inc., Holliston, MA, USA
Mini-PROTEAN® 3 cell	Bio-Rad Laboratories GmbH, München
Multipette® stream	Eppendorf AG, Hamburg
Odyssey® infrared imaging system	LI-COR Bioscience Corporate, Lincoln, NE; USA
Paraffin tissue floating bath Microm SB80	Thermo Fisher Scientific Inc., Waltham, MA, USA
PCR-Thermocycler T-1	Biometra biomedizinische Analytik GmbH, Göttingen
pH-Meter	WTW GmbH, Weilheim
Pipetus®	Hirschmann Laborgeräte GmbH&CoKG, Eberstadt
Power supply E844, E822, EV243	Consort, Turnhout, Belgium

Technical equipment	Source
Precision balance Kern FTB	Gottlieb Kern & Sohn GmbH, Balingen-Frommerns
Schott Duran® glass ware	Schott UK Ltd, Stafford, UK
Spectrophotometer ND-1000	PEQLAB Biotechnologie GmbH, Erlangen
StepOnePlus™ Real-Time PCR system	Applied Biosystems Inc., Carlsbad, CA, USA
Thermomixer compact	Eppendorf AG, Hamburg
Thermoshake	Gerhardt GmbH, Königswinter
VacuGene pump	GE Healthcare Europe GmbH, Freiburg
VacuGene XL	GE Healthcare Europe GmbH, Freiburg
Vortex Reax 2000	Heidolph Instruments GmbH, Schwabach
Vortex VF2	IKA-Werke GmbH, Staufen
Wallac MicroBeta® Trilux 1450	PerkinElmer Inc., Waltham, MA, USA
Water bath 1003	GFL Gesellschaft für Labortechnik GmbH, Burgwedel
Zeiss LSM 510	Carl Zeiss AG, Oberkochen

2.2. Disposables

Disposable	Source
27-gauge needles	BD Bioscience, Franklin Lakes, NJ, USA
Amersham Hybond™-N membrane	GE Healthcare Europe GmbH, Freiburg
Amersham illustra ProbeQuant™ G-50 micro columns	GE Healthcare Europe GmbH, Freiburg
Amersham Rediprime™ II DNA labelling system	GE Healthcare Europe GmbH, Freiburg
BioPur® combitips	Eppendorf AG, Hamburg

Disposable	Source
Cell culture plastics	BD Bioscience, Franklin Lakes, NJ, USA; TPP Tissue Culture Labware, Trasadingen, CH
Cell scrapers	TPP Tissue Culture Labware, Trasadingen, CH
Chromatography paper 3 mm	Whatman plc, Kent, UK
Cover slips	Menzel-Gläser, Braunschweig
Cryotubes™	Nunc™ Brand Products, Napeville, IL, USA
Cuvettes	Greiner Bio-One GmbH, Frickenhausen
Ethilon 5-0	Ethicon, Johnson&Johnson MEDICAL GmbH, Norderstedt
Feather disposable scalpel	Feather Safety Razor Co., Ltd, Osaka, Japan
Gene pulser/Micropulser cuvettes (0.2 cm gap)	Bio-Rad Laboratories GmbH, München
Immobilon transfer membrane	Millipore Corporate, Billerica, MA, USA
Kodak BioMax MS film	Sigma-Aldrich Chemie GmbH, Steinheim
MicroAmp® optical 96-well reaction plate	Applied Biosystems Inc., Carlsbad, CA, USA
Microtiterplate 96-well µclear® white	Greiner Bio-One GmbH, Frickenhausen
Microtome blades S35	Feather Safety Razor Co, Ltd., Osaka, Japan
PCR reaction tubes	Eppendorf AG, Hamburg
Petri dishes	Sarstedt AG&Co., Nümbrecht
Phase lock gel light tubes	5’ prime GmbH, Hamburg
Polystyrene tubes (round-bottom)	Sarstedt AG, Nümbrecht
Reaction tubes 1.5 and 2 mL	Eppendorf AG, Hamburg
Safe-lock reaction tubes BioPur®	Eppendorf AG, Hamburg
Serological pipettes	BD Bioscience, Franklin Lakes, NJ, USA

Disposable	Source
Single use syringe	CODAN Medizinische Geräte GmbH, Lensahn
Sterile pipet tips	Biozym Scientific GmbH, Hessisch Oldendorf
Superfrost® Plus glass slides	Menzel-Gläser, Braunschweig
Wound clips	MEDICON eG, Tuttlingen

2.3. Reagents and Enzymes

All restriction endonucleases were obtained from New England Biolabs (Frankfurt).

Reagent	Source
1,4-Dithiothreitol (DTT)	Carl Roth GmbH, Karlsruhe
1 kb extension ladder	Invitrogen GmbH, Karlsruhe
2log DNA ladder	New England Biolabs, Frankfurt
3-(4,5-deimethylthiazol-2-yl)-2,5-diphenyl tetrazolium bromide (MTT)	Carl Roth GmbH, Karlsruhe
4-hydroxytamoxifen (4-OHT)	Sigma-Aldrich Chemie GmbH, Steinheim
5-Bromo-2´-deoxyuridine (BrdU)	Sigma-Aldrich Chemie GmbH, Steinheim
Agarose	PEQLAB Biotechnologie GmbH, Erlangen
alpha-32P-dCTP, 9.25 Mbq, 250 µCi, ~3000 Ci/mmol	PerkinElmer Life and Analytical Scientices, Inc., Rodgau-Jürgesheim
Amersham Rapid-hyb™ buffer	GE Healthcare Europe GmbH, Freiburg
Amersham Rediprime™ II DNA labeling system	GE Healthcare Europe GmbH, Freiburg
Ampicillin (100 mg/mL)	Carl Roth GmbH, Karlsruhe
API-2	Tocris Bioscience, Ellisville, MO, USA
BBXF agarose gel loading dye mixture	BIO 101, Inc. Carlsbad, CA, USA

Reagent	Source
Bio-Rad Precision Plus protein standard	Bio-Rad Laboratories GmbH, München
Bio-Rad protein assay	Bio-Rad Laboratories GmbH, München
Bovine serum albumin (BSA) standard	Thermo Fisher Scientific, Piece Biotechnology, Rockford, IL, USA
Bromphenol blue	Sigma-Aldrich Chemie GmbH, Steinheim
BX-912	Axon Medchem BV, Groningen, The Netherlands
Chloramphenicol (30 mg/mL)	Applichem, Darmstadt
Chloroform	Carl Roth GmbH, Karlsruhe
Cre Recombinase	(Novagen) EMD Chemicals Inc., Gibbstown, NJ, USA
Dimethylsulfoxide (DMSO)	Carl Roth GmbH, Karlsruhe
D-luciferin	Synchem, Felsberg/Altenburg
DNAse I	Qiagen GmbH, Hilden
Erlotinib	LC Laboratories, Woburn, MA, USA
Ethanol 100%	Carl Roth GmbH, Karlsruhe
Ethidium bromide (10 mg/mL)	Carl Roth GmbH, Karlsruhe
Gateway® LR Clonase™ enzyme mix	Invitrogen GmbH, Karlsruhe
GDP (10x)	Millipore Corporate, Billerica, MA, USA
Gelatine	Carl Roth GmbH, Karlsruhe
Glycerol	Sigma-Aldrich Chemie GmbH, Steinheim
Glycin	Carl Roth GmbH, Karlsruhe
γ-GTP	Cytoskeleton, Denver, CO, USA
H-1152	Tocris Bioscience, Ellisville, MO, USA
HCl	Carl Roth GmbH, Karlsruhe

Reagent	Source
HEPES	Sigma-Aldrich Chemie GmbH, Steinheim
HotStarTaq DNA polymerase	Qiagen GmbH, Hilden
Isofluran Forene	Abbott GmbH, Wiesbaden
Isopropanol	Carl Roth GmbH, Karlsruhe
Kanamycin (100 mg/mL)	Carl Roth GmbH, Karlsruhe
LB agar and broth Luria/Miller	Carl Roth GmbH, Karlsruhe
Lipofectamin2000	Invitrogen GmbH, Karlsruhe
LR Clonase® II Plus enzyme	Invitrogen GmbH, Karlsruhe
LY294002	LC Laboratories, Woburn, MA, USA
Magnesiumchloride	Carl Roth GmbH, Karlsruhe
β-Mercaptoethanol	Sigma-Aldrich Chemie GmbH, Steinheim
Metacam	Boehringer Ingelheim Pharma GmbH, Ingelheim am Rhein
Methanol	Carl Roth GmbH, Karlsruhe
NaOH	Carl Roth GmbH, Karlsruhe
Nonidet NP-40	Sigma-Aldrich Chemie GmbH, Steinheim
NVP-BEZ235 hydrochloride	Chemdea, Ridgewood, NJ, USA
Odyssey blocking reagent	LI-COR Corp. Offices, Lincoln, NE, USA
Phosphatase inhibitor set	Roche Diagnostics Deutschland GmbH, Mannheim
PI-103	Selleck Chemicals LLC, Houston, TX, USA
Protease inhibitor set	Roche Diagnostics Deutschland GmbH, Mannheim
Proteinase K	Roche Diagnostics Deutschland GmbH, Mannheim
REDTaq® ReadyMix™ PCR reaction mix	Sigma-Aldrich Chemie GmbH, Steinheim

Reagent	Source
RNaseA	Fermentas GmbH, St. Leon-Rot
Roscovitine	(Calbiochem) EMD Chemicals Inc., Gibbstown, NJ, USA
Roti® Phenol/Chloroform/Isoamyl-alcohol	Carl Roth GmbH, Karlsruhe
Rotiphorese® Gel 30	Carl Roth GmbH, Karlsruhe
Saponin	Sigma-Aldrich Chemie GmbH, Steinheim
Sodium dodecyl sulphate (SDS)	Carl Roth GmbH, Karlsruhe
SSC buffer 20x concentrate	Sigma-Aldrich Chemie GmbH, Steinheim
S.O.C. medium	Invitrogen GmbH, Karlsruhe
Sodiumdeoxycholate	Sigma-Aldrich Chemie GmbH, Steinheim
Sunitinib	LC Laboratories, Woburn, MA, USA
SuperFect transfection reagent	Qiagen GmbH, Hilden
SuperScript II reverse transcriptase	Invitrogen GmbH, Karlsruhe
SYBR® Green PCR master mix	Applied Biosystems Inc., Carlsbad, CA, USA
T4 DNA ligase	Invitrogen GmbH, Karlsruhe
TEMED	Carl Roth GmbH, Karlsruhe
TrisHCl	Carl Roth GmbH, Karlsruhe
Tween-20	Carl Roth GmbH, Karlsruhe
Vectashield® mounting medium with DAPI	Vector Laboratories, Burlingame, CA, USA
Tamoxifen	Sigma-Aldrich Chemie GmbH, Steinheim
TO-PRO®3-iodid	Invitrogen GmbH, Karlsruhe
TritonX-100	Sigma-Aldrich Chemie GmbH, Steinheim

2.4. Kits

Kits	Source
Luciferase assay system	Promega GmbH, Mannheim
Plasmid Mini/Midi kit	Qiagen GmbH, Hilden
EndoFree Plasmid Maxi kit	Qiagen GmbH, Hilden
RNeasy Mini kit	Qiagen GmbH, Hilden
TaqMan® reverse transcription reagents	Applied Biosystems Inc., Foster City, CA, USA
Venor® *GeM* kit	Minerva Biolabs GmbH, Berlin
Zero Blunt® TOPO® PCR cloning kit	Invitrogen GmbH, Karlsruhe

2.5. Antibodies

Antibody	Source
AlexaFluor® 680 goat anti-mouse IgG (# A21058)	Invitrogen GmbH, Karlsruhe
AlexaFluor® 750 goat anti-mouse IgG (# A21037)	Invitrogen GmbH, Karlsruhe
AlexaFluor® 680 goat anti-rabbit IgG (# A21076)	Invitrogen GmbH, Karlsruhe
AlexaFluor® 750 goat anti-rabbit IgG (# A21039)	Invitrogen GmbH, Karlsruhe
Anti-β-Actin (mouse) (# A5316)	Sigma-Aldrich Chemie GmbH, Steinheim
Anti-Akt (rabbit) (# 9272)	Cell Signaling Technology, Inc, Danvers, MA, USA
Anti-BrdU (rat) (# MCA2060)	AbD Serotec, Düsseldorf
Anti-firefly luciferase (goat) (# ab81823)	Abcam Inc., Cambridge, MA, USA
Anti-Oct1 C-21 (rabbit) (# sc-232)	Santa Cruz Biotechnology Inc., Santa Cruz, CA, USA

Antibody	Source
Anti-pan Ras clone 10 (mouse) (# 05-516)	Millipore Corporate, Billerica, MA, USA
Anti-PCNA PC10 (mouse) (# sc-56)	Santa Cruz Biotechnology Inc., Santa Cruz, CA, USA
Anti-phospho-Akt Ser473 (rabbit) (# 9271)	Cell Signaling Technology, Inc, Danvers, MA, USA
Anti-phospho-Akt Thr308 (rabbit) (# 9275)	Cell Signaling Technology, Inc, Danvers, MA, USA
Anti-Tubulin (mouse) (# T6199)	Sigma-Aldrich Chemie GmbH, Steinheim
Biotinylated Anti-Goat IgG (rabbit) (# BA-5000)	Vector Laboratories, Burlingame, CA, USA
Biotinylated Anti-Mouse IgG (goat) (# BA-9200)	Vector Laboratories, Burlingame, CA, USA
Biotinylated Anti-Rabbit IgG (goat) (# BA-1000)	Vector Laboratories, Burlingame, CA, USA
Biotinylated Anti-Rat IgG (goat) (# BA-9400)	Vector Laboratories, Burlingame, CA, USA

2.6. Primers

All primers were synthesized by MWG (sequencing, real-time PCR) or Operon (cloning). If not stated otherwise, genotyping primer pairs are used for genomic tail PCR.

Designation	Name	Sequence
Cloning	ER-T2_XhoI_for	5'- CTCACTCGAGCCATCTGCTGGAGAC- 3´
	ER-T2_NdeI_SalI_rev	5'- CTGAGTCGACCATATGTCAAGCTGTGG CAGGGAAAC-3'
Cloning	Kras_KpnI_AaTII_for	5'- GAGGTACCGACGTCGATATGACTGAGT ATAAGCTTGTG- 3'
	Kras_ohne Stop_XhoI_rev	5'- CTATCTCGAGCATAACTGTACACCTTGT CCTTGACTTC- 3'
Cloning	EGFP Xho Linker_for	5'- CTCACTCGAGCCATCTGCTGGAGACAT GGTGAGCAAGGGCGAG- 3'
	EGFP Xho_ rev	5'- CTATCTCGAGCTTGTACAGCTCGTCCATGCC-3'

Designation	Name	Sequence
ES cell screening	Rosa-26-Prom-UP-3	5'- CCTAAAGAAGAGGCTGTGCTTTGG- 3'
	Soriano-SA-LP	5'- CATCAAGGAAACCCTGGACTACTG- 3'
Genotyping $Kras^{G12D}$ (tail, cells and tissue)	Kras-UP1-WT	5'- CACCAGCTTCGGCTTCCTATT- 3'
	Kras-LP-URP1	5'- AGCTAATGGCTCTCAAAGGAATGTA- 3'
	$Kras^{G12D}$mut-UP	5'- CCATGGCTTGAGTAAGTCTGC- 3'
Genotyping $Rosa26^{KE}$ (tail, cells and tissue)	R26-tva-GT-UP	5'- AAAGTCGCTCTGAGTTGTTAT- 3'
	pGl3-pA-Pause 4645 UP	5'- TGAATAGTTAATTGGAGCGGCCGCAATA- 3'
	Kras_ohne Stop_XhoI_rev	5'- CTATCTCGAGCATAACTGTACACCTTGT CCTTGACTTC- 3'
Genotyping $Ptf1a^{Cre}$	p48-Cre-GT-LP-URP	5'- CCTCGAAGGCGTCGTTGATGGACTGCA- 3'
	p48-Cre-GT-wt-UP	5'-CCACGGATCACTCACAAAGCGT-3'
	p48-Cre-GT-mut-UP-neu	5'-GCCACCAGCCAGCTATCAA-3'
Genotyping $Trp53^{R172H}$ (tail, cells and tissue)	$Trp53^{R172H}$-WT-UP2	5'-AGCCTTAGACATAACACACGAACT-3'
	$Trp53^{R172H}$-URP-LP	5'-CTTGGAGACATAGCCACACTG-3'
	$Trp53^{R172H}$-mut UP4	5'-GCCACCATGGCTTGAGTAA-3'
Genotyping $PCNA^{fLuc}$	PCNA-ATG_UUP	5'-GCACAGCTCGATTTGCCTG- 3'
	PCNA-ATG-Mut_LP	5'- TACGAACGGTAATTAACAATTCGATATCAAG- 3'
	PCNA-ATG-WT_LP	5'- CCCGACACCATAGACCAATCAG- 3'
Genotyping LSL-$PCNA^{fLuc/+}$ stop	pGL3-pA-pause-4645-UP	5'- TGAATAGTTAATTGGAGCGGCCGCAATA- 3'
	pGL_3LP	5'- CTTTATGTTTTTGGCGTCTTCC- 3'
LSL-$PCNA^{fLuc/+}$ stop (cells, tissue)	PCNA-ATG_UUP	5'-GCACAGCTCGATTTGCCTG- 3'
	pGL_3LP	5'- CTTTATGTTTTTGGCGTCTTCC- 3'

Designation	Name	Sequence
Genotyping Pdx1-Cre	Pdx1-GT-UP1	5’- TTGAAACAAGTGCAGGTGTTCG- 3’
	Cre-neu-LP	5’- CAGGGTGTTATAAGCAATCCC- 3’
	Gabra1-UP	5’- AACACACACTGGAGGACTGGCTAGG-3’
	Gabra1-LP	5’- CAATGGTAGGCTCACTCTGGGAGATGATA- 3’
Genotyping Rosa26 Locus	R26-Tva-GT-UP	5'- AAAGTCGCTCTGAGTTGTTAT -3'
	R26-Tva-GT-SA-mut-LP	5'- GCGAAGAGTTTGTCCTCAACC- 3'
	R26-Tva-GT-WT-LP	5'- GGAGCGGGAGAAATGGATATG- 3'
Real-time PCR	mCyclophilin UP	5'- ATGGTCAACCCCACCGTGT- 3'
	mCyclophilin LP	5'- TTCTGCTGTCTTTGGAACTTTGTC- 3'
Real-time PCR	mKras UP	5’-TGTGGATGAGTATGACCCTACGA- 3’
	mKras LP	5’- CTTGACCTGCTGTGTCGAGAATA- 3’
Real-time PCR	KrasERT2_UP-Taq	5’- AGTCCGAGAAATTCGAAAACA- 3’
	KrasERT2_LP-Taq	5’- AGATGGCTCGAGCATAACTG- 3’
Real-time PCR	mROSA26-TM-UP-1	5’- CTATGGGATGCTCAGGCTCTGT- 3’
	mROSA26-TM-LP-1	5’- CCTCTATTGGTATTGCCCCTGTT- 3’
Real-time PCR	mTVA UP	5'- CTCTGCCAGCCAGGAATCAC- 3'
	mTVA LP	5'- CATCTCACCAGCTCACAGCAA- 3'

Table 2-1: Primer sequences

2.7. Plasmids

Plasmid	Source
pBC SK+	Stratagene Cloning System, Inc., La Jolla, CA, USA
pBC ER^{T2}	Modified in our lab from Stratagene Cloning System, Inc., La Jolla, CA, USA
pBluescript	Stratagene Cloning System, Inc., La Jolla, CA, USA
pcDNA3.2	Invitrogen GmbH, Karlsruhe
pcDNA3.2-Kras-EGFP-ER^{T2}	Modified in our lab from Invitrogen GmbH, Karlsruhe
pEGFP-fLuc	Modified in our lab from pEGFP, Clontech Laboratories, Inc. Mountain View, CA, USA
pENTRdsRed	Modified in our lab from pENTR™/TOPO-D®, Invitrogen GmbH, Karslruhe
pENTR-LSL (pENTR with floxed transcriptional stop element)	Modified in our lab from pENTRTM/TOPO-D®, Invitrogen GmbH, Karlsruhe
pRCASdsRed-$KrasER^{T2}$	Generated in our lab

2.8. Bacterial Strains

Bacterial strain	Source
One Shot® TOP10 chemically competent cells	Invitrogen GmbH, Karlsruhe
One Shot® Stbl3™ chemically competent cells	Invitrogen GmbH, Karlsruhe

2.9. Buffers and Solutions

Buffer	Composition
50x TAE-buffer pH 8.5	2 M TRIS 100 mM EDTA 5.71% acetic acid (100%)
5x Protein loading buffer pH 6.8	10% SDS 50% glycerol 228 mM TrisHCl 0.75 mM bromphenol blue 5% β-mercaptoethanol
Collecting gel buffer pH 6.8	1 M TrisHCl
ES cell lysis buffer	100 mM Tris pH 8.5 5 mM EDTA 0.8 mM HCl 2% SDS 200 mM NaCl 0.1 mg/mL proteinase K (add prior to use)
Fixative solution A pH 7.4	81 mM Na_2HPO_4 pH 9.0 25 mM NaH_2PO_4 pH 4.0
Fixative solution B pH 7.4	8% para-formaldehyd
Glycerol stock solution	65% glycerol 0.1 M $MgSO_4$ 25mM TrisHCl pH 8.0

Buffer	Composition
Gitschier's buffer (10x)	670 mM Tris pH 8.8
	166 mM $(NH_4)_2SO_4$
	67 mM $MgCl_2$
IP-buffer pH 7.9	50 mM HEPES
	150 mM NaCl
	1 mM EDTA
	0.5% NP-40
	10% glycerol
	1% phosphatase inhibitor (add prior to use)
	1% protease inhibitor (add prior to use)
KCM buffer	500 mM KCl
	150 mM $CaCl_2$
	250 mM $MgCl_2$
Loading buffer orange G (6x)	60% glycerol
	60 mM EDTA
	0.24% orange G
	0.12% SDS

Buffer	Composition
Mg^{2+} lysis buffer	25 mM HEPES pH 7.5
	150 mM NaCl
	1% NP-40
	0.25% sodiumdeoxycholate
	10% glycerol
	10 mM $MgCl_2$
	1 mM EDTA
Nuclear extracts buffer A	10 mM HEPES pH 7.9
	10 mM KCl
	0.1 mM EDTA
	0.1 mM EGTA
	1 mM DTT
Nuclear extracts buffer C	20 mM HEPES pH 7.9
	0.4 M NaCl
	1 mM EDTA
	1 mM EGTA
	0.1 mM DTT
Paraffin lysis buffer	10 mM TrisHCl
	1 mM EDTA
	1% SDS
	20 mg/mL proteinase K (add prior to use)
PBS pH 7.4	20 mM Na_2HPO_4
	50 mM NaCl

Buffer	Composition
PCR lysis buffer (Soriano)	0.5% Triton X-100 1% β-Mercaptoethanol 10% 10x Gitschier's buffer 400 µg/mL proteinase K (add prior to use)
Running buffer	19 mM TrisHCl 192 mM glycin 0.1% SDS
Separation gel buffer pH 8.8	1.5 M TrisHCl
TE buffer pH 8.0	10 mM TrisHCl 1 mM EDTA
Transfer buffer	19 mM TrisHCl 192 mM glycin 0.1% SDS 20% methanol

All buffers were prepared with H_2O bidest.

2.10. Histochemistry Reagents

Histochemistry Reagent	Source
Avidin/Biotin blocking kit	Vector Laboratories, Burlingame, CA, USA
DAB peroxidase substrate kit	Vector Laboratories, Burlingame, CA, USA
Eosin	Waldeck GmbH, Münster
Goat serum (# G9023)	Sigma-Aldrich Chemie GmbH, Steinheim
H_2O_2	Merck KgaA, Darmstadt

Histochemistry Reagent	Source
Haematoxylin	Merck KgaA, Darmstadt
Pertex mounting medium	Medite GmbH, Burgdorf
Rabbit serum (# R9133)	Sigma-Aldrich Chemie GmbH, Steinheim
Roti® Histofix (4% Formalin)	Carl Roth GmbH, Karlsruhe
Roti® Histol	Carl Roth GmbH, Karlsruhe
Antigen unmasking solution, citric acid based	Vector Laboratories, Burlingame, CA, USA
VECTASTAIN® Elite ABC solution	Vector Laboratories, Burlingame, CA, USA

2.11. Cell Culture

Cells	Source
DF-1 cells	American Type Culture Collection, Manassas, VA, USA
HEK293 FT tva cells; Modified in our lab from HEK-293	American Type Culture Collection, Manassas, VA, USA
MiaPaCa-CMV-fLuc cells; Modified in our lab from MiaPaCa2 cells	American Type Culture Collection, Manassas, VA, USA
BxPC3-CMV-fLuc cells; Modified in our lab from BxPC3 cells	American Type Culture Collection, Manassas, VA, USA
W4/129S6 ES Cells	Taconic Farms Inc., Hudson, NY, USA

2.11.1 Cell Culture Reagents and Media

Reagent	Source
Collagenase	Worthington Biochemical Corporation, Lakewood, NJ, USA
Fetal calf serum (FCS)	Biochrom AG, Berlin
Gelatine	Invitrogen, Karlsruhe

Reagent	Source
L-Glutamine	Invitrogen, Karlsruhe
Geniticin	Biochrom AG, Berlin
Hygromycin	Merck KgaA, Darmstadt
LIF	(Chemicon) Millipore Corporate, Billerica, MA, USA
Non-essential amino acids (100x)	Invitrogen GmbH, Karlsruhe
Sodium pyruvate	Invitrogen GmbH, Karlsruhe
PAN-FCS	PAN-Biotech GmbH, Aidenbach
PBS	Invitrogen GmbH, Karlsruhe
Penicillin-Streptomycin	Invitrogen GmbH, Karlsruhe
DMEM	Invitrogen GmbH, Karlsruhe
Trypsin-EDTA	Invitrogen GmbH, Karlsruhe

Medium	
DF-1 Medium	DMEM
	10% PAN-FCS
	1% Penicillin-Streptomycin
	1% Non-essential amino acids
Tumor cell medium	DMEM
	10% FCS
	1% Penicillin-Streptomycin
HEK-293 FT tva cell medium	DMEM
	10% FCS
	1% Penicillin-Streptomycin
	1% Non essential amino acids
	500 µg/mL Geniticin
	100 µg/mL Hygromycin

Medium	
MiaPaCa-CMV-fLuc cell medium	DMEM 10% FCS 1% Penicillin-Streptomycin 500 µg/mL Geniticin
BxPC3-CMV-fLuc cell medium	DMEM 10% FCS 1% Penicillin-Streptomycin 1 mg/mL Geniticin
PMEF medium	DMEM 10% EU-FCS 1% Penicillin-Streptomycin 1% L-Glutamine
ES cell medium	DMEM 15% EU-FCS 1% Penicillin-Streptomycin 1% L-Glutamine 1% Sodium pyruvate 1% Non-essential amino acids 0.1% 10^{-1}M β-Mercaptoethanol 1000 U/mL LIF
Freezing Medium	7 mL DMEM 2 mL FCS 1 mL DMSO

3 Methods

3.1. Generation of the *LSL-Rosa26^{KE}* Mouse Line

Limitations in common mouse models of pancreatic cancer lead to the development of a new mouse strain, *LSL-Rosa26^{KE}*, which carries *Kras* with the activating G12D mutation fused to the tamoxifen inducible modified estrogen receptor ER^{T2}. The fusion protein was silenced by a 5' transcriptional stop element flanked by *loxP* sites. The targeted locus was the ubiquitously active murine *Rosa26* locus. The transgene was introduced into murine embryonic stem (ES) cells by homologous recombination and correct ES cell clones were sent to PolyGene AG, Switzerland, for blastocyst injection and generation of chimeras.

3.1.1 Inactivation of Mouse Embryonic Fibroblasts (MEFs)

ES cells need to be grown on a monolayer of mitotically inactivated primary murine embryonic fibroblasts. These cells provide an environment which promotes growth and prevents differentiation of ES cells due to secreted proteins and growth factors. Inactivation of mitosis can be achieved by either treatment with mitomycin C or, as in this case, with irradiation.

Isolated MEFs were existing in the lab. To allow ES cell selection with geniticine, MEFs had been isolated at embryonic development day E12 from animals which carried a Neo^{R}-cassette.

To mitotically inactive MEFs, they were irradiated with 34 gray and then frozen in MEF freezing medium as described in 3.4.1.

3.1.2 Generation of Transgenic Embryonic Stem Cells

3.1.2.1 Preparation of the Targeting Construct

The plasmids containing the targeting construct were generated as described in 3.5.1.1. Fresh LB broth was inoculated from glycerol stock and bacteria were grown until an OD600 of 1-1.2. Plasmid preparation was performed according to manufacturer's protocol using EndoFree Plasmid Maxi kit (Qiagen). After elution from QIA-filter cartridge, isopropanol precipitation and additional ethanol (EtOH) precipitation was performed. The pellet was dissolved in sterile filtered TE buffer.

Singularity of Pac I restriction site was verified by control digestion of DNA. For electroporation 30 µg of plasmid DNA were digested with Pac I (60 units) for 2 h at 37 °C. The enyzme was heat inactivated at 65 °C for 20 min. Linearization was controlled on a 0.8% agarose gel.

3.1.2.2 Embryonic Stem Cell Culture

As described in 3.1.1, ES cells need to be grown on a monolayer of MEFs. Therefore, MEFs were always seeded on gelatine-coated plates of appropriate size one day before ES cells were seeded. W4/129S6 ES cells (Taconic) were grown in ES cell medium at 37 °C and 5% CO_2. ES cell medium was renewed daily.

3.1.2.3 Transfection and Selection

The transgene was introduced into ES cells by electroporation. Therefore, $1x10^7$ ES cells were diluted in 750 µL ice-cold PBS. Cell suspension was pipetted into pre-cooled electroporation cuvettes (Bio-Rad) and mixed with linearized targeting construct (see 3.1.2.1). Electroporation was performed at 250 V/500 µF.
Suspension was pipetted onto MEF covered dishes. A residue of ES cells, which were not electroporated, was seeded onto gelatine-coated 6-well plates for isolation of wild type (WT) genomic stem cell DNA.
18 h after electroporation, ES cell medium was replaced by selective ES cell medium containing 200 µg/mL geniticine. After 7 days single clones were picked into 24-well plates with MEFs for expansion of the clone and, in parallel, into gelatine coated 96-well plates for polymerase chain reaction (PCR) screening. ES cell clones which were positive in PCR screening (see 3.1.2.4) were subcloned according to the scheme shown in Figure 3-1. ES cells were cryopreserved from a 6-well plate and a 6 cm dish as described in 3.4.1 using ES cell medium containing 10% DMSO instead of freezing medium.

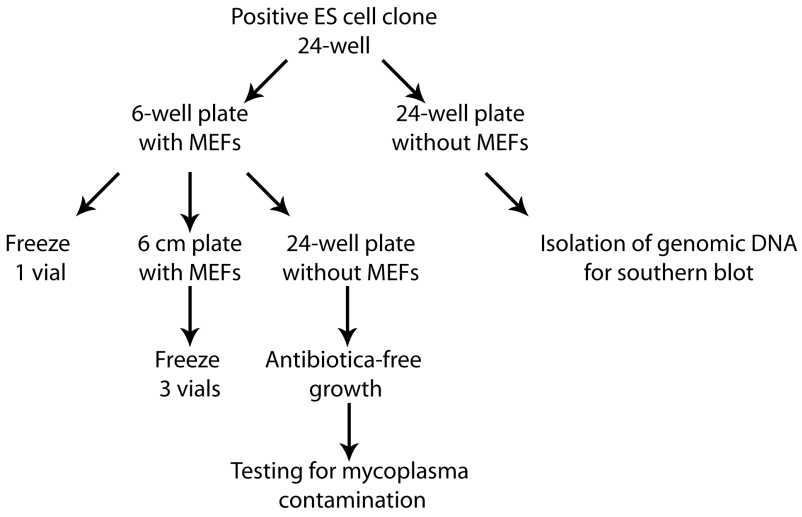

Figure 3-1: Procedure for ES cell clones positive in screening PCR.

3.1.2.4 PCR Screening of ES Cell Clones

For screening purpose DNA of ES cells was isolated out of the 96-well plates by incubation with 20 µL PCR lysis buffer for 1 h at 55 °C (wet chamber). After transfer of DNA into PCR tubes, proteinase K was heat inactivated at 95 °C for 10 min and 2 µL of DNA solution was used for screening PCR. HotStarTaq (Qiagen) was used according to manufacturer's protocol. Soriano-SA-LP and Rosa-26-Prom-UP-3 were used as primers. Conditions can be seen in Table 3-1. PCR products were loaded onto agarose gel for determination of correct size.

Temperature	Time	Number of cycles
95 °C	16 min	1
95 °C	35 sec	42
58 °C	45 sec	
72 °C	4 min +3 sec each cycle	
72 °C	10 min	1
4 °C	hold	

Table 3-1: PCR conditions for ES cell screening

3.1.2.5 Genomic DNA Isolation of ES Cells

ES cell medium on 6-well/24-well plates was changed daily and cells were grown to 100% confluency. Cells were lysed with ES cell lysis buffer in a wet chamber at 55 °C

over night. After addition of 100% EtOH, plates were incubated at room temperature (RT) over night. Next day, EtOH was removed, DNA was washed 3 times with 70% EtOH, dried at RT, dissolved in 200 µL water and stored at 4 °C until further use.

3.1.3 Southern Blot

Genomic DNA isolated from positive clones and WT ES cells was digested in duplicates with each Bgl I and EcoRV for 24 h at 37 °C and then used for Southern blot hybridization with 3 different probes (see Table 3-2) using a standard Southern blot protocol (Southern, 1975; Jurk, 1998). After addition of 10x BBXF Agarose gel loading dye mixture (Bio 101) samples as well as positive control and 1 kb extension ladder (Invitrogen) were loaded onto 1% agarose gel. Horizontal gel electrophoresis was run for approximately 14 h at 40 V. A strip containing digested WT DNA and 1 kb extension ladder was stained in ethidium bromide (EtBr), aligned with a transparent ruler and photographed under UV illumination.
DNA was transferred onto a Hybond-N+ membrane using a vacuum blotter with 55 mbar. To obtain improved transfer efficiency the gel was depurinated by incubation in 0.25 M HCl for 60-75 min. Subsequently, HCl was replaced by 0.4 M NaOH for denaturation. After blotting for 4 h, the membrane was incubated shortly in 2x SSC buffer and then baked at 80 °C for 2 h to fix the DNA on the membrane.

Probe	Source	Length
5' probe	pBroad3, digested with Not I	330 bp
3' probe	pRosa 26-3-2 digested with Acc/Drd	370 bp
neo probe	pMC1-neo digested with Mlu/Sal	850 bp

Table 3-2: Probes for Southern blots

Prehybridization was carried out in a roller bottle with 0.1 mL Amersham Rapid-hyb™ buffer per 1 cm^2 membrane for 2 h at 65 °C. During prehybridization 25 ng of each probe were labeled with [α-^{32}P]-dCTP using Rediprime™ II DNA labeling system (Amersham) and purified with illustra ProbeQuant™ G-50 micro columns (Amersham) both according to manufacturer's protocol. After denaturation at 95 °C for 5 min followed by 5 min on ice, freshly labelled probes were pipetted into pre-warmed Rapid-hyb™ buffer (Amersham). The membrane was hybridized at 65 °C

over night with gentle agitation. After hybridization, membranes were washed as described in Table 3-3. After the last washing step, the blot was exposed to X-Ray film.

Probe	Buffer	Temperature	Duration	Repeats
5' probe/ neo probe	2x SSC/0.1% SDS	65 °C	20 min	1
	1x SSC/0.1% SDS	65 °C	20 min	2
	0.1x SSC/0.1% SDS	65 °C	20 min	1
3' probe	2x SSC/0.1% SDS	65 °C	20 min	1
	2x SSC/0.1% SDS	65 °C	20 min	1
	2x SSC/0.1% SDS	65 °C	15 min	1

Table 3-3: Stringency washing of membranes after hybridization with radioactively labeled probes

3.2. Animal Experiments

For animal experiments the conditional *Cre/LoxP* system was applied. By interbreeding mice which carry a transgene silenced by a transcriptional stop element flanked by *loxP* sites with mice strains expressing *Cre recombinase* under control of a tissue-specific promoter, conditional deletion of *LSL* and, therefore, tissue-specific expression of the transgene could then be found in offspring.

LSL-Kras^{G12D} and *LSL-Trp53*$^{R172H/+}$ mouse strains were kindly provided by Dr. T. Jacks (Massachusetts Institute of Technology, Cambridge, MA, USA) and *Ptf1a*$^{Cre/+}$ mice were kindly provided by Dr. H. Nakhai (Klinikum rechts der Isar, TU Munich, Munich, Germany). *Pdx1-Cre* mouse strain was kindly provided by Dr. D. Melton (Harvard Stem Cell Institute, Cambridge, MA, USA). *Prm1-Cre* mice were purchased from The Jackson Laboratory (Bar Harbor, Maine, USA).

All animal studies were conducted meeting the requirements of the European guidelines for the care and use of laboratory animals and were approved by the local authorities.

3.2.1 Mouse Strains and Breeding

3.2.1.1 *LSL-Rosa26^{KE}* Mice

To obtain mice expressing the *KrasER^{T2}* in the pancreas, the *LSL-Rosa26^{KE}* strain was crossed with *Ptf1a$^{Cre/+}$* mice (Nakhai et al., 2007). Tumor growth was accelerated by introduction of *LSL-Trp53^{R172H}* (Hingorani et al., 2005) into a subcohort of animals.

For tamoxifen experiments mice were fed 4 mg tamoxifen for 3 days using a feeding needle. 2 h after last dosage, dissection was performed as described in 3.2.3.

2 h before mice were sacrificed they were injected intraperitoneally (i.p.) with 50 mg/kg Bromodeoxyuridine (BrdU).

3.2.1.2 *LSL-PCNA$^{fLuc/+}$* Mice

Several approaches were carried out for the characterization of the new *LSL-PCNA$^{fLuc/+}$* mouse strain.

To generate mice carrying *fLuc* in one or two alleles *LSL-PCNA$^{fLuc/+}$* mice were crossed homo- or heterozygously. For ubiquitous deletion of the transcriptional stop element, *LSL-PCNA$^{fLuc/+}$* mice were interbred with the general deleter strain *Prm1-Cre* (O'Gorman et al., 1997). To obtain pancreas-specific recombination *LSL-PCNA$^{fLuc/+}$* mice were interbred with *Ptf1a$^{Cre/+}$* (Nakhai et al., 2007) or *Pdx1-Cre* (Hingorani et al., 2003) mouse strains. To express *fLuc* in PanIN lesions and PDAC *LSL-PCNA$^{fLuc+/-}$* mice were crossed with the genetically defined model of pancreatic cancer (*Pdx1-Cre* or *Ptf1a$^{Cre/+}$;LSL-Kras$^{G12D/+}$;(LSL-Trp53$^{R172H/+}$)*).

3.2.2 *In Vivo* Bioluminescence Imaging

For *in vivo* measurement of luciferase activity, mice were anesthetized by i.p. injection of MMF (5 mg/kg midazolam, 500 µg/kg medetomidine, 50 µg/kg fentanyl). Simultaneously D-luciferin (225 mg/kg body weight) (Synchem) was administered i.p.. After 15 min mice were measured with a cooled back-thinned, charge-coupled device camera (ORCA II-ER-1394, Hamamatsu) equipped with an image intensifier as previously described (Saur et al., 2005; von Burstin et al., 2008). A bright field grey-scale image was taken to see positioning of mice. Afterwards several bioluminescence images with highest gain (900) and various exposure times (10-300 sec) were taken, displayed in pseudo colors and projected on the grey-scale image

using SimplePCI software (Hamamatsu). Signal intensity was measured over the region of interest using SimplePCI software.
If desired, anesthesia was antagonized by subcutaneous injection of AFN (750 µg/kg atipamezole, 500 µg/kg flumazenil, 1.2 mg/kg naloxone). Otherwise mice were sacrificed and analyzed as described in 3.2.3.

3.2.3 Tumor Mice Dissection and Isolation of Tumor Cell Lines

Mice were sacrificed by isoflurane inhalation (Abbott). After disinfection with 70% ethanol, dissection of the animal was carried out in as sterile conditions as possible. As desired size and weight of tumor, pancreas and other organs were determined and appropriate samples were taken. Samples for DNA isolation were stored at –20 °C or directly lysed using PCR lysis buffer. Tissue samples for luciferase assay and Western blot were snap frozen and stored at –80 °C. RNA samples were homogenized in RLT buffer containing β-mercaptoethanol (Qiagen), snap frozen and stored at –80 °C.
For tumor cell isolation samples were cut with into small pieces and incubated with medium containing 200 U/mL collagenase type II until completely digested (approx. 24 h). After removal of collagenase type II cells were cultured as described in 3.4.1. Cell lines were cryopreserved at passage three to four and cells were seeded for protein and DNA isolation and luciferase assay at passage five to seven.
After desired samples were taken, the rest of the organs were fixed in formalin for paraffin-histological analysis.

3.2.4 Orthotopic Transplantation of Tumor Cells

Tumor cells were diluted at 5000 cells/20 µL in serum free DMEM. Swiss nude mice (Charles River Laboratories, Sulzfeld, Germany) were anesthetized with MMF. After 15 min the abdominal skin was disinfected and a small cut was made in the skin and peritoneum. 20 µL of cell suspension were injected orthotopically into the pancreas using a microliter syringe with a 27-gauge needle (Hamilton Syringes). Ethilon 5-0 (Ethicon) was used to suture the peritoneum and the wound was sealed using wound clips. Anesthesia was antagonized by subcutaneous injection of AFN. Mice were analgenized with 1.5 µg/g Metacam (Boehringer Ingelheim) directly after the transplantation and every 24 h for 3 days.

3.2.5 Subcutaneous Transplantation of Tumor Cells

Tumor cells were diluted at 10,000 cells/20 µL, 50,000 cells/20 µL or 250,000 cells/20 µL in serum free DMEM. Swiss nude mice (Charles River) were anesthetized and antagonized as described in 3.2.4. Dorsal skin was disinfected and 20 µL of cell dilution series were injected subcutaneously in each side of the back. Within the 2 weeks after transplantation tumor size and luciferase activity were monitored *in vivo* by using a caliper and bioluminescence imaging as described in 3.2.2.

3.3. Histological Staining

3.3.1 Paraffin Sections

Tissue was fixed in Roti® Histofix for 24 h, dehydrated using ASP300 Tissue Processor (Leica) and embedded in paraffin. A series of 20 3-4 µm thick sections were cut for staining.

3.3.2 Haematoxylin and Eosin (HE) Staining of Tissue Sections

Roti® Histol (Carl Roth) was used for removal of wax from paraffin embedded tissue sections. Subsequently rehydration was obtained by the decreasing alcohol series. (2x 100%, 2x 98% and 2x 80% EtOH). Sections were then stained in haematoxylin for 5 sec, washed in tab water for 10 min and then stained in eosin for approx. 20 sec. Dehydration was achieved by an increasing alcohol series (2x 80%, 2x 96% and 2x 100% ethanol). After 2x 5 min in Roti® Histol (Carl Roth) slides were mounted in Pertex (Medite).

3.3.3 Immunohistochemistry

Tissue sections were dewaxed and rehydrated as described above. Microwave antigen retrieval using unmasking solution (Vector Labs) was performed for 9 min. After a cooling period of at least 15 min slides were washed in H_2O. To block endogenous peroxidase reactivity, slides were incubated in 3% H_2O_2 for 10 min. After washing (1x H_2O, 2x PBS) incubation with 5% serum in PBS for 1 h was done to block unspecific antibody binding. Primary antibody was diluted to desired concentration in PBS with 3% serum and incubated as stated in Table 3-4. In the

case of anti-firefly luciferase antibody Avidin/Biotin blocking kit (Vector Labs) was used according to manufacturer's protocol.

Primary Antibodies	Dilution	Blocking serum	Incubation
Anti- firefly luciferase (goat)	1:500	Rabbit serum plus Avidin	o/n at RT and afterwards o/n at 4 °C
Anti- BrdU (rat)	1:250	Goat serum	1 h at RT
Anti- PCNA (mouse)	1:250	Goat serum	1 h at RT
Anti- phospho- Akt Ser473 (rabbit)	1:50	Goat serum	1 h at RT

Table 3-4: Conditions for primary antibodies in IHC

Primary antibody was removed by washing with PBS. Biotinylated secondary antibody was diluted 1:200 and incubated for 1 h at RT. After washing, VECTASTAIN® Elite ABC solution (Vector Labs) was added and subsequently slides were incubated with 3,3'-diaminobenzidine tetrahydrochloride (DAB) (Vector Labs) until suitable brown staining developed. Slides were finally counterstained with haematoxylin and mounted as described in 3.3.2.
For correlation of Brdu positive cells to tumor volume the number of stained tumor cells were counted in 5 visual fields of 2-6 slides (magnification 100x).

3.3.4 Isolation of DNA from Paraffin Embedded Tissue

To verify recombination in pancreatic tissue, DNA was isolated from paraffin embedded tissue. Therefore, 2-3 10 µm thick sections were cut and rehydrated as described in 3.3.2. Pancreatic tissue was then scraped into a reaction tube with a pipette tip and incubated over night at 52 °C in paraffin lysis buffer. After phenol-chloroform-extraction and isopropanol precipitation, DNA pellet was resuspended in H_20 and 2 µL were used for genotyping PCR.

3.4. Cell Culture

3.4.1 Culture Conditions, Handling and Cryopreservation

Isolated tumor cells, HEK293 FT tva cells, MiaPaCa-CMV-fLuc cells and BxPC3-CMV-fLuc cells were cultured at 37 °C and 5% CO_2. DF-1 cells were cultured at 39 °C and 5% CO_2. All work was conducted in a laminar flow bench.

To subculture cells they were washed with sterile PBS, trypsinated 1-5 min at 37 °C and passaged into a new flask containing fresh medium. For cryopreservation cells were taken up in fresh medium after trypsination and centrifuged at 1200 rpm for 5 min. Supernatant was discarded, the pellet was resolved in ice-cold freezing medium and proceeded to –80 °C. After 24 h at –80 °C cells were moved to liquid nitrogen. In the case of ES cell cryopreservation a freezing container with isopropanol was used to obtain optimal freezing conditions.

3.4.2 Transduction of Cells via the RCAS-tva System

For stable expression of a desired gene in tumor cell lines the RCAS-tva system was used. As described in Fisher et al., 1999, DF-1 cells are transfected with a plasmid containing RCAS sequences and the gene of interest. Transfected cells produce virus carrying the gene of interest, which subsequently can infect DF-1 and all other tva-receptor positive cells. In non-avian, tva-receptor positive cells the gene of interest is expressed, but no infectious virus particles are build (Fisher et al., 1999).
In this case, DF-1 cells were transfected with SuperFect transfection reagent (Qiagen) according to manufacturer's protocol using 2.5 µg plasmid DNA (pRCAS-KrasER^{T2}-dsRed). Transfection and infection efficiency were checked by fluorescence microscopy using the reporter gene *dsRed*. When DF-1 cells produced high viral titers, supernatant was harvested, centrifuged at 3000 g for 10 min and filtered through 0.45 µm pores to avoid contamination with DF-1 cells. Viral supernatant was then added to growth medium of tva-receptor positive, isolated murine PDAC cells. Infection was repeated daily for one week. Transfected DF-1 cells and transduced tumor cells were cryopreserved.

3.4.3 Transfection of HEK293 FT tva Cells and Fluorescent Staining for Confocal Microscopy

HEK293 FT tva cells were seeded in 6-well plates and transfected with Lipofectamin2000 (Invitrogen) according to manufacturer's protocol. The plasmid used for transfection was pcDNA3.2-Kras-EGFP-ER^{T2}. 6 h after transfection either tamoxifen (1 µM) or ethanol were added to medium. Medium containing tamoxifen was renewed daily. 2 days after transfection, cells were transferred into 24-well plates, which contained collagen-coated coverslips. On the following day wells were

washed once with PBS and coverslips were fixed in fixative (3 parts fixative solution A and 1 part fixative solution B) for 10-15 min at RT. After washing, cells were permeabilized and blocked for 10 min at RT by incubation with PBS containing 3% BSA, 0.1% TritionX-100 and 1% saponin. TOPRO®-3 was diluted 1:3000 and added to cells for 1-4 h at RT in a dark, wet chamber. Cells were washed twice with PBS containing 3% BSA, 0.1% TritionX-100 and 1% saponin and once with PBS. After removal of PBS, one drop of Vectashield with DAPI was put on coverslips, they were transferred onto slides and sealed with nail polish. Confocal images were taken with Zeiss LSM 510 confocal microscope.

3.4.4 Correlation of Cell Number and Luciferase Signal

For determination of the correlation between cell number and luciferase signal $5x10^4$ $mPCNA^{fLuc}$ cells were seeded on 6-well plates for each cell counting and luciferase assay. Cells were harvested for luciferase assay and cell counting after 16 h, 24 h, 40 h, 48 h, 60 h and 72 h after seeding. $mPCNA^{fLuc}$ cells were counted in a hemocytometer (Neubauer improved, LO-Laboroptik). Luciferase assay was peformed as described in 3.6.5.
Experiments were done in triplicates in three independent experiments.

3.5. Molecular Techniques

3.5.1 Cloning of Plasmids

Kras was amplified from pRCAS-Kras plasmid with primer set Kras_KpnI_AatII_for and Kras_ohne Stop_XhoI_rev by PCR. The ER^{T2} sequence was amplified from pBC-ER^{T2} with primer set ER-T2_XhoI_for and ER-T2_NdeI_SalI_rev. Enhanced green fluorescent protein (EGFP) was amplified from pEGFP-fLuc (Clontech; modified in our lab) with primer set EGFP_Xho_Linker_for and EGFP_Xho_ rev. In all three amplifications appropriate restriction sites and, in the case of ER^{T2} and EGFP amplification, a linker sequence were introduced. PCR products were subcloned into pCR®- Blunt II TOPO® using Zero Blunt® TOPO® PCR cloning kit (Invitrogen).
$KrasER^{T2}$ fusion protein was generated by subcloning both Kras and ER^{T2} from pCR®- Blunt II TOPO® vectors into pBC-SK+ (Stratagene). pBC-$KrasER^{T2}$ was then

used as a starting point for cloning of targeting construct as described in 3.5.1.1, of RCAS vector as described in 3.5.1.2 and pcDNA3.2-Kras-EGFP-ER^{T2} as described in 3.5.1.3.

3.5.1.1 Cloning of Targeting Construct

KrasER^{T2} fusion protein was excised from pBC-KrasER^{T2} and subcloned into pENTR-LSL, resulting in pENTR-LSL-KrasER^{T2}. The LSL-KRasER^{T2} sequence was transferred into the Rosa26 targeting vector via clonase reaction with aqt-RosaRFA targeting vector using Gateway® LR Clonase™ enzyme mix (Invitrogen).

3.5.1.2 Cloning of pRCAS-KrasER^{T2}

KrasER^{T2} fusion protein was excised from pBC-KrasER^{T2} and cloned into pENTRdsRed. Clonase reaction was performed with pRCAS vector resulting in pRCASdsRed-KrasER^{T2}.

3.5.1.3 Cloning of pcDNA3.2-Kras-EGFP-ER^{T2}

KrasER^{T2} fusion protein was excised from pBC-KrasER^{T2} and subcloned into pENTR-LSL. The transcriptional stop element was removed using Cre recombinase (Novagen). Via clonase reaction KrasER^{T2} was transferred into pcDNA3.2. From the resulting construct KrasER^{T2} and flanking sequences were excised and subcloned into pBluescript. After in frame insertion of EGFP into KrasER^{T2}, the triple fusion protein was cloned back into pcDNA3.2 resulting in pcDNA3.2-Kras-EGFP-ER^{T2}.

3.5.2 Transformation of Competent Bacteria and Isolation of Plasmid DNA

Transformation of competent bacteria was achieved using KCM method. Clonase reaction or 200-500 ng of plasmid DNA were diluted in 100 µL 1x KCM buffer and mixed with 100 µL of either One Shot® TOP10 or One Shot® Stbl3™ chemically competent cells (Invitrogen). Reactions were kept at 4 °C for 20 min and at RT for 10 min. Afterwards, 1 mL of S.O.C medium (Invitrogen) was added and bacteria were incubated on a horizontal shaker at 25 °C or 37 °C for 1 or 2 h depending on optimal growth temperature of bacteria. Transformed cells were then streaked onto agar plates containing the appropriate antibiotic for selection and incubated over night at 25° or 37 °C.

Before amplification of plasmids, verification of correct insert and orientation was performed with screening PCR (see 3.5.3.1). Of positive clones verified by PCR, a colony from backup plate (see 3.5.3.1) was used to inoculate selective growth medium which then was incubated over night at 25 °C or 37 °C with agitation. Glycerol stocks were prepared by mixing equal volumes of glycerol stock solution and freshly grown bacteria (storage –80 °C). Depending on the amount of plasmid DNA needed, Qiagen Plasmid Mini or Midi kits were used according to manufacturer's protocol. For isolation of targeting construct DNA Endofree Plasmid Maxi kit (Qiagen) was used. Verification of correctness of the plasmid was done by digestion with restriction endonucleases followed by agarose gel electrophoresis.

3.5.3 PCR

3.5.3.1 Screening PCR

Screening PCR was used to minimize effort on plasmid preparation by excluding false positive clones. Colonies were picked from agar plates, streaked into a PCR tube and onto a fresh selective agar plate (backup plate). Bacteria were heat denatured at 95 °C in 50-60 µL H_2O for 5 min. Specific primers were used to check correct insert and orientation in the plasmid.

3.5.3.2 Genotyping

Genotyping of mice was done by genomic tail PCR. Therefore, a 2-3 mm piece of mouse tail was lysed in PCR lysis buffer at 55 °C for 1.5 h. Inactivation of proteinase K was performed at 95 °C for 20 min. Samples were vortexed 20 sec and centrifuged at 14,000 rpm and 4 °C for 10 min. Supernatant was used for PCR reactions. For PCR conditions see Table 3-5. Amplification was done with 40 cycles.

Primer sets for PCR were designed to specifically amplify fragments of different sizes in the case of WT or mutated allele. Genotyping PCRs were also used to check recombination of the transcriptional stop element in DNA samples isolated from tissue or cell lines. Primer sets may vary from genomic tail PCR. For details see Table 2-1.

PCR products were loaded onto a 1.5% agarose gel to determine genotypes.

Type of PCR	Denaturation	Annealing	Extension	Band size (bp)
$Kras^{G12D}$	95 °C 45 sec	55 °C 1 min	72 °C 1 min 30 sec	170 (mut w/ stop) 270 (WT) 300 (mut w/o stop)
$KrasER^{T2}$	95 °C 45 sec	60 °C 1 min	72 °C 1 min 30 sec	900 (mut w/ stop) 1100 (mut w/o stop)
$Ptf1a^{Cre/+}$	95 °C 45 sec	60 °C 1 min	72 °C 1 min 30 sec	400 (mut) 600 (WT)
$Trp53^{R172H}$	95 °C 45 sec	60 °C 1 min	72 °C 1 min 30 sec	270 (mut) 570 (WT)
$PCNA^{fLuc/+}$	95 °C 45 sec	60 °C 1 min	72 °C 1 min 30 sec	490 (mut) 780 (WT)
$PCNA^{fLuc/+}$ Stop	95 °C 45 sec	64 °C 1 min	72 °C 1 min 30 sec	330 bp (w/ stop)
Pdx1-Cre	95 °C 45 sec	58 °C 45 sec	72 °C 1 min	800 bp (Pdx1 Cre) 290 bp (Gabra Cre)
Rosa26 Locus	95 °C 45 sec	62 °C 1 min	72 °C 1 min 30 sec	310 bp (tva) 430 bp ($KrasER^{T2}$) 600 bp (WT)

Table 3-5: PCR conditions for genotyping. mut=mutated, WT=wild type; w/ stop=with transcriptional stop element; w/o stop= without transcriptional stop element after recombination

3.5.4 RNA Isolation, Reverse Transcription and Quantitative Real-Time PCR

For expression analysis from *Rosa26* locus and *Kras* locus in murine pancreatic tumor cells, RNA was isolated from murine pancreatic cancer cell lines isolated in our lab. For RNA isolation cells were grown to 70-80% confluency, washed with PBS, lysed with RLT buffer (Qiagen) containing β-mercaptoethanol and scraped into a BioPur® safelock reaction tube (Eppendorf). Samples were stored at –80 °C until further analysis. For expression analysis of *$KrasER^{T2}$* and *Kras* in mice, RNA was isolated from murine tissue as described in 3.2.3.

RNA from samples in RLT buffer was isolated using RNeasy kit (Qiagen) and treated with DNAse I according to manufacturer's protocol. 5 µg RNA were reverse transcribed using random hexamer primers, TaqMan Reverse Transcription Reagents (Applied Biosystems) and SuperScript II reverse transcriptase according to manufacturer's protocol (Invitrogen). cDNA was stored at –20 °C until further use.

Real-time PCR primers were designed using Primer Express software (Applied Biosystems) according to the manufacturer's guidelines. Real-time PCR was

performed in triplicates with SYBR® Green PCR Master Mix and 300 nM each primer using StepOnePlus™ real-time PCR system and software (Applied Biosystems).
All samples were normalized to cyclophilin as housekeeping gene. PCR conditions can be seen in Table 3-6. Primer sequences are listed in Table 2-1. Analysis was performed in triplicates in three independent experiments.
For quantification standard curves were employed as stated in Table 3-7.

Temperature	Time	Number of cycles
50 °C	2 min	1
95 °C	10 min	1
95 °C	15 sec	40
60 °C	1 min	

Table 3-6: Conditions for quantitative real-time PCR

Gene	Copies of gene					
Cyclophillin	$5x10^6$	$7,5\ x10^5$	$1,5\ x10^5$	$3\ x10^4$	$6\ x10^3$	
Kras	$1\ x10^6$	$2\ x10^5$	$4\ x10^4$	$8\ x10^3$	$1.6\ x10^3$	$3.2\ x10^2$
$KrasER^{T2}$	$1\ x10^5$	$2\ x10^4$	$4\ x10^3$	$8\ x10^2$	$1.6\ x10^2$	
Rosa	$1\ x10^6$	$2\ x10^5$	$4\ x10^4$	$8\ x10^3$	$1.6\ x10^3$	$3.2\ x10^2$

Table 3-7: Standard curves employed for quantitative real-time PCR

3.6. Protein Isolation and Detection

3.6.1 Protein Isolation from Tumor Cells and Tissue Samples

To obtain whole cell lysates, cells were grown to 80% confluency, washed twice with ice-cold PBS and lysed in IP-buffer. Lysates were stored at –80 °C for at least 1 h.
Protein samples from murine tissue were thawed on ice, IP-buffer was added and samples were homogenized with Silent Crusher M with tool 6F (Heidolph). Snap frozen samples were then stored at –80 °C until further analysis.
Both cell and tissue samples were centrifuged at 13,000 rpm and 4 °C for 30 min prior further use. Protein content was determined by Bradford assay (BioRad).

3.6.2 Nuclear and Cytosolic Extracts

To analyze shuttling of the KrasER^{T2} fusion protein, nuclear and cellular extracts were generated. Cells were incubated with 100 nM 4-hydroxytamoxifen (4-OHT) or ethanol at the same dilution for 5 days and medium was renewed every second day. Cells were washed with ice-cold PBS twice, scraped into tubes and centrifuged at 1100 rpm for 5 min. All centrifugation steps were performed at 4 °C. Pellet was washed with PBS, centrifuged at 1600 rpm for 2 min and resuspended with nuclear extracts buffer A containing 1% protease and phosphatase inhibitors. To allow cell swelling, samples were incubated on ice for 15 min and afterwards mechanically disrupted using a 27-gauge needle. After centrifugation at 6800 rpm for 2 min supernatant containing the cytosolic fraction was collected and kept on ice until further processed. The pellet containing nuclei and cell membrane was washed six times with nuclear extracts buffer A. To obtain nuclear proteins, the samples containing the nuclei and membrane faction were incubated at 4 °C with strong agitation in nuclear extracts buffer C containing 1% protease and phosphatase inhibitors for 30-60 min. Subsequently, cytosolic fraction and nuclear fraction were centrifuged at 13,000 rpm for 30 min to remove cell debris. Protein content was determined by Bradford assay (BioRad).

3.6.3 Western Blot

Western blot was performed employing standard denaturating SDS polyacrylamide gel electrophoresis (SDS-Page) (Burnette, 1981). 50-200 µg of protein were boiled in 1x protein loading buffer and loaded onto 10% or 12.5% acrylamide gels. After separation according to their molecular weight, proteins were immobilized on Immobilon transfer membrane (Millipore). Wet blot was performed either for 3 h at 100 V or over night at 30 V.

To block unspecific antibody binding, membrane was incubated for 1 h at RT in a 1:1 dilution of Odyssey® Blocking Reagent (LI-COR) and PBS. Subsequently, the membrane was incubated with primary antibody for 2-3 h at RT or over night at 4 °C. After washing, secondary antibody (1:2000) was added for 2 h at RT in the dark before detection was performed in Odyssey® infrared imaging system (LI-COR).

Primary Antibody	Dilution	Secondary Antibody
Anti-β-Actin	1:2000	Anti-mouse
Anti-Akt	1:1000	Anti-rabbit
Anti-Oct1	1:200	Anti-rabbit
Anti-pan Ras clone 10	1:5000	Anti-mouse
Anti-phospho-Akt Ser473	1:1000	Anti-rabbit
Anti-phospho-Akt Thr308	1:1000	Anti-rabbit

Table 3-8: Antibody dilutions for Western blotting

3.6.4 Ras Activation Assay

Ras activation assay was adapted from Millipore Ras activation kit protocol (Millipore) and from a protocol by S. Taylor (Stephen J. Taylor, 2001). All steps were performed very quickly and samples were kept on ice all the time. For Ras activation assay cells were incubated with 4-OHT (500 nM) or EtOH for 5 days.

Cells were harvested or tissue was homogenized in Mg^{2+} lysis buffer containing 1% phosphatase and protease inhibitors. For the assay 1 mg protein lysate was used and diluted in a total volume of 500 µL Mg^{2+} lysis buffer. For positive and negative control 1 mg protein was diluted in 500 µL Mg^{2+} lysis buffer plus 10 µL 0.5 M EDTA. For positive control 1x GTPγS and for negative control 1x GDP was added and incubated with agitation at 30 °C for 30 min. To stop control reactions 1 M $MgCl_2$ was added.

Raf-RBD agarose beads were added to each sample, positive and negative control and incubated with agitation at 4 °C for 1 h. Beads were then collected by centrifugation at 13,000 rpm for 10 sec at 4 °C, pellet was washed and protein was released from agarose beads by boiling in 2x protein loading dye. Samples were then loaded onto a 12% acrylamide gel and detected as described in 3.6.3.

3.6.5 Luciferase Assay

For determination of luciferase activity in murine samples or cell culture the luciferase assay system (Promega) was used. Murine samples were collected as described in 3.2.3, thawed on ice and homogenized in cell culture lysis buffer (CCLR) with Silent Crusher M with tool 6F (Heidolph). Cells were grown according to experiment, washed twice with PBS, lysed in passive lysis buffer (PLB) for 10 min at room

temperature with agitation and scraped into tubes. Both murine and cell samples were centrifuged for 15 min at 13,000 rpm and 4 °C to remove cell debris. Luciferase activity was measured in the luminometer by adding 50 µL of sample to 50 µL of luciferase assay reagent. Protein content was determined by Bradford assay (BioRad).

3.7. Development of a Screening Platform

To generate a screening platform, mPCNA^{fLuc} cells (1x10^4 cells/well) were seeded on 96-well plates and incubated with various inhibitors (see Table 3-9). Luciferase activity and cell viability (MTT assay) were determined after defined incubation periods. To correlate luciferase activity to cell number, mPCNA^{fLuc} cells were counted in a hemocytometer (Neubauer improved, LO-Laboroptik).

Inhibitor	Concentration range			Mode of action
API-2	5 µM	20 µM	40 µM	Inhibition of Akt1/2/3 phosphorylation targeting an Akt effector molecule other than PI3-kinase or Pdk-1
Bx-912	1 µM	5 µM	10 µM	Pdk-1 inhibitor
Erlotinib	9 µM	18 µM	36 µM	Tyrosine-kinase inhibitor (EGF receptor)
H-1152	0.1 µM	1 µM	10 µM	Rock inhibitor
LY294002	5 µM	10 µM	20 µM	PI3-kinase inhibitor
NVP-BEZ235	5 nM	10 nM	50 nM	Dual mTOR and PI3-kinase inhibitor
PI-103	2.5 µM	-	-	PI3-kinaseα inhibitor 1
Roscovitine	5 µM	25 µM	100 µM	Cdk inhibitor
Sunitinib	25 µM	-	-	Receptor-tyrosine kinase inhibitor

Table 3-9: Inhibitors used for the development of a screening platform

3.7.1 MTT- Assay

MTT assay is a colorimetric assay in which MTT (3-(4,5-Dimethylthiazol-2-yl)-2,5-diphenyltetrazolium bromide) is reduced to a purple formazan by mitochondrial reductase. It can be used to determine cell viability (Mosmann, 1983).

In each well 10 µL MTT reagent (5 mg/mL MTT in PBS) per 100 µL media were added after desired incubation time with inhibitor and plates were incubated at 37 °C

for 4 h. Subsequently, media was carefully removed, cells were lysed in 200 µL DMSO:EtOH (1:1), incubated at RT with agitation for 10 min and OD600 was determined.
Experiments were done in triplicates in three independent experiments.

3.7.2 High-Throughput Luciferase Measurement

Luciferase assay was mainly performed as described in 3.6.5. For high-throughput experiments, medium was aspirated from 96-well plate after desired incubation time with inhibitor, cells were washed twice with PBS and lysed in 20 µL PLB. After 10 min incubation at room temperature with agitation 96-well plate was measured in FLUOstar with injection of 50 µL luciferase assay reagent into each well.
Experiments were done in triplicates in three independent experiments.

3.8. Statistical Analysis

Graphical depiction, data correlation and statistical analysis were done with GraphPad Prism5 software (La Jolla, USA). Data are presented in arithmetic mean +/- standard error of the mean, if not stated otherwise.
Survival curves were done by Kaplan-Meier survival analysis. To analyze statistical significance of different groups t-test or log rank test were used.
To analyze correlation between data sets Pearson's nonparametric correlation was applied. As significance levels error probability p was employed ($p<0.05$ (*), $p<0.005$ (**), $p<0.001$ (***)).

4 Results

4.1. Generation of the *LSL-Rosa26^{KE}* Mouse Model

To characterize aspects of pancreatic tumor development which cannot be analyzed with existing mouse models, e.g. the inactivation of oncogenic Kras after onset of PanIN or invasive cancer development, the *LSL-Rosa26^{KE}* mouse strain was generated. Herein, the system established by Feil et al. was adopted (Feil et al., 1996). The coding sequence of the murine *V-Ki-Ras2* gene (*Kras*) with the activating G12D point mutation was fused to the triple mutated *LBD* of the human estrogen receptor (ER^{T2}). The resulting sequence for the fusion protein, *KrasER^{T2}*, was knocked into the first intron of the murine *Rosa26* locus by homologous recombination. This locus is ubiquitously expressed, but does not exhibit any known function. Homo- or heterozygous deletion of this locus does not show any apparent phenotype in mice (Zambrowicz et al., 1997). To obtain tissue-specific expression, the fusion protein is silenced by a transcriptional stop element which is flanked by *loxP* sites (Seidler et al., 2008). Upon Cre recombination the KrasER^{T2} fusion protein is expressed.

In vitro experiments were performed to analyze expression levels of the targeted locus and functionality of the KrasER^{T2} fusion protein.

4.1.1 Expression Analysis of *Rosa26* Locus and *Kras* Locus

Expression of genes from different loci may result in differences in the gene expression level. To assure that *KrasER^{T2}* under control of the murine *Rosa26* promoter can be transcribed at a level comparable to endogenous *Kras*, quantitative real-time PCR was performed to acquire information about transcriptional levels of relevant loci.

Ptf1a$^{Cre/+}$;LSL-Kras$^{G12D/+}$ mice express *Kras* from one allele of the *Kras* locus which induces PDAC development (Hingorani et al., 2003). Ten different cell lines isolated from PDACs of *Ptf1a$^{Cre/+}$;LSL-Kras$^{G12D/+}$* mice were tested for mRNA level of *Rosa26* gene product from *Rosa26* locus and of *Kras* from *Kras* locus. Relative amounts of the transcripts were calculated using standard curves of defined copy numbers and normalized to the housekeeping gene *Cyclophilin* in the same RNA preparation. As

depicted in Figure 4-1 *Rosa* and *Kras* are equally expressed or expression is slightly higher from *Rosa26* locus, respectively. This leads to the assumption that *KrasER*^{T2} can be transcribed in equal amounts from one allele of the murine *Rosa26* locus compared to *Kras*^{G12D} transcribed from one allele of the endogenous *Kras* locus.

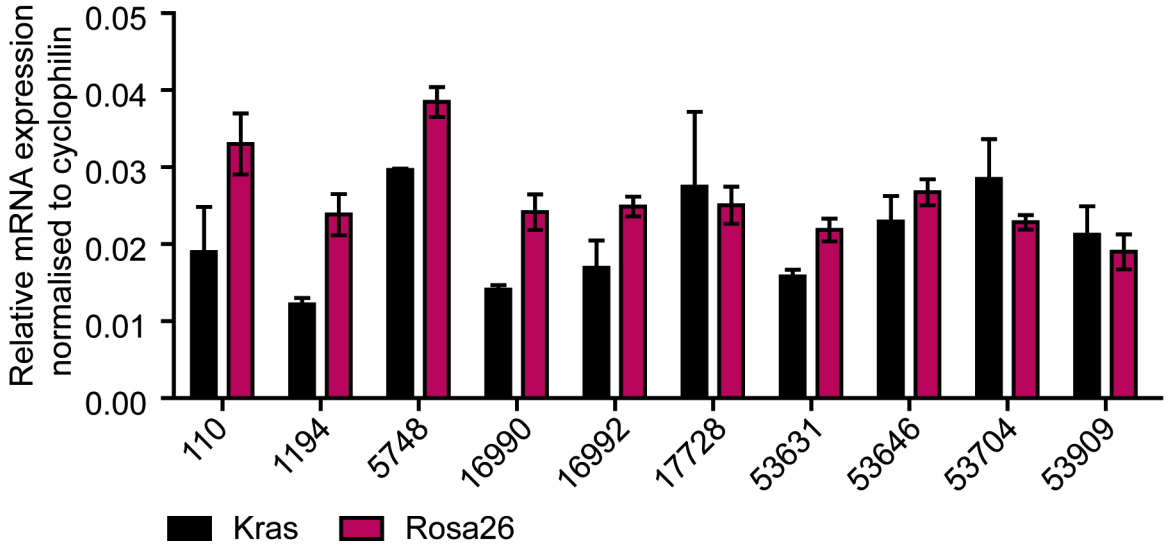

Figure 4-1: Relative mRNA expression of *Kras* and *Rosa26*: Murine PDAC cell lines were analyzed for their *Rosa26* and *Kras* expression level. Relative amounts of *Rosa26* and *Kras* transcripts were calculated using standard curves. Values were normalized to ubiquitously expressed *Cyclophillin* as housekeeping gene in the same RNA preparation.

4.1.2 *In Vitro Analysis* of the KrasER^{T2} Fusion Protein

The KrasER^{T2} fusion protein is composed of Kras^{G12D} and of the tamoxifen inducible modified ligand binding domain of the estrogen receptor, ER^{T2}. In the absence of ligand, in this case tamoxifen or 4-hydroxytamoxifen (4-OHT), the fusion protein is bound to heat shock protein 90 (Hsp90). Thus, translocation into the nucleus is disabled. Upon addition of tamoxifen or 4-OHT, Hsp90 is released and the fusion protein translocates into the nucleus (Danielian et al., 1998). Due to Kras being active in its membrane-bound state in the cytosol (Barbacid, 1987, Bar-Sagi, 2001), shuttling of KrasER^{T2} into the nucleus is supposed to lead to inactivation of Kras activity. Thus, the ability of KrasER^{T2} being shuttled is crucial for the new model, since then inactivation of Kras^{G12D} is possible.

HEK293 FT tva cells were transiently transfected with the coding sequence for triple fusion protein Kras-EGFP-ER^{T2} and tamoxifen or ethanol were added to growth medium. As seen in confocal microscopy, the triple fusion protein, indicated by green color of EGFP, colocalizes with the blue DAPI staining of the nucleus when cells are

treated with tamoxifen. In contrast, EGFP remains in the cytosol in ethanol controls Figure 4-2A). Worth mentioning is that in the confocal images the KrasER^{T2} fusion protein does not localize to the cell membrane as Kras localization would be expected from published data (Eisenberg et al., 2008).

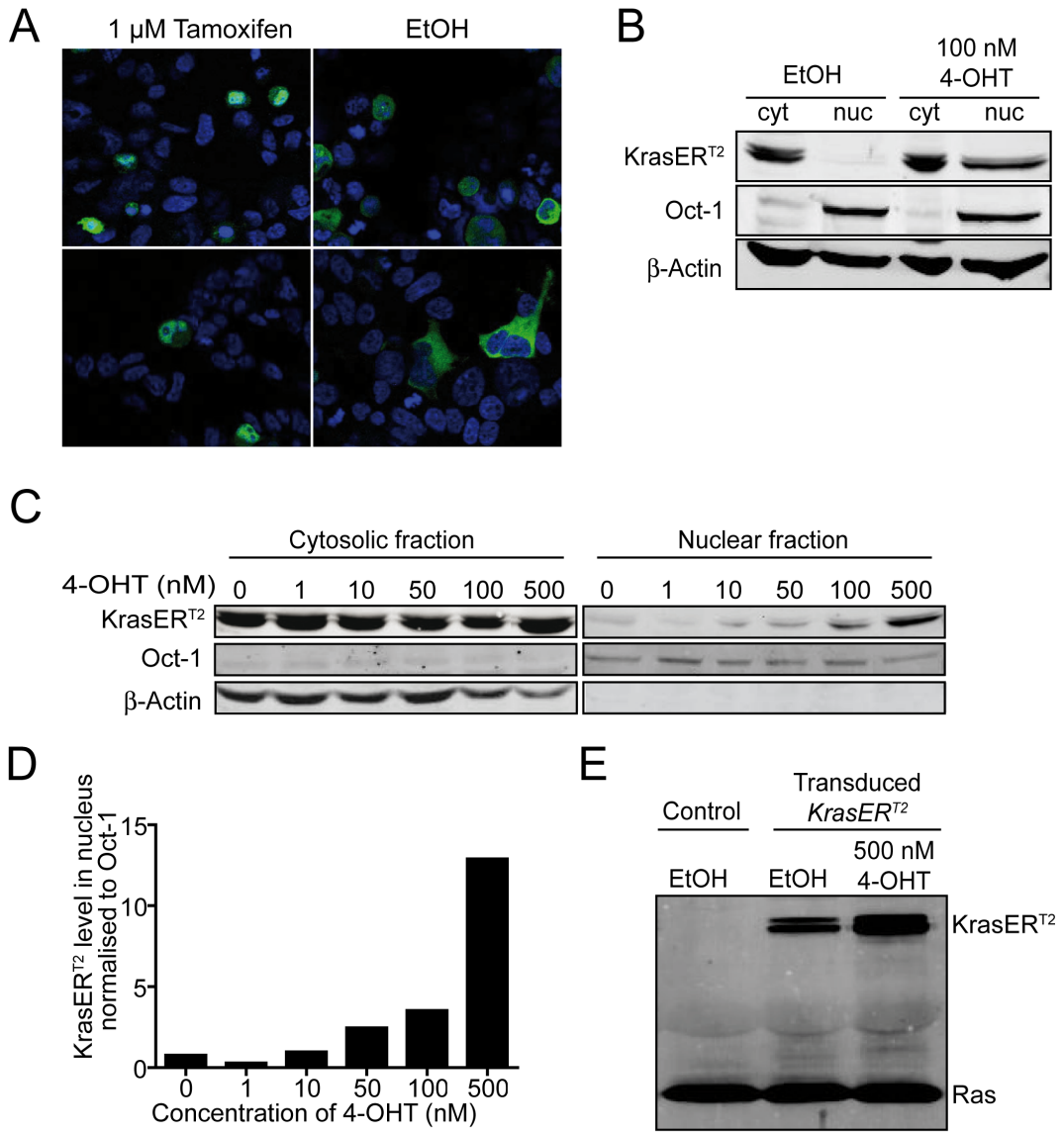

Figure 4-2: *KrasER^{T2}* is expressed *in vitro* and can be shuttled via 4-OHT treatment: A) Confocal microscopic images of HEK293 FT tva cells which were transiently transfected with Kras-EGFP-ER^{T2} triple fusion protein: When treated with 1 µM tamoxifen, Kras-EGFP-ER^{T2} can be localized in the nucleus by EGFP and DAPI colocalization. B) Western blots of cytosolic (cyt) and nuclear (nuc) fractions of murine PDAC cells stably transduced with KrasER^{T2} via the RCAS system: When treated with 100 nM 4-OHT, shuttling of the KrasER^{T2} fusion protein into the nucleus is observed. C and D) Level of KrasER^{T2} in the nucleus can be increased in a dose-dependent manner as seen after quantification of KrasER^{T2} in the nuclear fraction (normalized to Oct-1 level) (D). E) Using Raf-RBD agarose beads, activated Ras protein and, after transduction with KrasER^{T2}, activated KrasER^{T2} was pulled down in murine PDAC cells (*Ptf1a$^{Cre/+}$;LSL-Kras$^{G12D/+}$;LSL-p53$^{R172H/R172H}$;LSL-R26$^{tva-lacZ}$*). Upon 4-OHT treatment (500 nM), the level of activated KrasER^{T2} is elevated compared to ethanol treated cells. The original, not transduced cell line was used as control.

Shuttling can also be seen on protein level. Murine PDAC cells were transduced with the KrasER^{T2} fusion protein via the RCAS-tva system (Fisher et al., 1999). After five days of 4-OHT treatment, nuclear and cytosolic fractions of cells were generated and Western blot with anti-Ras antibody and specific nuclear (Oct-1) and cytosolic (β-Actin) antibodies was performed. As seen in Figure 4-2B, KrasER^{T2} fusion protein was detectable in the nuclear fraction after 4-OHT treatment, but not in ethanol controls. Probably due to high overexpression of KrasER^{T2} in these cells, KrasER^{T2} cannot completely be shuttled into the nucleus, but remains in the cytoplasma despite 4-OHT treatment. As seen in Figure 4-2C and D, shuttling occured in a dose-dependent manner as KrasER^{T2} level in the nucleus increases with higher 4-OHT concentrations. In contrast, no decrease, but rather an increase, of KrasER^{T2} protein expression was observed in the cytosolic fraction, indicating a stabilization of the fusion protein by 4-OHT treatment.

To prove activity of the fusion protein, a Ras activation assay was performed. Herein, one can take advantage of Ras' specificity to interact with the Ras binding domain (RBD) of its cellular down-stream target Raf-1 kinase. Using a fusion protein of Raf-RBD and glutathione S-transferase which is immobilized on agarose beads, active Ras can be affinity precipitated and detected by Western blotting with Ras antibody (Taylor et al., 2001). Ras activation assay was performed with a murine PDAC cell line (*Ptf1a*$^{Cre/+}$*;LSL-Kras*$^{G12D/+}$*;LSL-p53*$^{R172H/R172H}$*;LSL-R26*$^{tva\text{-}lacZ}$) which has been transduced with KrasER^{T2} via the RCAS-tva system. By 4-OHT treatment of KrasER^{T2}-transduced cells, an increase of activated KrasER^{T2} can be detected compared to control treated cells (EtOH) (Figure 4-2E).

In summary, these experiments show that 4-OHT treatment activates and stabilizes the KrasER^{T2} fusion protein rather than the proposed inactivation by nuclear shuttling.

4.1.3 Generation of the *LSL-Rosa26*^{KE} Knock-In Mouse Model

The KrasER^{T2} fusion protein with a 5' floxed transcriptional stop element was introduced into the murine *Rosa26* locus by homologous recombination (see schematic representation of targeting in Figure 4-3A).

After verification of correctness of targeting construct, it was introduced into murine W4/129S6 embryonic stem cells by electroporation. Subsequently, cells were grown

in selective medium, single clones were picked and tested for correct knock-in via screening PCR and Southern blots. Out of 83 picked clones, two were positive in PCR screening and Southern blot analysis. Figure 4-3 displays Southern blots of positive clones with the appropriate 4.2 kb fragment (lines 1 and 3 in Figure 4-3B). The presence of the Rosa26 WT allele which was not clearly visible in Southern blot analysis (11.5 kb fragment) was verified by PCR (Figure 4-3 and data not shown). Positive clones were tested for mycoplasma contamination before they were sent to PolyGene AG, Switzerland, for blastocyst injection and generation of chimeras.

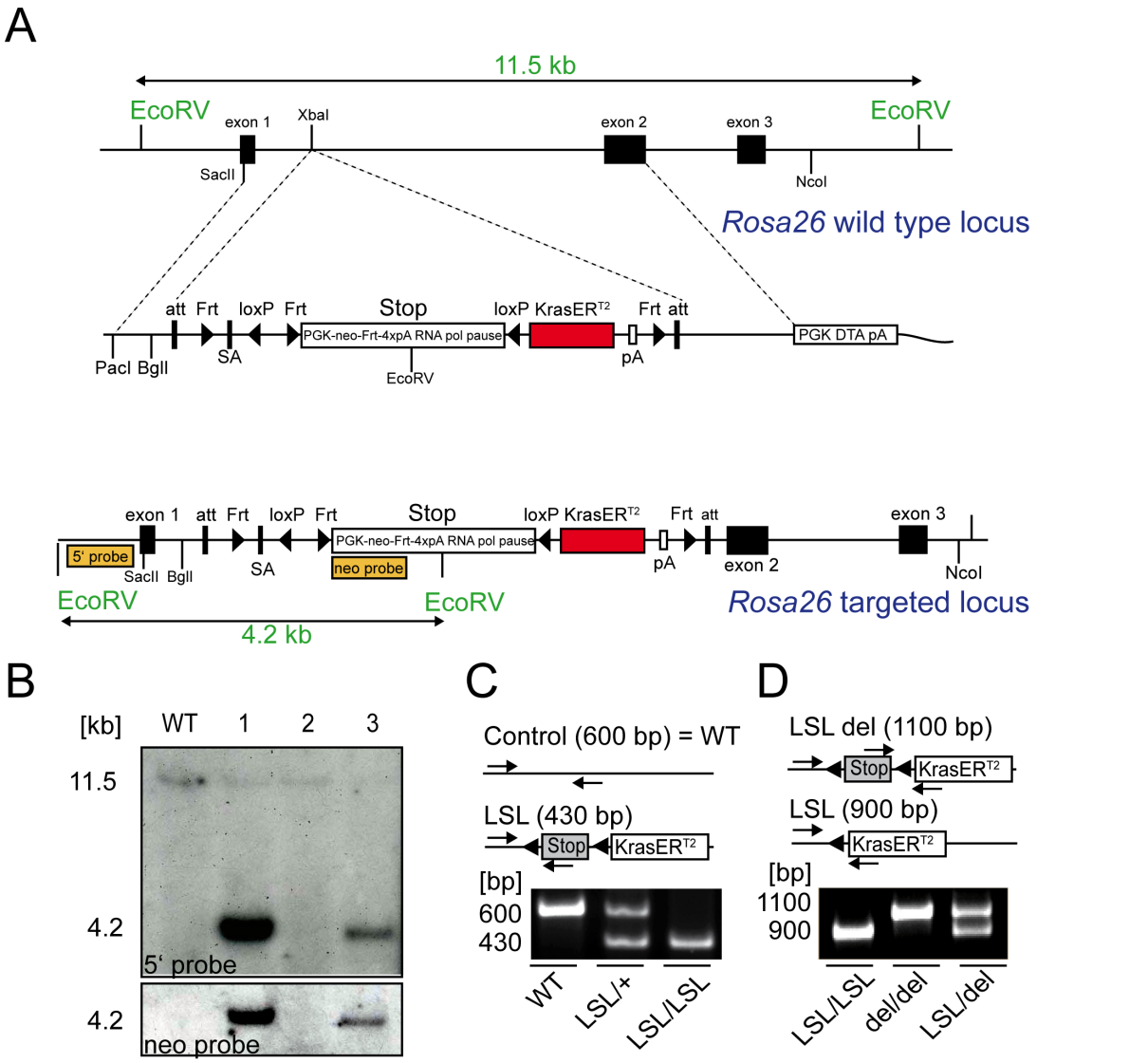

Figure 4-3: Targeting *KrasER^{T2}* to the murine *Rosa26* locus: A) Schematic representation of targeting *LSL-KrasER^{T2}* to the murine *Rosa26* (*R26*) locus. B) Southern blot and C) PCR analysis showed successful targeting. In Southern blot the 11.5 kb fragment represents WT allele and the 4.2 kb fragment represents targeted allele. D) Presence of *LSL* was confirmed by PCR.

4.1.4 *In Vivo* Characterization of the *LSL-Rosa26^{KE}* Mouse Model

Genotyping of the new mouse strain *LSL-Rosa26^{KE}* was carried out as described in 3.5.3.2. The WT allele resulted in a PCR product of 600 bp, heterozygous *LSL-Rosa26$^{KE/+}$* mice displayed two bands at 600 bp and 430 bp. A 430 bp PCR product was found for homozygous *LSL-Rosa26$^{KE/KE}$* mice (Figure 4-3C). The integrity of the transcriptional stop element in genomic tail DNA was confirmed by PCR resulting in a PCR product of 900 bp whereas a band at 1100 bp could be observed after Cre mediated recombination (Figure 4-3D). PCR, as depicted in Figure 4-3D, was used to confirm recombination in murine pancreas samples.

To verify expression of *KrasER^{T2}*, quantitative real-time PCR was performed on pancreatic tissue. *KrasER^{T2}* was expressed in a gene-dose-dependent manner in *Ptf1a$^{Cre/+}$;LSL-Rosa26^{KE}* mice whereas no expression was seen in *Ptf1a$^{Cre/+}$;LSL-Kras$^{G12D/+}$* mice (Figure 4-4A).

The activation of the KrasER^{T2} fusion protein *in vivo* was analyzed by Ras activation assay. Endogenous Ras could be detected in pancreatic samples of 6 weeks old *Ptf1a$^{Cre/+}$;LSL-Rosa26$^{KE/+}$* and *Ptf1a$^{Cre/+}$;LSL-Kras$^{G12D/+}$* mice as well as in an isolated PDAC cell line (*Ptf1a$^{Cre/+}$;LSL-Kras$^{G12D/+}$;LSL-p53$^{R172H/R172H}$;LSL-R26$^{tva\text{-}lacZ}$*). In contrast, KrasER^{T2} fusion protein was solely pulled down in *Ptf1a$^{Cre/+}$;LSL-Rosa26$^{KE/+}$* mice. Treatment of *Ptf1a$^{Cre/+}$;LSL-Rosa26$^{KE/+}$* mice with tamoxifen lead to an increase of activated KrasER^{T2} similar to the effects observed *in vitro* (Figure 4-4B).

Western blot analysis of proteins isolated from murine pancreata demonstrated that KrasER^{T2} can be detected in *Ptf1a$^{Cre/+}$;LSL-Rosa26$^{KE/+}$*, but not in *LSL-Rosa26$^{KE/+}$* mice. Again, a stronger band of KrasER^{T2} was observed after treatment with tamoxifen (Figure 4-4C). Thus, Western blot analysis argues for a stabilization of KrasER^{T2} *in vivo* which is in concordance with published data reporting stabilization of fusion proteins containing the LBD of hormon receptors upon tamoxifen treatment *in vitro* (Samuels et al., 1993; Greulich and Erikson, 1998; De Vita et al., 2005).

One cell line isolated from a *Ptf1a$^{Cre/+}$;LSL-Rosa26$^{KE/+}$;LSL-Kras$^{G12D/+}$* mouse (B567PPT) showed strong expression of KrasER^{T2} (left lane in Figure 4-4C). After treatment with 100 nM 4-OHT, a small amount of KrasER^{T2} was detected in the nuclear fraction (Figure 4-4D).

In summary, *in vivo* data, as observed in *in vitro* experiments, show a stabilization of the KrasER^{T2} fusion protein and an elevation of Kras activity by tamoxifen treatment rather than complete translocation, and thus inactivation, of the fusion protein.

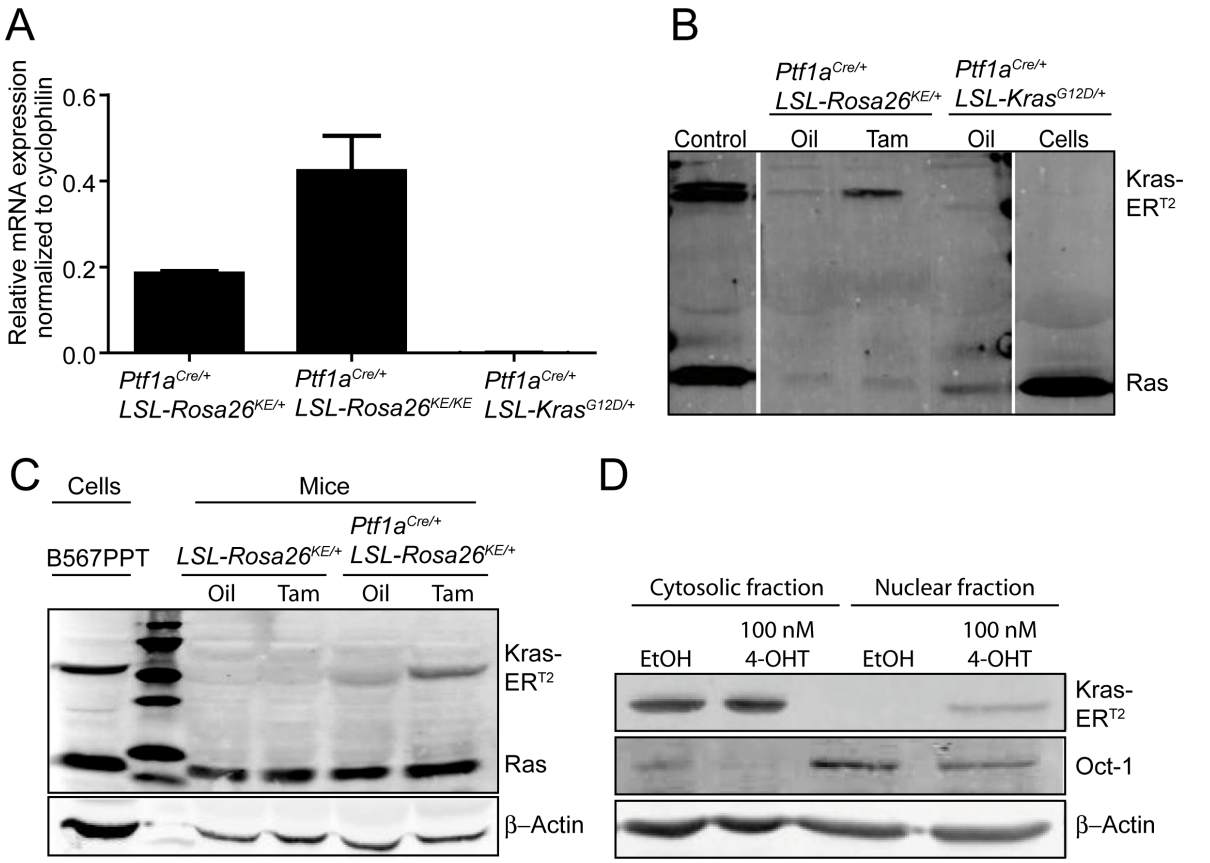

Figure 4-4: *KrasER^{T2}* is expressed and activated *in vivo*: A) *KrasER^{T2}* was expressed in a gene-dose-dependent manner in pancreatic tissue of 6 weeks old *Ptf1a$^{Cre/+}$;LSL-Rosa26^{KE}* mice, but not of *Ptf1a$^{Cre/+}$;LSL-Kras$^{G12D/+}$* mice. B) Activated Ras protein was pulled down using Raf-RBD agarose beads in pancreatic tissue of 6 weeks old *Ptf-1a$^{Cre/+}$;LSL-Rosa26$^{KE/+}$* mice, but not of *Ptf1a$^{Cre/+}$, LSL-Kras$^{G12D/+}$* mice or isolated cells. Activated KrasER^{T2} was increased upon tamoxifen treatment (4 mg/day for 3 subsequent days). As positive control, isolated PDAC cell lines from *Ptf1a$^{Cre/+}$;LSL-Kras$^{G12D/+}$* mice were transduced with KrasER^{T2} (left lane). C) KrasER^{T2} fusion protein was detected in pancreatic tissue of *Ptf1a$^{Cre/+}$;LSL-Rosa26$^{KE/+}$* mice, but not of *LSL-Rosa26$^{KE/+}$* mice via Western blot. Treatment with 4 mg tamoxifen per day for 3 days lead to an increase of KrasER^{T2} protein level. A high expression of KrasER^{T2} was seen in murine PDAC cells isolated from a *Ptf1a$^{Cre/+}$;LSL-Kras$^{G12D/+}$;LSL-Rosa26$^{KE/+}$* mouse (B567). D) In murine PDAC cells (B567PPT) isolated from a *Ptf1a$^{Cre/+}$;LSL-Kras$^{G12D/+}$;LSL-Rosa26$^{KE/+}$* mouse nuclear KrasER^{T2} protein level was increased by treatment with 100 nM 4-OHT for 5 days.

Comparison of age matched *Ptf1a$^{Cre/+}$;LSL-Rosa26$^{KE/+}$* mice with *Ptf1a$^{Cre/+}$;LSL-Kras$^{G12D/+}$* mice shows that, at the age of four months, *Ptf1a$^{Cre/+}$;LSL-Kras$^{G12D/+}$* mice developed PanIN lesions whereas pancreata of *Ptf1a$^{Cre/+}$;LSL-Rosa26$^{KE/+}$* mice displayed normal pancreas histology (Figure 4-5). Additional histological analysis of homo- or heterozygous *Ptf1a$^{Cre/+}$;LSL-Rosa26^{KE}* mice with or without *LSL-Trp53^{R172H}*

revealed that KrasER^{T2} was not sufficient to induce formation of PanIN lesions or tumor in the absence of tamoxifen. Whether stabilization and activation of KrasER^{T2} by tamoxifen treatment is sufficient to induce tumorigenesis is currently under investigation.

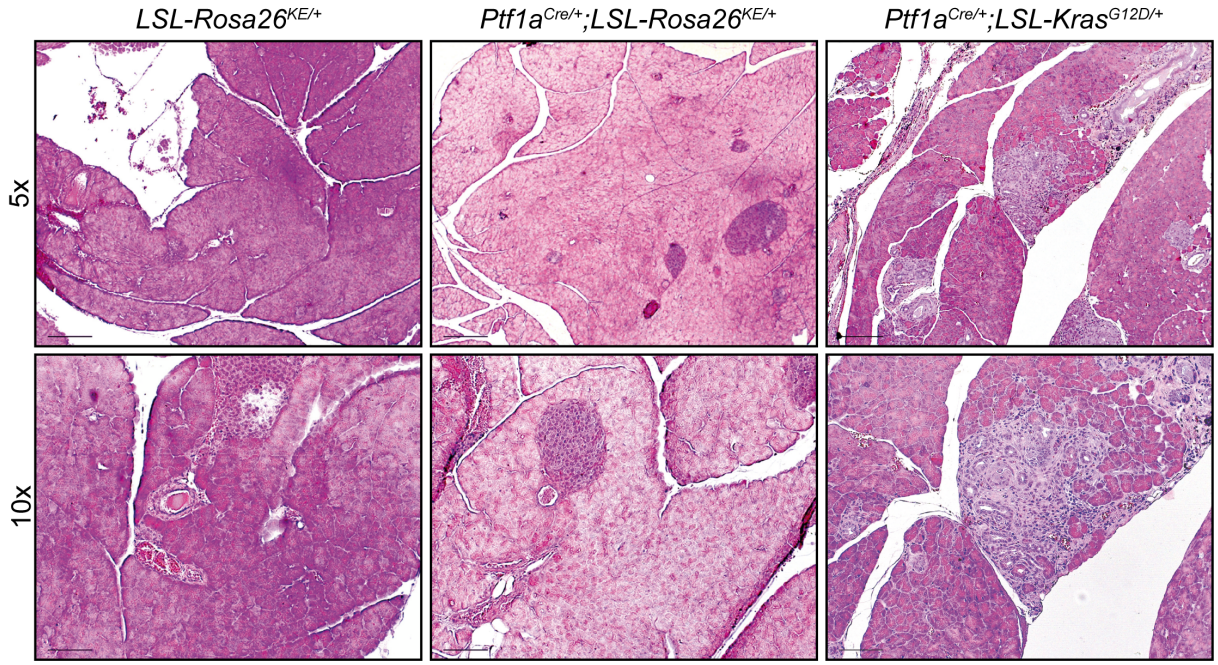

Figure 4-5: HE staining *of LSL-Rosa26$^{KE/+}$* mice: Histological analysis of age-matched, 4 month old *LSL-Rosa$^{KE/+}$*, *Pft1a$^{Cre/+}$;LSL-Rosa26$^{KE/+}$* and *Ptf1a$^{Cre/+}$;LSL-Kras$^{G12D/+}$* mice showed normal pancreas in animals of the new *LSL-Rosa26$^{KE/+}$* strain with or without Cre recombinase expression in the absence of tamoxifen treatment. In contrast, *Ptf1a$^{Cre/+}$;LSL-Kras$^{G12D/+}$* mice developed PanIN lesions (scale bar 200 µm top panel and 100 µm bottom panel).

4.2. Characterization of the *LSL-PCNA$^{fLuc/+}$* Knock-In Mouse Model

In our lab the *LSL-PCNA$^{fLuc/+}$* mouse model was generated in order to establish a model which allows surveillance of cell proliferation *in vivo* and *in vitro*. Therein, *firefly luciferase* is expressed from the *proliferating cell nuclear antigen* (*PCNA*) locus. The ubiquitously expressed PCNA is an auxiliary protein for DNA polymerase δ and is essential for DNA replication. Its synthesis correlates with the proliferation state of the cell (Celis et al., 1987, Travali et al., 1989). Therefore, the *PCNA* locus provides suitable properties to express *fLuc* in a proliferation dependent manner. The targeting vector contained the *fLuc* sequence and a 5'-floxed transcriptional stop element to silence *fLuc* expression. The targeting construct was knocked into the ATG start codon of the first exon of the *PCNA* gene by homologous recombination resulting in

the *LSL-PCNA*$^{fLuc/+}$ mouse (See Figure 4-6). By crossing this model with *Cre* expressing mouse strains, tissue-specific expression of *fLuc* takes place in proliferating recombined cells. By introducing *LSL-PCNA*$^{fLuc/+}$ into the Kras^{G12D}-dependent PDAC mouse model, proliferation of PDAC cells can be visualized *in vivo* by bioluminescence imaging.

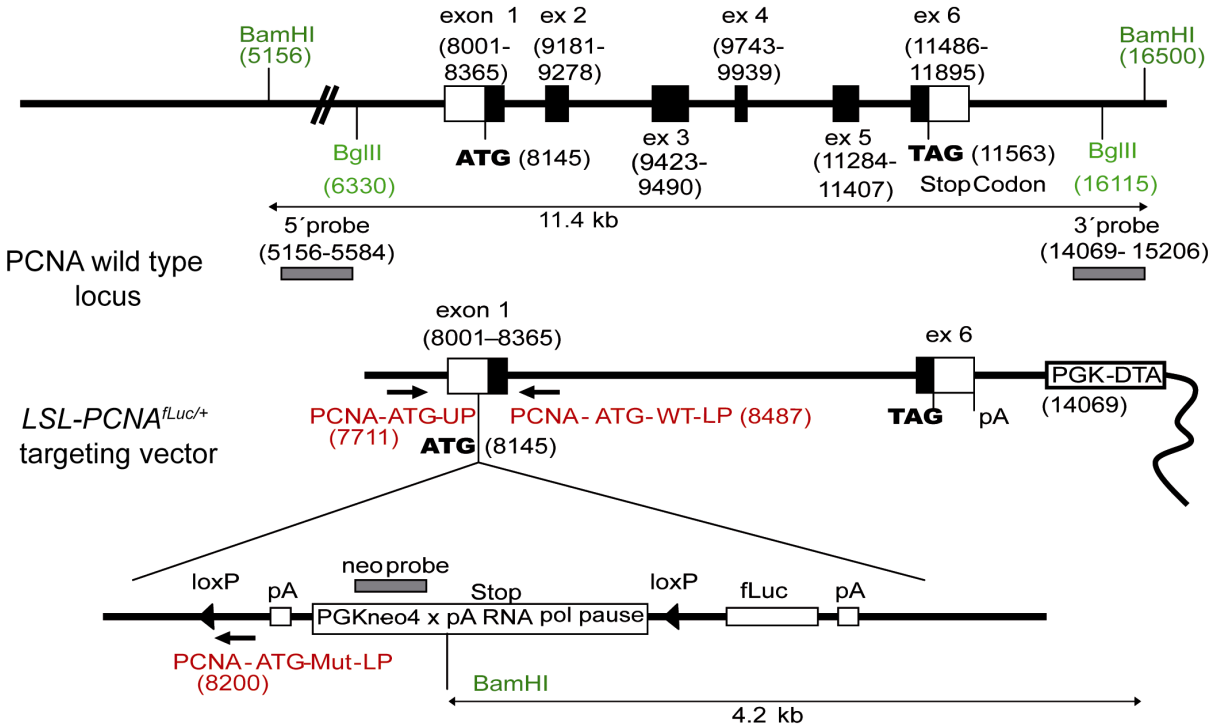

Figure 4-6: Targeting of *the fLuc* to the murine *PCNA* locus: Schematic representation of the murine *PCNA* locus (top) and the targeting vector (bottom). Scheme kindly provided by D. Saur.

4.2.1 Impact of Homo- and Heterozygous *PCNA* Deletion

Before crossing the *LSL-PCNA*$^{fLuc/+}$ line into the Kras^{G12D}-dependent PDAC model the influence of homo- and heterozygous *PCNA* deletion was analyzed. Mice with homozygous deletion of *PCNA* are not viable as none of the offspring carried homozygous *LSL-PCNA*$^{fLuc/fLuc}$ (Figure 4-7A). Also, analysis of embryos at E4.5, E6.5 and E12.5 revealed no homozygous *PCNA* deleted offspring. Therefore, *PCNA* deletion results in embryonic lethality before day E4.5. Since *PCNA* expression is an obligatory event in G1-S phase transition, this is not astonishing (Celis et al., 1987).

Wild type (WT) and *LSL-PCNA*$^{fLuc/+}$ male and female mice were weighted to determine whether growth retardation occurs due to heterozygous deletion of *PCNA*. As seen in Figure 4-7, there is no significant difference in body weight (Figure 4-7B)

or organ weight (Figure 4-7C) of WT mice and age-matched *LSL-PCNA*$^{fLuc/+}$ mice. Thus, it is assumed that normal development and growth are not impaired in *LSL-PCNA*$^{fLuc/+}$ mice.

A

	WT	Hetero-zygous	Homo-zygous
LSL-PCNA$^{fLuc/+}$ x *LSL-PCNA*$^{fLuc/+}$	17 (31.5%)	37 (68.5%)	0 (0%)
LSL-PCNA$^{fLuc/+}$ x WT	364 (43.5%)	280 (56.5%)	N.A.

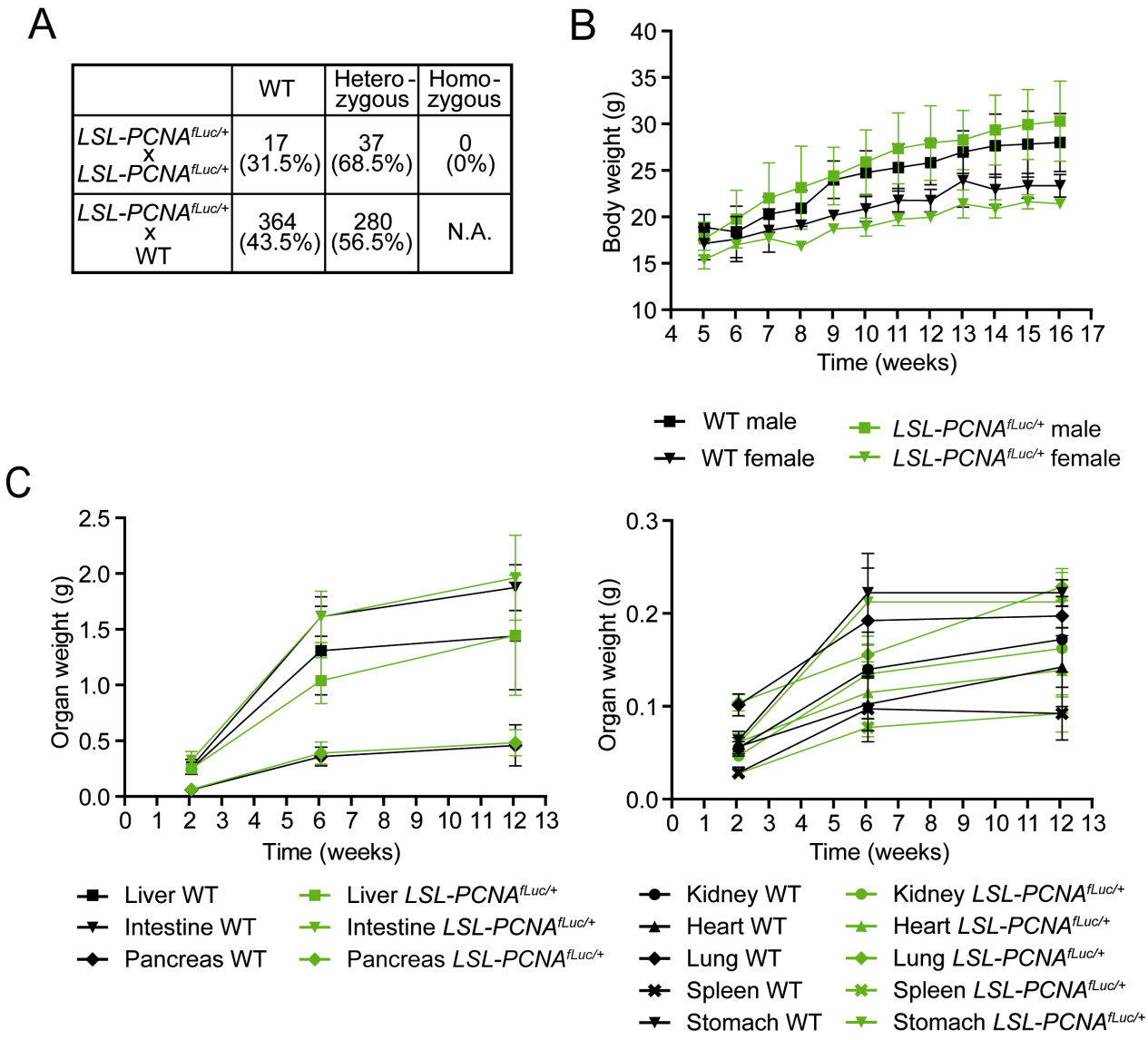

Figure 4-7: Characterization of *LSL-PCNA*$^{fLuc/+}$ mice: A) Analysis of offspring shows no homozygote animals (N.A.= not available). B) Body weight of wild type (WT) and *LSL-PCNA*$^{fLuc/+}$ mice showed no significant difference (male: p=0.4452, female: p= 0.0660) (t-test). C) Organ weight (C) of WT and *LSL-PCNA*$^{fLuc/+}$ mice showed no significant difference (p= 0.8250-0.9480) (t-test).

4.2.2 Tissue-Specific Deletion of Transcriptional Stop Element

In the *LSL-PCNA*$^{fLuc/+}$ mouse model *fLuc* is only expressed after Cre mediated recombination as it is silenced by a floxed transcriptional stop element. To verify this, *LSL-PCNA*$^{fLuc/+}$, *Pdx1-Cre;LSL-PCNA*$^{fLuc/+}$, *Ptf1a*$^{Cre/+}$*;LSL-PCNA*$^{fLuc/+}$ and *Prm1-Cre;LSL-PCNA*$^{fLuc/+}$ mice were analyzed. *Prm1-Cre* mice express *Cre* unter control of the *Protamin1*-promoter (*Prm1*) which is expressed during the terminal stages of spermatogenesis (O'Gorman et al., 1997). Thus, in the second generation of male *Prm1-Cre;LSL-PCNA*$^{fLuc/+}$ mice the transcriptional stop element is ubiquitously deleted in offspring. Expression of *Cre* in *Ptf1a*$^{Cre/+}$ mice is restricted to pancreatic ducts, exocrine and endocrine cells of the pancreas, GABAergic cells in the neural tube and cerebellum as well as the neuroretina (Kawaguchi et al., 2002; Nakhai et al., 2007). *Pdx1-Cre* mice display mosaic expression of *Cre* in the pancreas (Hingorani et al., 2003).

In vivo and *ex vivo* BLI images were acquired of all four genotypes. Additionally, luciferase activity in organ lysates was determined. Bioluminescence images clearly showed pancreas restricted luciferase activity in *Pdx1-Cre;LSL-PCNA*$^{fLuc/+}$ and *Ptf1a*$^{Cre/+}$*;LSL-PCNA*$^{fLuc/+}$ mice whereas luciferase was active in all organs of *Prm1-Cre;LSL-PCNA*$^{fLuc/+}$ mice (Figure 4-8). Leakage of the transcriptional stop element was not observed in *LSL-PCNA*$^{fLuc/+}$ mice. As expected, luciferase activity was higher in organs which have a higher rate of self-renewal, e.g. stomach vs. kidney. It could also be seen that luciferase activity was higher in *Ptf1a*$^{Cre/+}$*;LSL-PCNA*$^{fLuc/+}$ mice compared to *Pdx1-Cre;LSL-PCNA*$^{fLuc/+}$ mice.

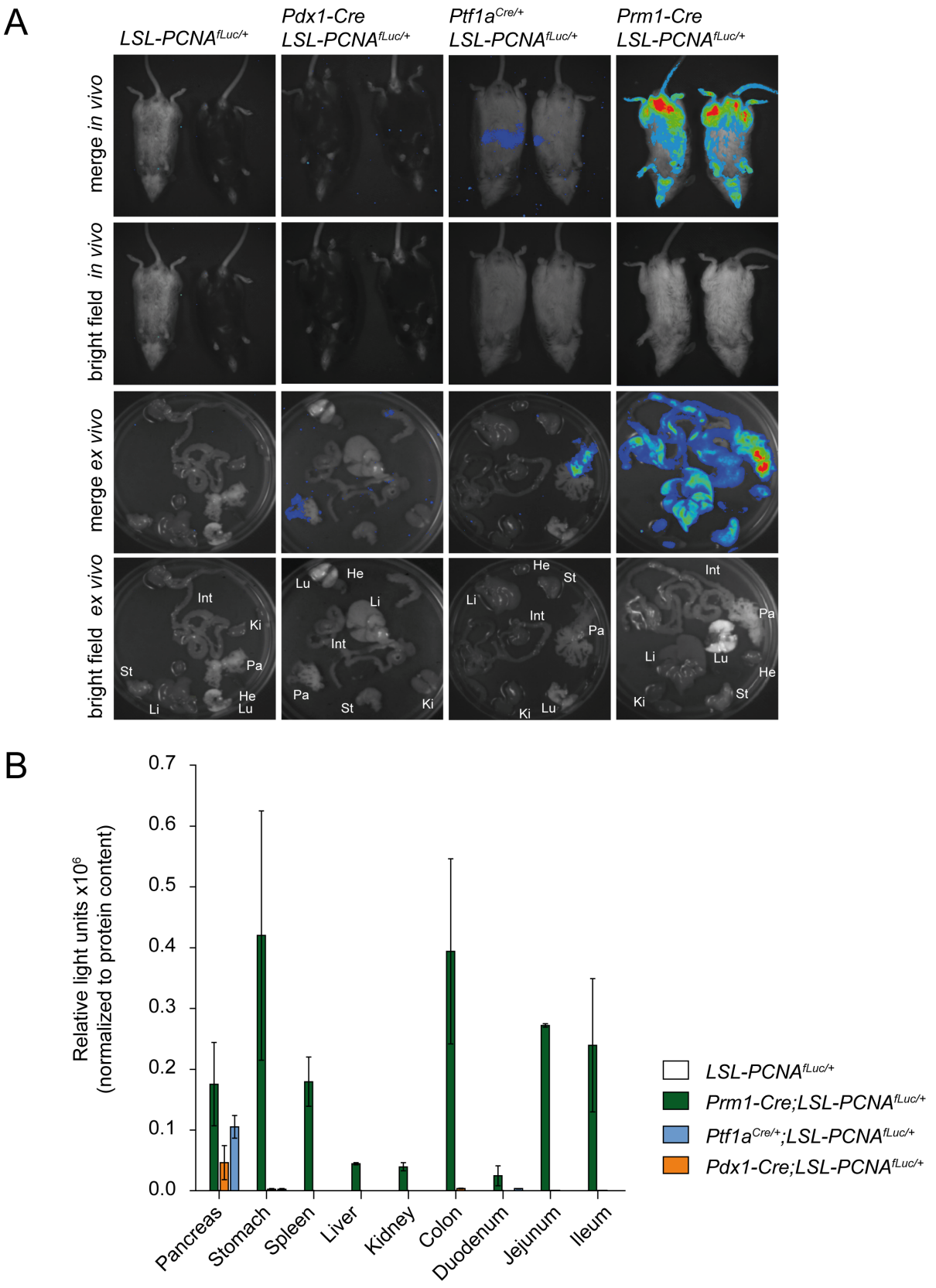

Figure 4-8 Expression of *fLuc* is organ-specific: *In vivo* bioluminescence imaging (A) and *ex vivo* luciferase assay (B) showed pancreas-specific expression of *fLuc* in *Pdx1-Cre;LSL-PCNA*$^{fLuc/+}$ and *Ptf1a*$^{Cre/+}$*;LSL-PCNA*$^{fLuc/+}$ mice. Ubiquitous deletion of the transcriptional stop element by a deleter mouse strain (*Prm1-Cre*) lead to *fLuc* expression in all organs. (He = heart; Int = small intestine; Ki = kidney; Li = liver; Lu = lung; Pa = pancreas; St = stomach).

4.2.3 *In Vivo* Bioluminescence Imaging of PDAC

The new *LSL-PCNA*$^{fLuc/+}$ mouse model was crossed into the well-established Kras^{G12D}-dependent pancreatic tumor model (Hingorani et al., 2003). Kaplan-Meier survival analysis indicates that there is no significant difference in survival rates of *Pdx1-Cre;LSL-Kras*$^{G12D/+}$*;LSL-p53*$^{R172H/+}$ mice with or without knock-in of *LSL-PCNA*$^{fLuc/+}$ into the *PCNA* locus (Figure 4-9). For the other genotypes under investigation (*Pdx1-Cre;LSL-Kras*$^{G12D/+}$, *Pdx1-Cre;LSL-Kras*$^{G12D/+}$*;LSL-p53*$^{R172H/R172H}$, *Ptf1a*$^{Cre/+}$*;LSL-Kras*$^{G12D/+}$, *Ptf1a*$^{Cre/+}$*; LSL-Kras*$^{G12D/+}$*;LSL-p53*$^{R172H/+}$, *Ptf1a*$^{Cre/+}$*;LSL-Kras*$^{G12D/+}$*;LSL-p53*$^{R172H/R172H}$ each with and without *LSL-PCNA*$^{fLuc/+}$) cohorts were too small for statistical analysis.

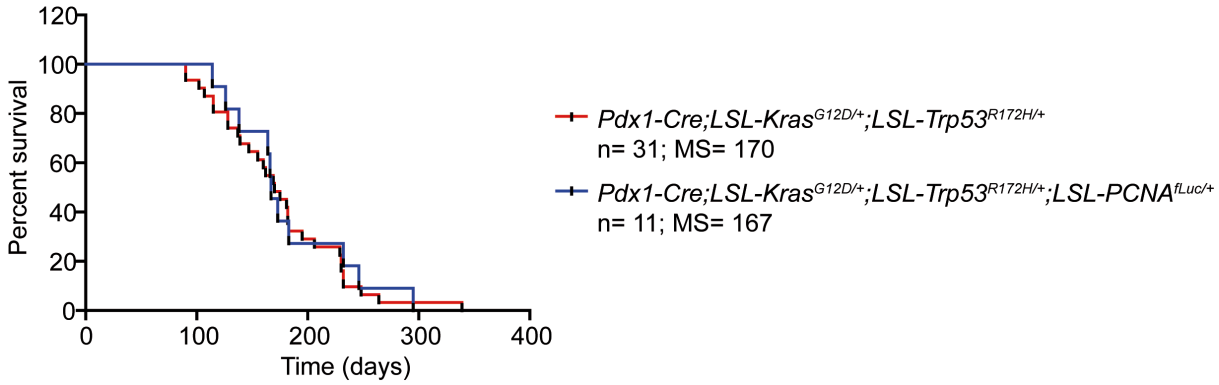

Figure 4-9. Kaplan-Meier survival curves of *LSL-PCNA*$^{fLuc/+}$ tumor mice: Survival rates of *Pdx1-Cre;LSL-Kras*$^{G12D/+}$*;LSL-Trp53*$^{R172H/+}$ mice with or without *LSL-PCNA*$^{fLuc/+}$ were compared. No statistically significant difference in survival rates was observed (log-rank test) (n = cohort size; MS = median survival).

In vivo imaging of pancreatic tumor proliferation revealed a luciferase signal which varied highly between different mice. After dissection it was shown by *ex vivo* bioluminescence imaging that luciferase signal was restricted to the pancreas and the tumor (Figure 4-10 and data not shown). All animals were checked for deletion of *LSL* of *Kras*$^{G12D/+}$ and *PCNA*$^{fLuc/+}$ and were only included into analysis if both transcriptional stop elements were deleted.

Statistical analysis of correlation between the luciferase signal and the tumor volume or the number of BrdU positive cells within the tumor was not possible due to small number of animals in each cohort. As the pancreas is located retroperitoneally, it can be hidden behind the stomach during the measurement. Thus, the luciferase signal can be attenuated depending on the amout of digested food in the stomach. As not

all of the animals could be starved before bioluminescence imaging, they have to be analyzed separately, thus further reducing cohort size.

It was observed that the luciferase signal was mostly stronger in brown animals compared to black animals. In living animals no metastasis was detected by bioluminescence imaging.

Histologically no difference was observed between PDAC tumor mice with or without *LSL-PCNA*$^{fLuc/+}$.

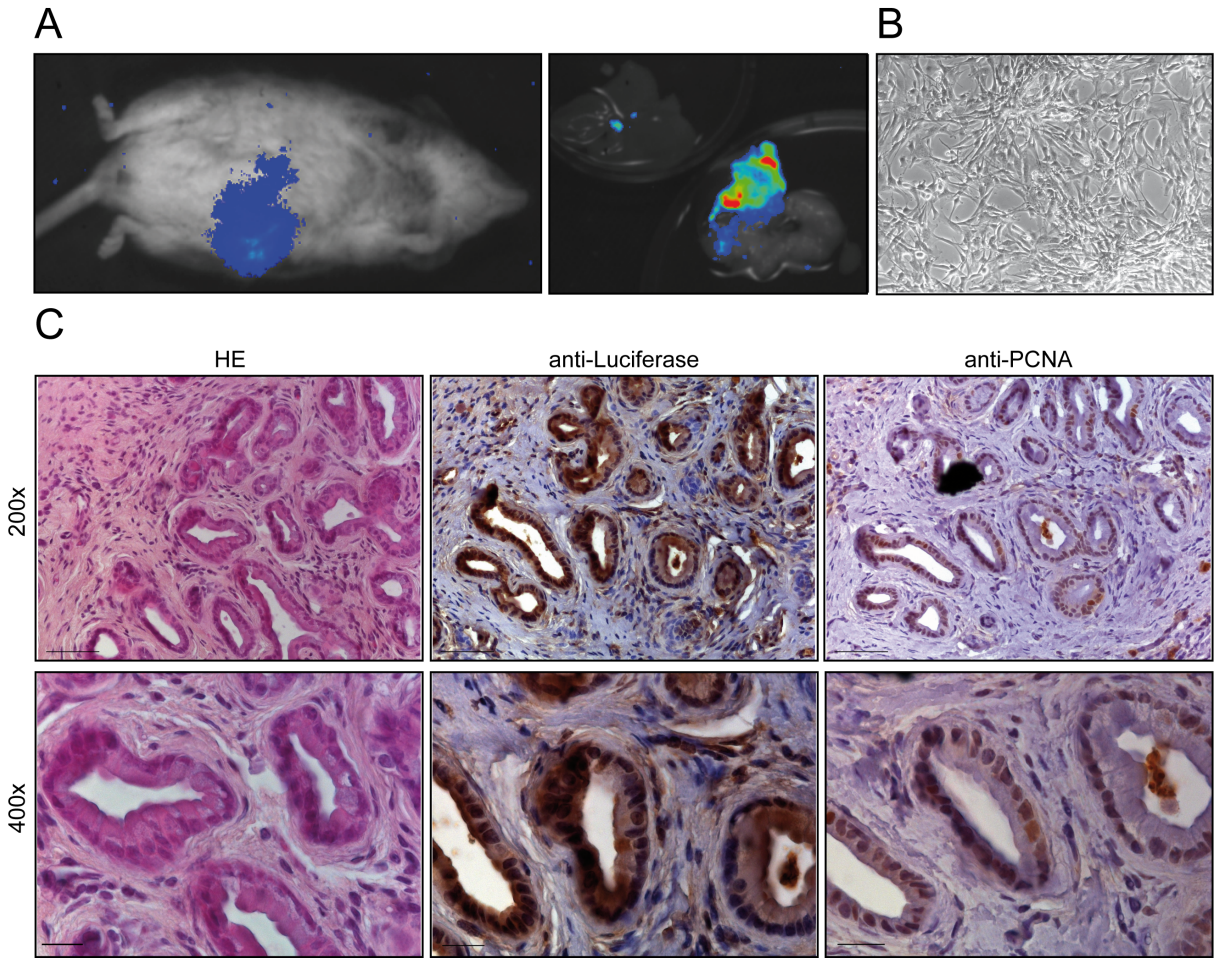

Figure 4-10: *In vivo* imaging of pancreatic tumors in the endogenous Kras^{G12D}-dependent PDAC model: A) Bioluminescence imaging of *Ptf1a*$^{Cre/+}$;*LSL-Kras*$^{G12D/+}$;*LSL-PCNA*$^{fLuc/+}$ mouse showed a strong luciferase signal *in vivo* and *ex vivo*. B) mPCNA^{fLuc} cells were isolated from tumor and used for *in vitro* experiments. C) Luciferase and PCNA immunohistochemistry of pancreatic tumor.

4.3. Establishing of an *In Vitro* Screening Platform for Novel PDAC Therapeutics

I set out to develop a potent tool which allows high-throughput screening of drugs and inhibitors for treatment of pancreatic cancer by bioluminescence imaging of proliferation using the conditional *LSL-PCNA*$^{fLuc/+}$ mouse. Therefore, it needs to be verified that luciferase signal resembles proliferation rate. It is also important to assure that it can be distinguished between a cytotoxic and a cytostatic response as proliferation reoccurs after removal of the cytostatic inhibitor.

Tumors of *Ptf1a*$^{Cre/+}$ or *Pdx1-Cre;LSL-Kras*$^{G12D/+}$*;LSL-PCNA*$^{fLuc/+}$ mice with or without *LSL-Trp53*^{R172H} served as a source for mPCNA^{fLuc} cell lines which were isolated as described in 3.2.3. Even though cell lines showed variations in their luciferase signal intensity and proliferation rate, the luciferase signal of all cell lines correlated exactly with cell proliferation (R=0.9355-0.9813; p<0.0001; Pearson's correlation) (Figure 4-11 and data not shown).

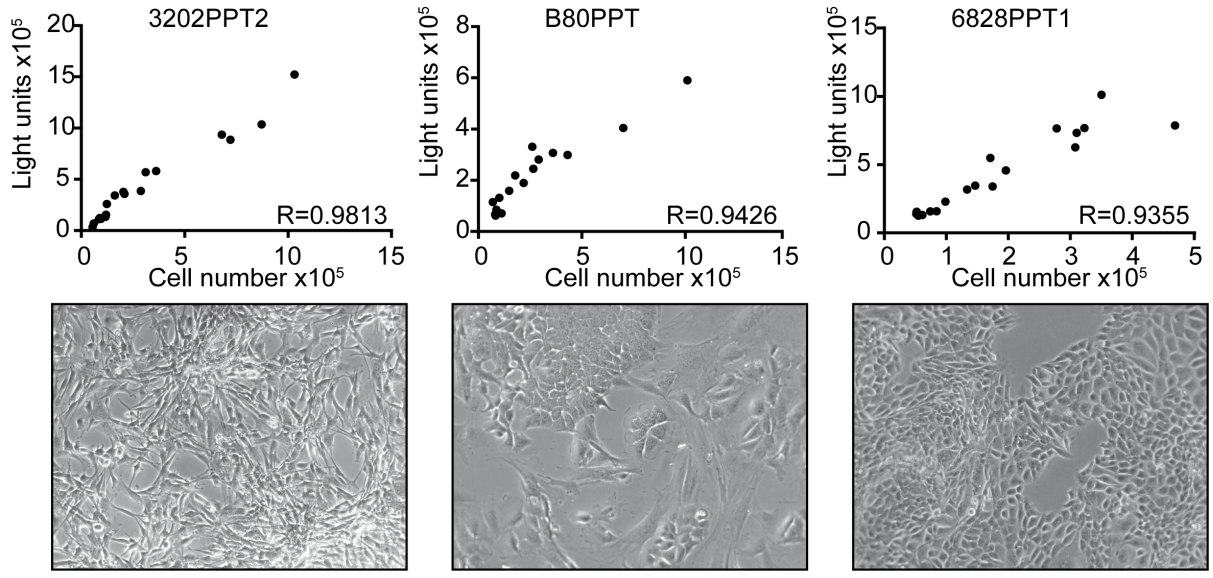

Figure 4-11. Correlation of luciferase signal and cell proliferation: mPCNA^{fLuc} cell lines were isolated from murine PDAC. Cell number and luciferase signal were determined at six time points over three days. Data analysis showed an exact correlation between cell number and luciferase signal (p<0.0001; Pearson's correlation).

To address the question whether luciferase activity in mPCNA^{fLuc} cells can be used to monitor treatment response, various inhibitior experiments were performed. LY294002 is a synthetic flavinoid that acts as a potent, competitive, reversible inhibitor of the ATP-binding site of class I PI3-kinases (Vlahos et al., 1994, Bondar et

al., 2002). mPCNA^{fLuc} cells were incubated with LY294002 for 48 h and luciferase activity, cell viability (MTT assay) and cell number were determined every 24 h. As seen in Figure 4-12 treatment with LY294002 lead to a proliferation stop as well as inhibition of luciferase signal and reduction of cell viability. Comparison of the Pearson's correlation of luciferase signal, cell viability and cell proliferation reveals an overall exact correlation (R=0.9475-0.9574; p<0.0001). Since cell viability defined by MTT assay correlates with cell number, MTT was chosen as control for further experiments (Figure 4-12F).

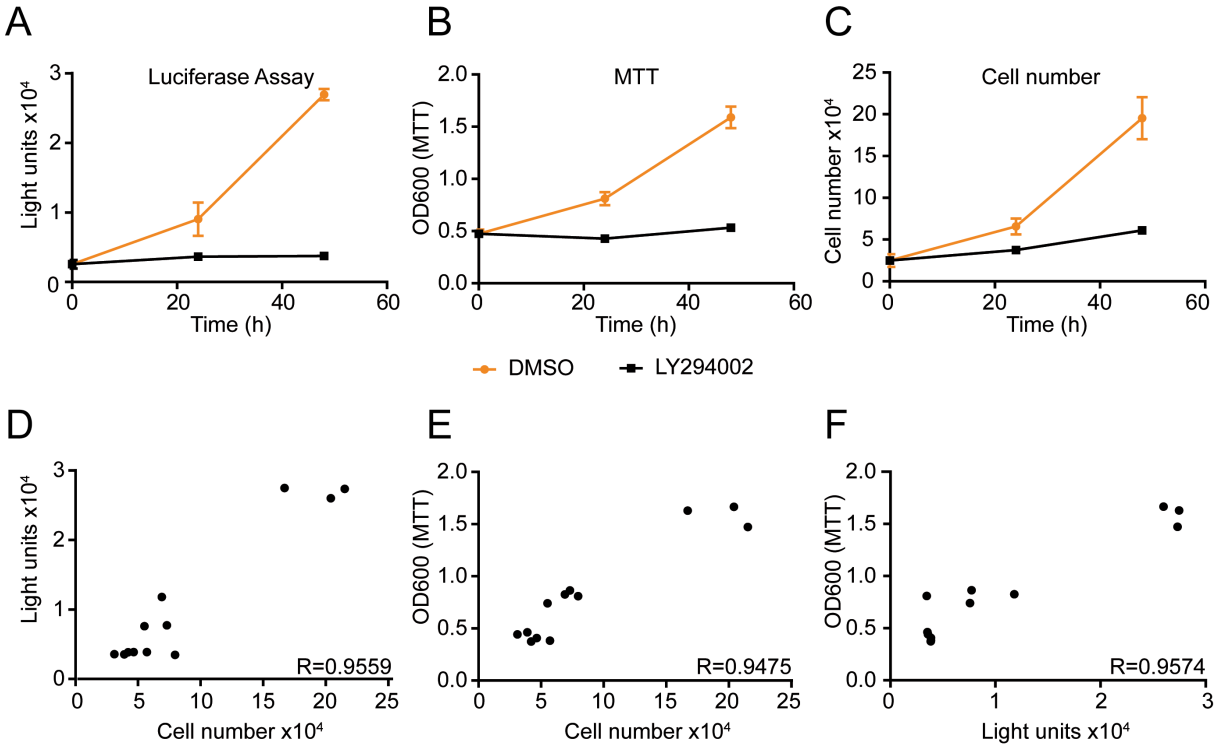

Figure 4-12: Luciferase assay correlates with MTT assay and cell number when mPDAC^{fLuc} cells were treated with LY294002: A-C) mPCNA^{fLuc} cells (3202PPT2) were treated with LY294002 (20 µM) or DMSO for 48 h. Luciferase signal (A), MTT (B) and cell number (C) were measured every 24 h. Values are arithemtic mean +/- standard deviation. D-F) Pearson's correlation of data showed an exact correlation of luciferase signal, cell viability and cell numbers (p<0.0001) (n=1).

To verify whether LY294002 treatment inhibits PI3-kinase signaling in mPCNA^{fLuc} cells, 3202PPT2 cells were treated with LY294002, whole cell lysates were harvested every 24 h and Western blot was performed to analyze Akt phosphorylation status. LY294002 reduced Akt phosphorylation in a time dependent manner (Figure 4-13). After 48 h Akt phosphorylation is reduced to 50% and after 72 h to 15% compared to controls.

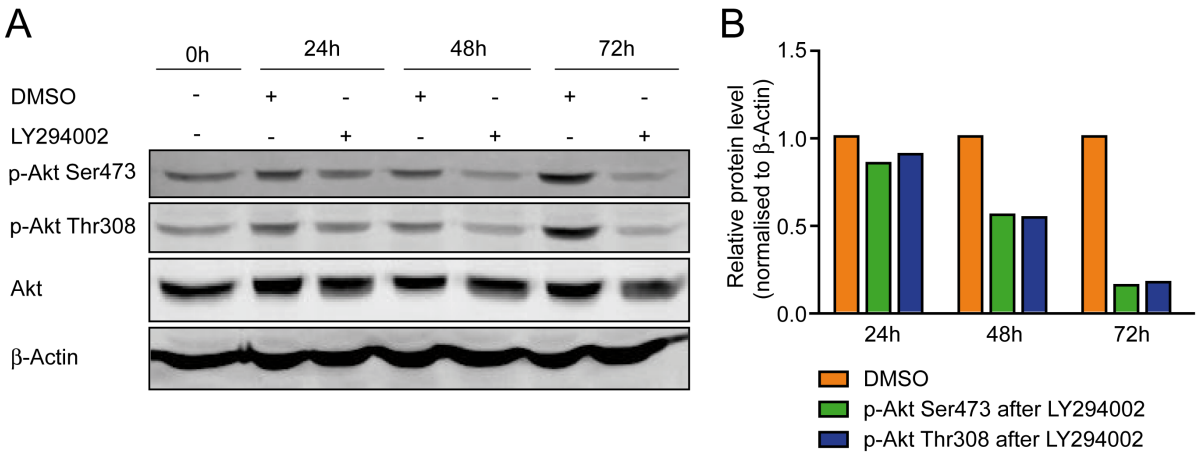

Figure 4-13: LY294002 reduces phospho-Akt level (serine 473 and threonine 308) in mPCNA^{fLuc} cells: A) Cells (3202PPT2) were treated with LY294002 (20 µM) for up to 72 h. Cell lysates were harvested every 24 h and Western blot analysis was performed. B) Quantification of the blot showed a time dependent reduction of phosphorylation of Akt at residues serine 473 and threonine 308.

To further analyze whether the exact correlation of luciferase signal and cell viability is true for different cell lines and for various inhibitors, experiments were extended. Three different mPCNA^{fLuc} cell lines with different genetic background (3202PPT2: *Ptf1a$^{Cre/+}$;LSL-Kras$^{G12D/+}$;LSL-PCNA$^{fLuc/+}$*; 1713PPT: *Pdx1-Cre;LSL-Kras$^{G12D/+}$;LSL-PCNA$^{fLuc/+}$;LSL-Trp53$^{R172H/+}$;LSL-R26$^{tva-lacZ}$*; B80PPT: *Pdx1-Cre;LSL-Kras$^{G12D/+}$;LSL-PCNA$^{fLuc/+}$;LSL-Trp53$^{R172H/R172H}$;LSL-R26$^{tva-lacZ}$*) were treated with Erlotinib, Roscovitine and LY294002. Erlotinib is a tyrosine kinase inhibitor, which acts on the epidermal growth factor receptor. Roscovitine is a cyclin-dependent kinase inhibitor.
As depicted in Figure 4-14 reduction of luciferase activity and cell viability was time dependent and inhibitor-specific. Even though reduction of luciferase activity and cell viability were varying slightly within cell lines, the same overall response could be observed. LY294002 treatment lead to reduction of luciferase activity to 40-60% after 24 h and to approximately 20% after 48 h treatment in all three cell lines. Even though, Iseki et al. could show a sensitivity of the human pancreatic cancer cell line BxPC3 towards Roscovitine treatment, I cannot report proliferation inhibition or reduction of cell viability of mPCNA^{fLuc} cells by Roscovitine (Iseki et al., 1998). Erlotinib lead to reduction of 40-50% in cell viability and luciferase activity. This is in accordance with previously published data where Erlotinib lead to a reduction of cell growth by approximately 50% in BxPC3 cells (Lu et al., 2008) In all three cell lines a correlation between luciferase signal and cell viability was seen (R=0.6106-0.9282; $p<0.0001$- $p=0.0071$; Pearson's correlation) (Figure 4-14).

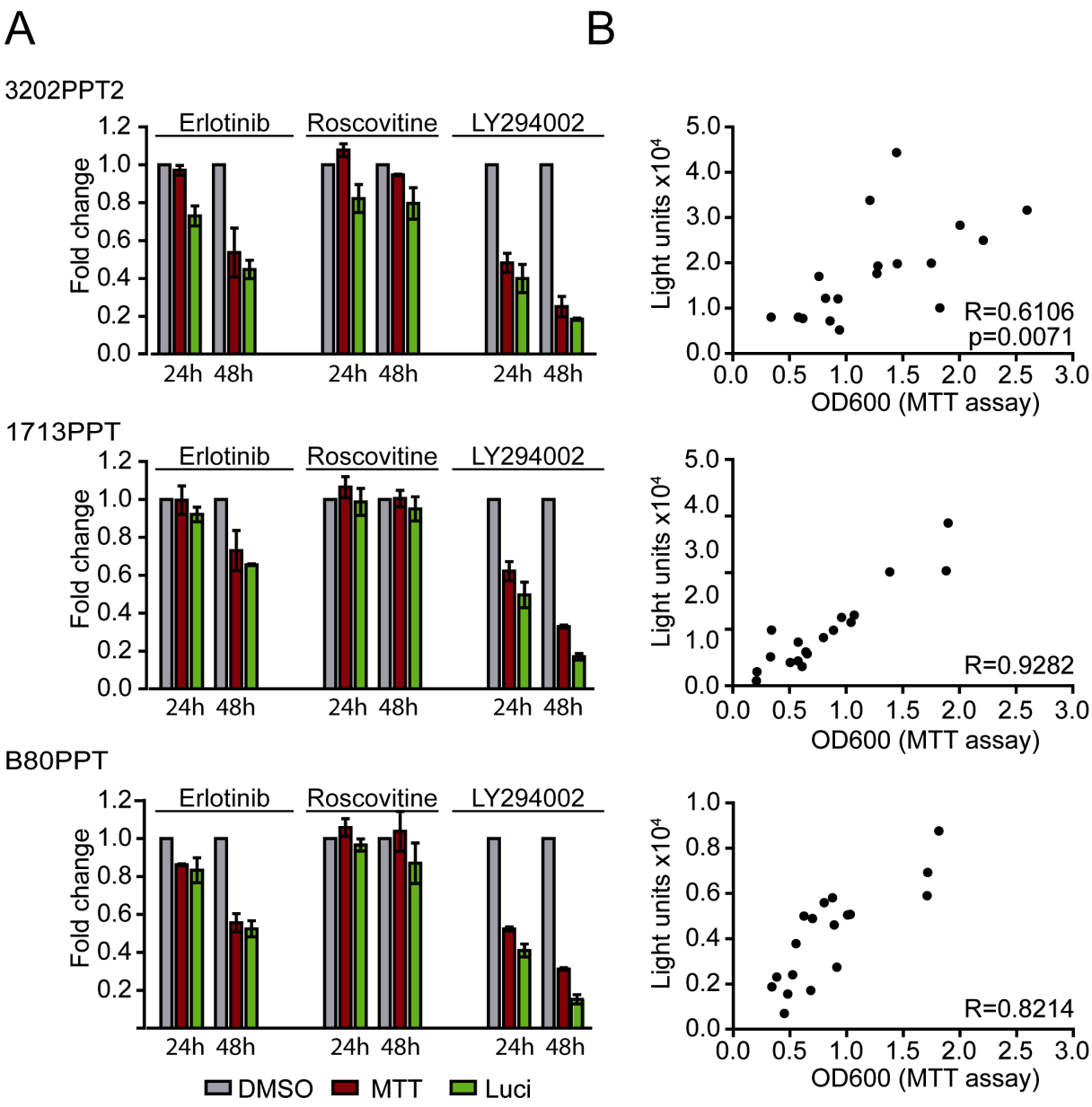

Figure 4-14: Luciferase signal correlates with MTT assay: A) Three different mPCNA^{fLuc} cell lines have been treated with inhibitors targeting different signaling pathways for 24 h and 48 h (Erlotinib 18 µM, Roscovitine 25 µM, LY294002 20 µM). Luciferase assay and MTT assay were performed every 24 h. B) Data of luciferase assay and MTT assay showed a good correlation ($p<0.0001$ if not stated otherwise; Pearson's correlation).

For the development of a screening tool, an important question is whether an effect achived by drug or inhibitor treatment is reversible. To answer this question, two mPCNA^{fLuc} cells were treated with LY294002 or DMSO for 120 h. After 48 h LY294002 was removed from some samples, but remained on the others for another 72 h. While luciferase activity was strongly inhibited during LY294002 treatment, luciferase signal increased up to 50% of control group after removal of LY294002 in

3250PPT cells (Figure 4-15A). In 3202PPT2 cells luciferase signal reached the level of control group (Figure 4-15B). This enables differentiation between inhibitors that induce cell death and those which lead to a reversible proliferation stop.

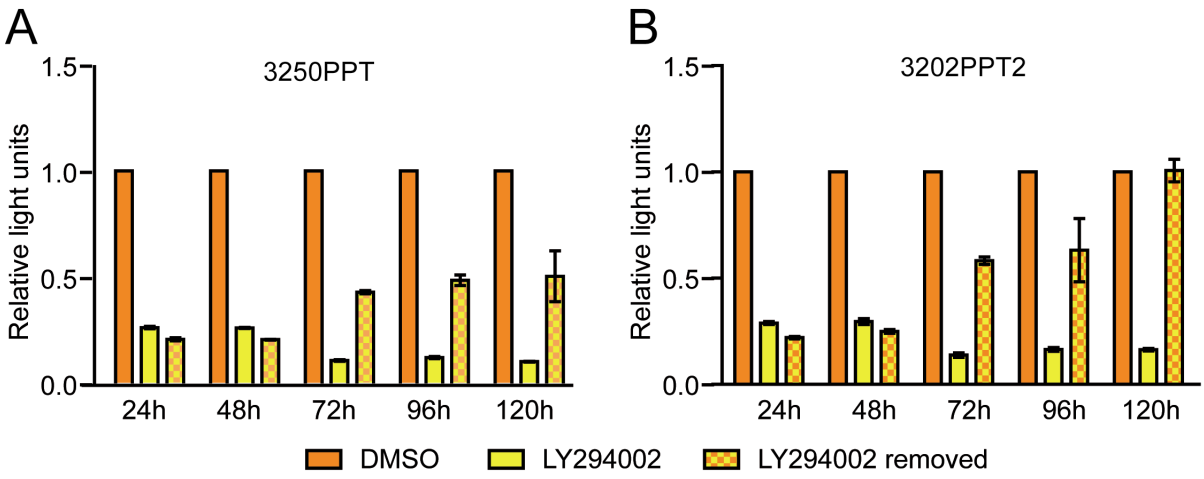

Figure 4-15: **Reduction of luciferase signal is reversible:** mPCNA^{fLuc} cells showed reduction of luciferase signal when PI3-kinase signaling was inhibited by LY294002 treatment (20 µM). After removal of LY294002 after 48 h the luciferase signal increased up to 50% in 3250PPT cells (A) and up to the level of controls in 3202PPT2 cells (B).

The previous experiments showed that expression of *fLuc* from the *PCNA* locus is proliferation dependent. To verify that luciferase activity also reflects proliferation under treatment conditions, and is not reduced due to altered translational control of the *fLuc* transgene, stably transfected cell lines expressing *fLuc* under control of the ubiquitously active *human cytomegalovirus* (*CMV*) promoter were compared with mPCNA^{fLuc} cells (3202PPT2: *Ptf1a$^{Cre/+}$;LSL-Kras$^{G12D/+}$;LSL-PCNA$^{fLuc/+;}$* 3250PPT: *Pdx1-Cre;LSL-Kras$^{G12D/+}$;LSL-PCNA$^{fLuc/+}$;LSL-R26$^{tva-lacZ}$*). The two human pancreatic adenocarcinoma cell lines (MiaPaCa-CMV-fLuc and BxPC3-CMV-fLuc) are stably transfected with *fLuc* under control of a constitutively active *CMV* promoter (kindly provided by S. Eser and S. Rasch). Both sets of cell lines were treated with LY294002 for 48 h and luciferase activity was determined at indicated time points. In the mPCNA^{fLuc} cell lines luciferase activity was decreased to 43% in 3202PPT2 and to 34% in 3250PPT cells after 24 h and to 25% in 3202PPT2 and 16% in 3250PPT after 48 h (Figure 4-16A). In contrast, luciferase activity was not altered in both cell lines which express *fLuc* proliferation independently from *CMV* promoter (Figure 4-16B). This shows that decreased luciferase expression levels are not altered due to impaired translational control of *fLuc* in response to treatment.

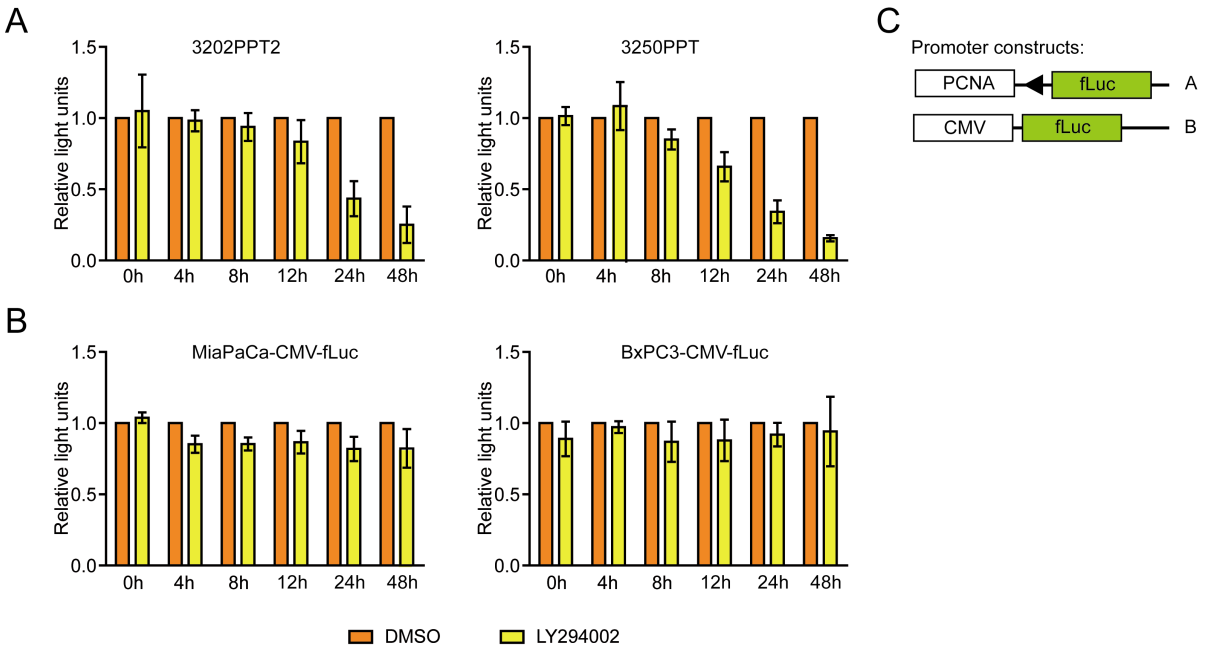

Figure 4-16: Luciferase signal is proliferation dependent in mPCNA^{fLuc} cell lines: Murine mPCNA^{fluc} cells and human PDAC cell lines, stably transfected with fLuc, were incubated with LY294002 (20 µM) for up to 48 h. Luciferase assay was performed at 4, 8, 12, 24 and 48 h after addition of inhibitor. Inhibition of PI3-kinase signaling by LY294002 treatment lead to a decrease of luciferase signal in mPCNA^{fLuc} cell lines (A), but not in cell lines which stably express *fLuc* under control of a *CMV* promoter (B). C) Promoter constructs of mPCNA^{fLuc} cells (upper scheme; triangle representing one *loxP* site after recombination) and cell lines expressing *fLuc* from *CMV* promoter (lower scheme).

In order to evaluate tumor heterogeneity in treatment response, several different mPCNA^{fLuc} cell lines can be screened with various inhibitors. First experiments showed that 3202PPT2 (*Ptf1a$^{Cre/+}$;LSL-Kras$^{G12D/+}$;LSL-PCNA$^{fLuc/+}$*) did not respond to Sunitinib treatment, whereas 3250PPT cells (*Pdx1-Cre;LSL-Kras$^{G12D/+}$;LSL-PCNA$^{fLuc/+}$;LSL-R26$^{tva-lacZ}$*) showed a decrease in luciferase activity and cell viability (Figure 4-17A and C). Sunitinib is a multitargeted tyrosine kinase inhibitor which inhibits several growth factor receptors, e.g. the vascular endothelial growth factor receptors, the platelet-derived growth factor receptors and KIT (stem cell factor receptor) (Le Tourneau et al., 2007). Thus, an alteration in response to Sunitinib treatment may indicate genetic variation in one of the mentioned receptor pathways in either of the cell lines. Still, this is speculative and remains to be verified.

In contrast to Sunitinib treatment, both cell lines strongly reacted upon PI-103 treatment (Figure 4-17B and D). PI-103 is a selective class I PI3-kinase inhibitor which is known to inhibit proliferation in various cancer cell lines and in xenograft transplantation models (Raynaud et al., 2007). As both cell lines under investigation

respond to PI-103 treatment, this indicates a sensitivity of mPDAC^{fLuc} cells towards PI-103. To verify this, a larger panel of cell lines needs to be investigated.
This experiment shows that by the treatment of a large panel of different mPCNA^{fLuc} cells it is possible to determine an overall response to an inhibitor, independently of genetic background, and the identification of resistance mechanisms.

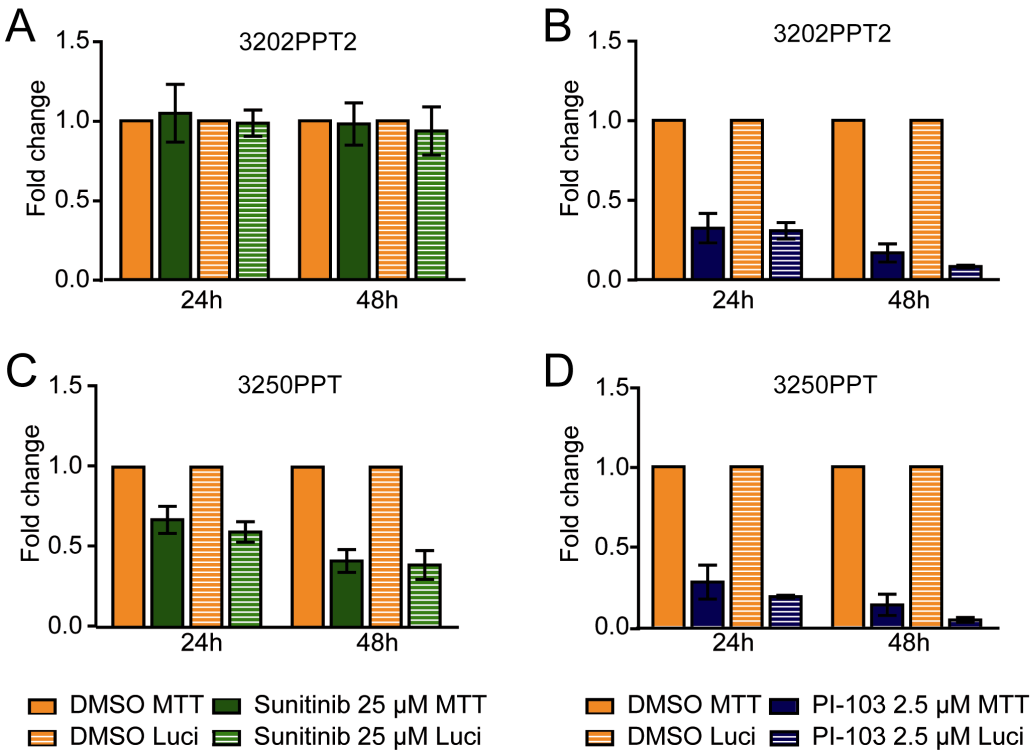

Figure 4-17: Differentiation between responsive and non-responsive mPCNA^{fLuc} cell lines: 3202PPT2 and 3250PPT cells were incubated with Sunitinib (25 µM) and PI-103 (2.5 µM) for 48 h. Cell viability and luciferase activity were determined every 24 h. 3202PPT2 cells did not respond to Sunitinib (A) but to PI-103 (B) whereas 3250PPT cells responded to both inhibitors (C and D).

After verifying that luciferase activity is proliferation-dependent and that it does resemble the cells' proliferative status, one mPCNA^{fLuc} cell line was used as an example for a drug screening platform. 3202PPT2 cells were treated with seven inhibitors at three different concentrations and luciferase signal as well as cell viability were determined after 48 h incubation. The inhibitors address different intracellular targets as listed in Table 3-9. A dose-dependent and inhibitor-dependent decrease in both luciferase activity and cell viability was observed (Figure 4-18). In all experiments it could be seen that the response of the luciferase signal was slightly higher than of cell viability. However, there was an exact correlation between luciferase activity and cell viability ($R=0.9205$; $p<0.0001$; Pearson's correlation).

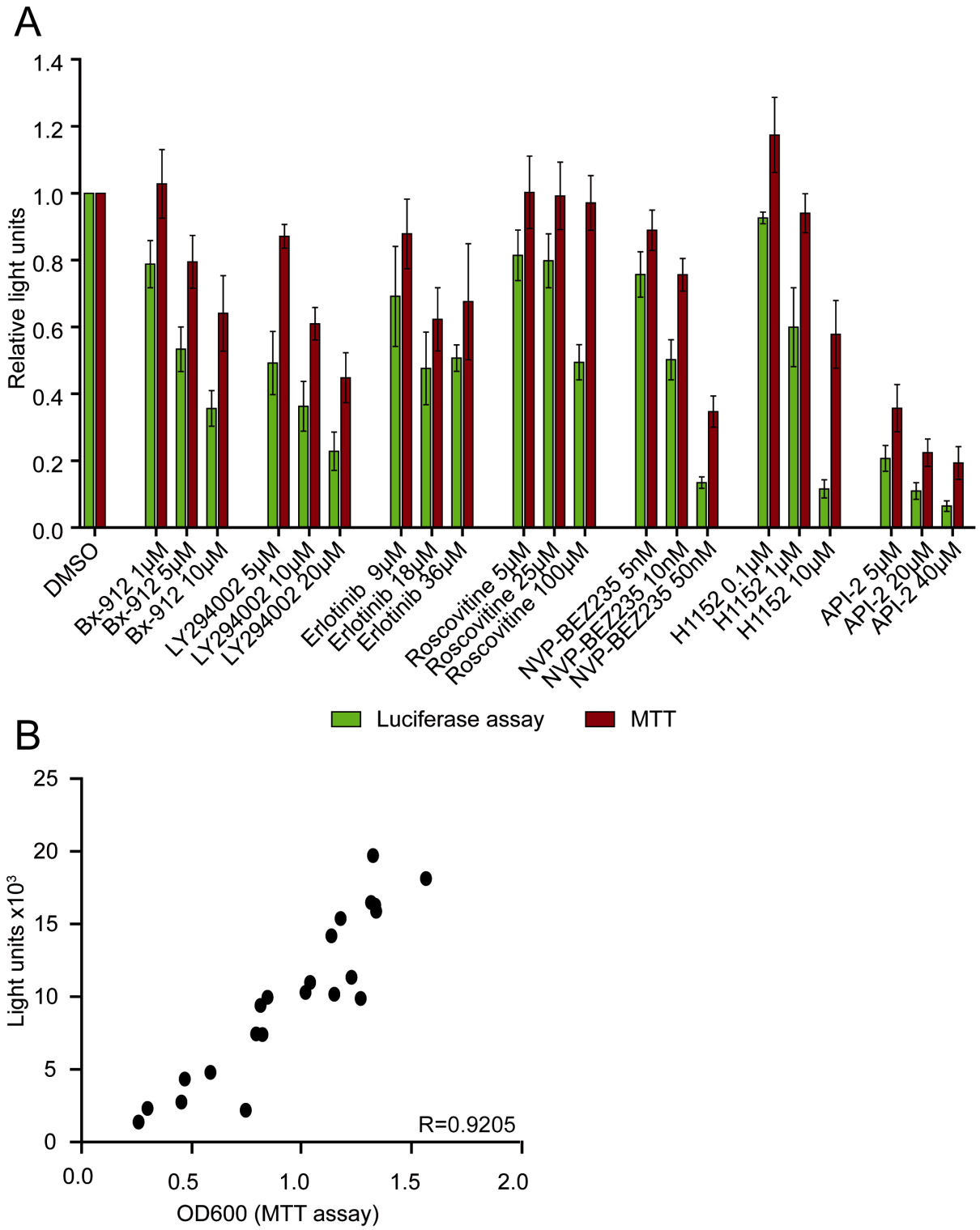

Figure 4-18: mPCNA^{fLuc} cells as a potent tool for the development of a drug screening platform: A) mPCNA^{fLuc} cells (3202PPT2) showed dose-dependent reduction of cell viability (MTT assay) and of proliferation (luciferase assay) after 48 h incubation with inhibitor. B) Luciferase signal correlated exactly with cell viability ($p<0.0001$; Pearson's correlation).

4.4. Transplantation Models for Validation of Drug Candidates

Once a candidate has been found in an *in vitro* screening assay, there is a need to validate results *in vivo*. To make sure that the luciferase signal correlates with the tumor size 10,000, 50,000 and 250,000 mPCNA^{fLuc} cells (3202PPT2: *Ptf1a$^{Cre/+}$;LSL-Kras$^{G12D/+}$;LSL-PCNA$^{fLuc/+}$*) were transplanted subcutaneously in each side of the back of immunocompromised Swiss nude mice. Tumor size was determined by caliper measurement and luciferase activity was determined by BLI. Data analysis showed an exact correlation of tumor volume, i.e. cell number, and luciferase activity *in vivo* (R=0.9210; p<0.0001; Pearson's correlation) (Figure 4-19). The number of BrdU positive cells per visual field of tumor section remained constant in all three tumors, independently of tumor size.

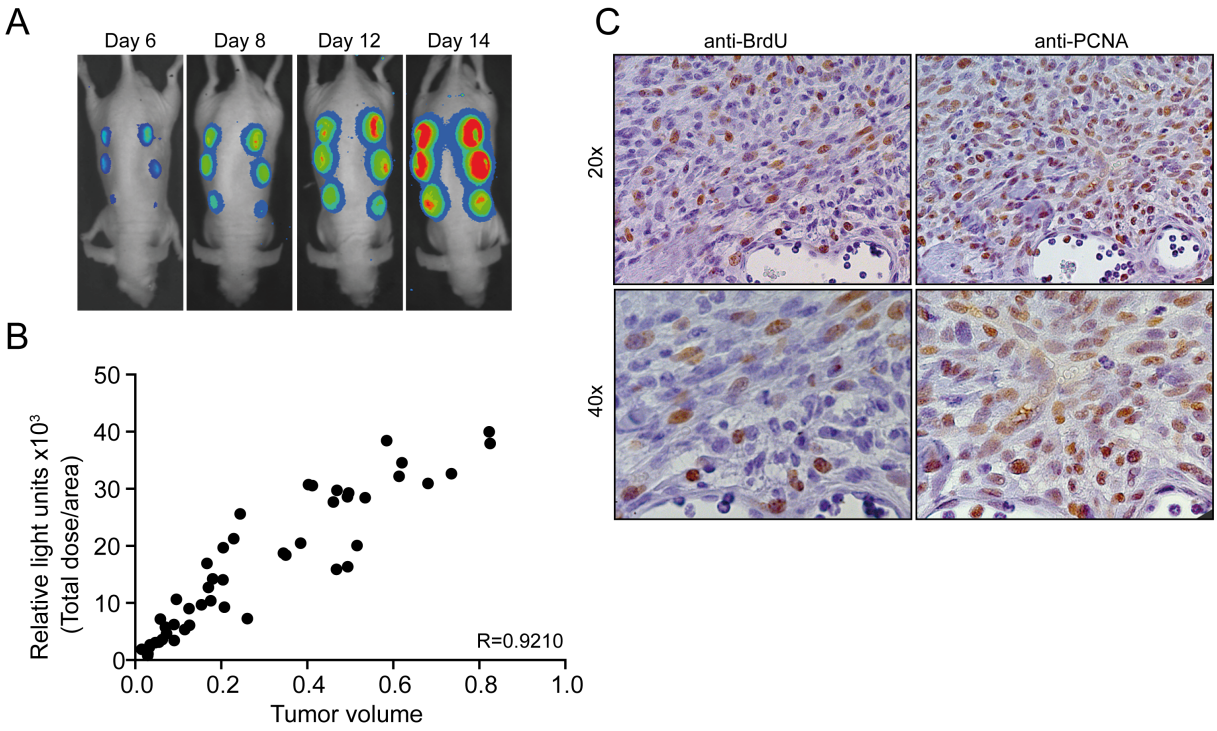

Figure 4-19: Luciferase signal correlates exactly with tumor size *in vivo*: A) and B) After subcutaneous transplantation of 10,000, 50,000 and 250,000 mPCNA^{fLuc} cells (3202PPT2), exact correlation between the *in vivo* luciferase signal and tumor size was shown. Tumor size was measured and BLI images were aquired at day 6, day 8, day 12 and day 14 after implantation (p<0.0001; Pearson's correlation). C) BrdU and PCNA immunohistochemistry of corresponding tumors.

To analyze the effect of the PI3-kinase inhibitor LY294002 on the proliferation of cells *in vivo* an orthotopic transplantation model was used. mPCNA^{fLuc} cells (3202PPT2) were transplanted into the pancreas of Swiss nude mice. Three weeks after transplantation animals were treated with 100 mg/kg LY294002 or DMSO as control.

Luciferase activity was measured after 3, 8 and 24 h. By quantification of the signal it was shown that luciferase signal decreased to 44% after 8 h compared to control animal. The reversibility of the effect can be seen as the signal was increasing again after 24 h (Figure 4-20). Data shown here are preliminary as they are based on a small number of experiments and need to be verified in larger cohorts and with further inhibitors. Still, they indicate that orthotopic transplantation models with mPCNA^{fLuc} cells can be used for validation of response to drug treatment *in vivo.*

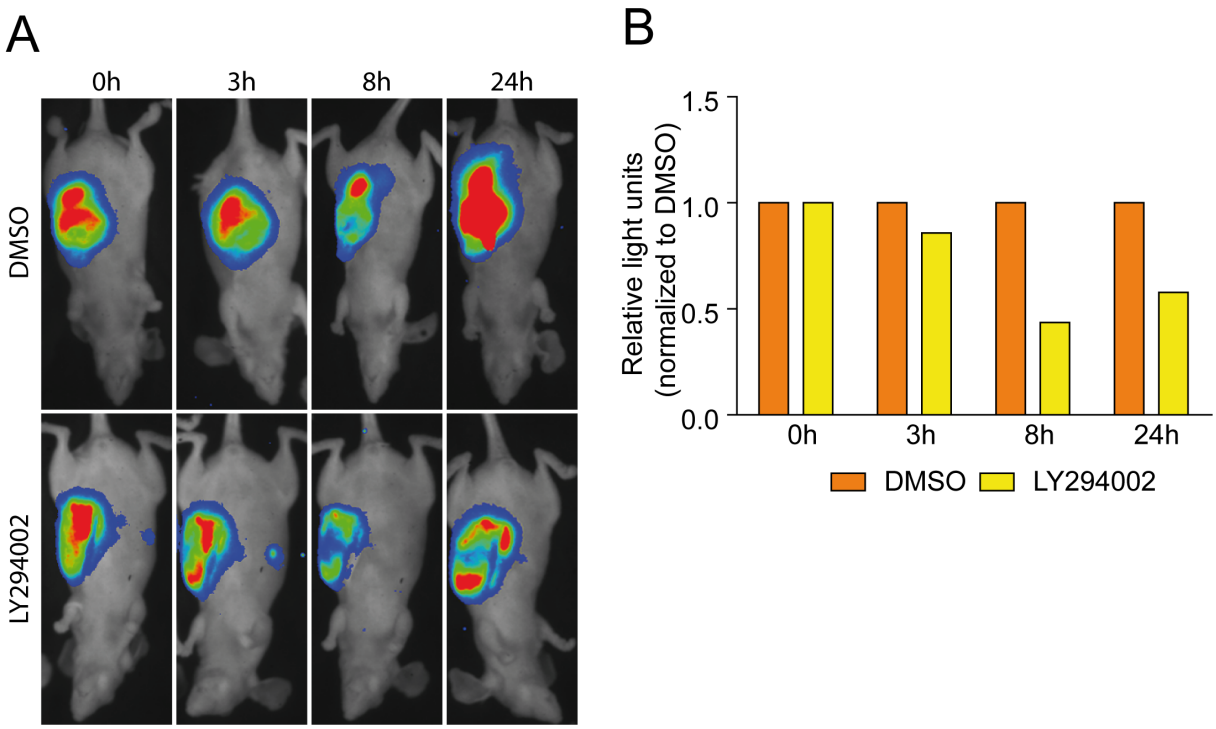

Figure 4-20: Blockade of PI3-kinase signaling pathway leads to a reversible proliferation arrest in an orthotopic transplantation model: A) Three weeks after orthotopic transplantation of mPCNA^{fLuc} cells (3202PPT2) mice were treated with LY294002 (100 mg/kg) or DMSO. Bioluminescence images were acquired before and 3, 8 and 24 h after drug administration. B) Quantification of luciferase signal showed a reduction of proliferation signal to 44% 8 h after treatment. After 24 h the signal was increasing again.

5 Discussion

5.1. Establishment of the *LSL-Rosa26^{KE}* Mouse Model

The well-established genetically defined Kras^{G12D}-dependent tumor mouse model of PDAC has been widely used to gain insight into pancreatic tumor development as it resembles all major hallmarks of human PDAC development (Hingorani et al., 2003). It has been interbred with a variety of mouse models which carry additional genetic alterations observed in PDAC, e.g. *Trp53* mutation (Hingorani et al., 2005), *Ink4A-Arf* or *Smad 4* deletion (Aguirre et al., 2003; Kojima et al., 2007), blockade of TGF-β signaling (Ijichi et al., 2006) or deletion of *PTEN* (Rose and Hill, 1996). Still, this model cannot address the question whether Kras^{G12D} is solely important for tumor initiation or also for tumor maintenance or promotion, since, once activated, Kras cannot be turned off.

With the new tamoxifen inducible *LSL-Rosa26^{KE}* mouse model, which allows spatio-temporal control of Kras^{G12D} activity, we planned to investigate the effects of adult-onset of Kras^{G12D} activity as well as of the removal of oncogenic Kras^{G12D} after tumor onset. Guerra et al. discovered that adult-onset of Kras^{G12V} activity does not result in PanIN or PDAC development if expressed upon Cre recombination in a doxycycline inducible *elastase-Cre* system (Guerra et al., 2007). Before that, it was already shown by Grippo et al. that expression of *Kras^{G12D}* from the *elastase* promoter does not lead to PDAC development (Grippo et al., 2003). At this stage, no data were published about an inducible system which expresses *Kras^{G12D}* after recombination by *Pdx1-Cre* or *Ptf1a$^{Cre/+}$*. In 2009, Gidekel Friedlander et al. used a tamoxifen-inducible *Pdx1-CreER^{TM}* transgenic mouse strain in combination with the *LSL-Kras$^{G12D/+}$* mouse model (Gidekel Friedlander et al., 2009). By tamoxifen treatment Cre recombination was induced in the pancreas of adult mice. Mice developed PanIN-1 and PanIN-2 lesions, but only one mouse developed PDAC, unless additional mutations in *Trp53* or *Ink4A/Arf* were induced. Therefore, it was concluded that younger mice are more susceptible to oncogenic transformation by Kras^{G12D} (Gidekel Friedlander et al., 2009).

The KrasER^{T2} construct was analyzed *in vitro*. I report that the Kras-EGPF-ER^{T2} triple fusion protein colocalized with DAPI staining of the nucleus upon tamoxifen

treatment. Still, confocal images indicated that the triple fusion protein seems to be disabled to localize to the cytoplasma membrane. Wild type Kras is targeted to the cytoplasma membrane by two distinct motifs. The C-terminal CAAX motif (C=cysteine, A=aliphatic amino acid, X=any amino acid) is posttranslationally farnesylated to gain a membrane anchor. Additionally, a polybasic domain comprising six consecutive lysine residues (amino acids 175-180) is required for membrane localization. If one of these motifs is disrupted, Kras cannot be targeted to the membrane (Hancock et al., 1990). By fusing EGFP-ER^{T2} to the C-terminus of Kras^{G12D}, one of the motifs might be inaccessible due to sterical hinderance in the triple fusion protein and, thus, membrane anchorage might be impaired. Membrane localization in KrasER^{T2} transduced cells was not analyzed by immunocytochemistry as specific antibodies are not available. However, KrasER^{T2} showed strong Ras activity in Ras activation assays, and therefore, Kras^{G12D} activity seems not to be impaired due to the fusion with ER^{T2}.

After successful targeting of the *LSL-KrasER^{T2}* to the murine *Rosa26* locus, mice were interbred with *Ptf1a$^{Cre/+}$* mice to specifically express *KrasER^{T2}* in the pancreas. By quantitative real-time PCR it was shown that *KrasER^{T2}* was expressed in a gene-dose dependent manner in *Ptf1a$^{Cre/+}$;LSL-Rosa26^{KE}* mice. Presence of the KrasER^{T2} fusion protein in pancreatic tissue samples was verified by Western blotting and its ability to bind its downstream interaction partner, Raf-1, was shown in Ras activation assay. Results from Western blots and the Ras activation assay displayed a strong increase of KrasER^{T2} protein level and Ras activity after tamoxifen treatment *in vitro* and *in vivo*. This is in concordance with previously published data, which describe stabilization of fusion proteins of Ras, MEK or Raf with LBD of the estrogen receptor (Samuels et al., 1993; Greulich and Erikson, 1998; De Vita et al., 2005). It remains to be determined whether an elevated KrasER^{T2} level and the observed increase in Ras activity due to tamoxifen treatment is sufficient to induce tumorigenesis. As seen in histological analysis of untreated *Pft1a$^{Cre/+}$;LSL-Rosa26^{KE}* mice, KrasER^{T2} is not sufficient to induce development of PanIN lesions or PDAC, even when interbred with the *LSL-Trp53^{R172H}* mice which accelerate tumor development in the Kras$^{G12D/+}$-dependent mouse model (Hingorani et al., 2005).

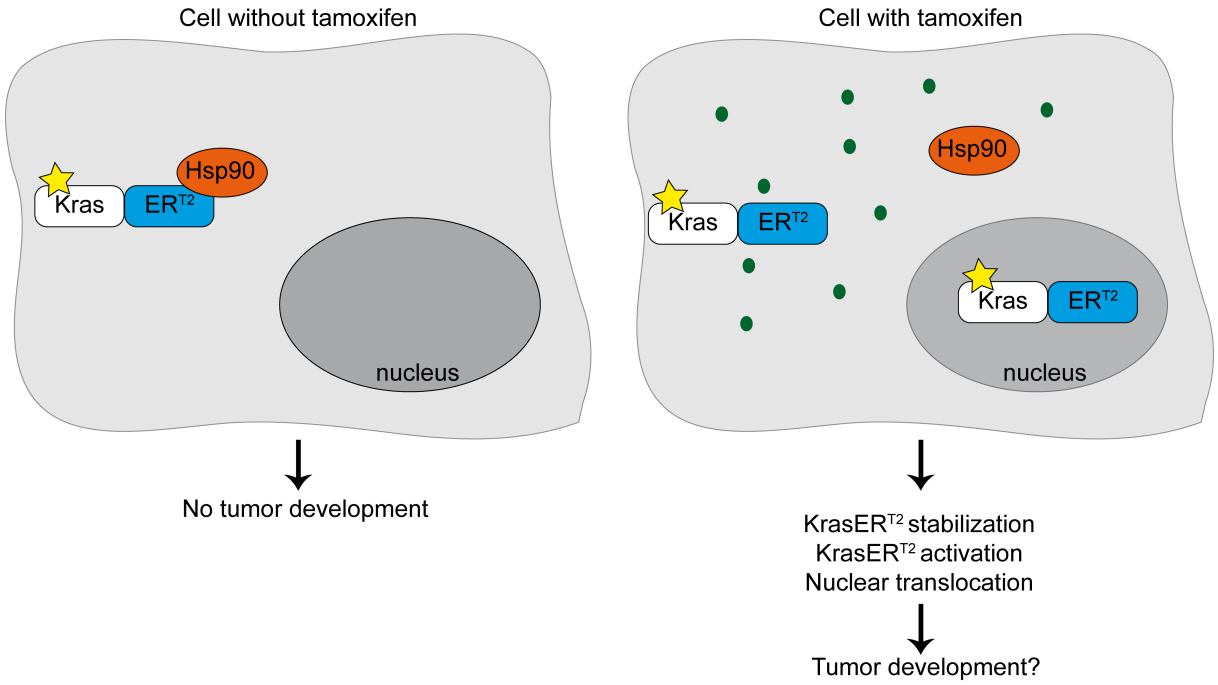

Figure 5-1: Schematic representation of KrasER^{T2} model: KrasER^{T2} is bound to Hsp90 in the absence of tamoxifen. Upon tamoxifen treatment, the KrasER^{T2} fusion protein gets stabilized. KrasER^{T2} is partly shuttled into the nucleus upon tamoxifen treatment (adapted from Leone et al., 2003).

According to these data, Kras^{G12D} protein abundance is increased and Ras activity is elevated by tamoxifen treatment rather than inactivated as proposed. In addition, a small amount of the KrasER^{T2} fusion protein can be shuttled into the nucleus by tamoxifen treatment. Therefore, a model as shown in Figure 5-1 is proposed. Without stabilization of the KrasER^{T2} fusion protein by tamoxifen treatment, Ras activity is insuffient to induce tumorigenesis. It remains to be determined whether stabilized KrasER^{T2} is sufficient for tumor development, despite partial translocation into the nucleus.

5.2. Bioluminescence Imaging of PDAC Development

Cancer development is a complicated process involving genetic changes, de-regulation of the immune system and modification of the surrounding tissue. Therefore, it is of high advantage to analyze the process of tumor development in real-time and in an intact organ system in living animals (Edinger et al., 1999). As bioluminescence imaging offers an easy to perform, non-invasive, sensitive and inexpensive method, it has recently been widely applied to study the intricate process

of tumor growth *in vivo.* Furthermore, as bioluminescence imaging is dependent on ATP, it reflects metabolically active cells (Jenkins et al., 2005).

Commonly used BLI systems are injection, orthotopic transplantation or subcutaneous transplantation of tumor cells which stably express *fLuc* from a constitutively active promoter (Jenkins et al., 2003; Saur et al., 2005; Miretti et al., 2008; Rehemtulla et al., 2000; Wetterwald et al., 2002; Klerk et al., 2007). These models enable non-invasive monitoring of tumor growth over a time course and show a direct correlation of luciferase output and tumor size (Mayr et al., 2008; Woolfenden et al., 2009). But it has to be taken into account that transplantation models do not completely resemble the naturally occurring situation in which tumor development is a stepwise process. Moreover, transplantation models use immunosuppressed mice. Therefore, tumor environment and immune system differ from the natural situation (Hawes and Reilly, 2010). There is a variety of transgenic mouse models that can be used as reporters. Buschow et al. conditionally expressed a SV40 Large T antigen-fLuc fusion protein under control of the *CAG* promoter to monitor oncogene expression (Buschow et al., 2010). Furthermore, Vooijs et al. put *fLuc* under the control of the *proopiomelanocortin* promoter to monitor Rb-dependent tumor development as *fLuc* is coexpressed with Cre recombinase which mediates expression of a mutated *Rb* in the pituitary gland (Vooijs et al., 2002). Still, these models can only address specific questions. Therefore, it was of interest to create more general reporter mouse strains. Lyons et al. created a Cre/loxP based transgenic model which expresses *fLuc* with a 5' transcriptional stop element flanked by *loxP* sites under control of the *β-actin* promoter and introduced it into pre-existing tumor mouse models (Lyons et al., 2003). Other approaches have been done by Safran et al. and Woolfenden et al. who placed *fLuc* under control of the constitutively active *Rosa26* or *CAG* promoter (Safran et al., 2003; Woolfenden et al., 2009). By silencing *fLuc* expression with transcriptional stop elements, expression can be directed to specific tissues. Even though it was shown that the luciferase signal is related to the tumor volume, it does not provide information about the proliferation status of the cells. To my knowledge, the only model which allows tissue-specific visualization of cell proliferation was published by the group around Eric Holland who monitored cell proliferation in a transgenic glioma mouse model. Therefore, *fLuc* expression is driven from the *E2F1* promoter. A drawback of this

model is that *E2F1-fLuc* mice display a high background signal as expression is not silenced by a transcriptional stop element (Uhrbom et al, 2004).

In our lab a reporter mouse model that enables visualizing of the proliferation state of the cells was generated. Therefore, *fLuc* was targeted to the endogenous *PCNA* locus. To take advantage of existing tumor models which express *Cre recombinase* under control of tissue-specific promoters, a transcriptional stop element was used to silence *fLuc* expression unless recombination takes place in targeted tissue. Thus, the *LSL-PCNA*$^{fLuc/+}$ mouse model can be interbred with *Cre/loxP* based (tumor) models of choice to monitor cell proliferation. In this thesis I set out to establish this reporter mouse model in context of the well-characterized Kras^{G12D}-dependent pancreatic tumor model.

I report that heterozygous deletion of *PCNA* did not impair normal development of any organ and of the whole body whereas homozygous deletion seems to be lethal during embryogenesis as PCNA is essential for DNA replication (Celis et al., 1987; Travali et al., 1989). Furthermore, I report that introduction of *fLuc* into the *PCNA* locus does not affect survival rates of *Pdx1-Cre;LSL-Kras*$^{G12D/+}$*;LSL-p53*$^{R172H/+}$ mice. Applying bioluminescence imaging *in vivo* and *ex vivo*, I showed that luciferase activity is restricted to tissue that expresses *Cre recombinase*.

After crossing *LSL-PCNA*$^{fLuc/+}$ into the endogenous Kras^{G12D}-dependent tumor mouse model, luciferase activity was determined before mice were sacrificed. However, in most mice weak or no obvious luciferase signal was detected *in vivo*. As a proof of principle I was able to show that it is possible to detect proliferation in pancreatic tumor cells as most mice with a clear luciferase signal displayed solid tumors. Although there is no direct comparison, the luciferase signal in PDAC mice appeared relatively low compared to endogenous models that express *fLuc* from a synthetic, constitutive active promoter (Lyons et al., 2003; Safran et al., 2003; Woolfenden et al., 2009). A limiting factor in BLI in pancreatic cancer might also be the lack of oxygen as it is described as hypoxic tumor (Duffy et al., 2003; Masamune et al., 2008).

In a recent publication from Zhang et al. it was shown that monitoring of pancreatic tumor is possible over a time course. They applied a double-transgenic mouse model of spontaneous pancreatic acinar cell carcinoma driven by SV40 T and t antigens (TAg) expression from a rat *elastase 1* promoter. Additionally, *fLuc* was driven from

the *elastase 1* promoter. Thus, they were able to label pancreatic tissue. Mice that developed tumors displayed a strong increase of luciferase activity. For the first time, they showed the possibility of *in vivo* bioluminescence imaging of tumors originating from the exocrine pancreas. Moreover, they were also able to show that luciferase activity stays at background level when animals were treated with rapamycin while luciferase signal increased with tumor size in untreated animals. In contrast to the *LSL-PCNA*$^{fLuc/+}$ PDAC mouse model presented in this thesis, Zhang et al. used the FVB/N strain, which has a white fur color (Zhang et al., 2009). In the *LSL-PCNA*$^{fLuc/+}$ PDAC model there is a tendency that mice with brown fur show higher luciferase signal compared to black fur. This is in concordance with data presented by Curtis et al. who studied the influence of fur and pigmentation on BLI and found that the signal can be attenuated up to 90% by pigmentation (Curtis et al., 2010). Thus, animals with bright hair are of advantage in bioluminescence imaging models. Alternatively, animals could be shaved to remove hair.

One major challenge of monitoring PDAC development in the murine model is the retroperitoneal localization of the pancreas. With each centimeter of tissue depth there is a 10-fold decrease of photon intensity (Sadikot and Blackwell, 2005). Therefore, it is easier to monitor tumors which are located closer to the surface and thus more accessible, e.g. gliomas which have been successfully monitored (Uhrbom et al., 2004). In literature several models are described which are able to visualize metastasis *in vivo*, but these models employ tail vein or intracardiac injection of tumor cells with stable expression of *fLuc* (Wetterwald et al., 2002; Jenkins et al., 2003; Saur et al., 2005). In our new model metastasis could not be observed by BLI in living animals.

In conclusion, location of the pancreas, the presence of fur and the strength of the *PCNA* promoter appeared as limiting factors for monitoring tumor development or early stage PDAC via bioluminescence imaging *in vivo*. However, a major advantage, the *LSL-PCNAfLuc/+* model enables monitoring of therapy response. When a luciferase signal of the tumor can be detected, it is possible to monitor changes in luciferase signal, and thus cell proliferation, within the same animal before and after treatment using each mouse as its own control. Providing the same conditions, e.g. food intake, these changes can be detected independently of fur color and location of the tumor and offer an enormous opportunity for surveillance of therapy response in

an endogenous system. Moreover, the *LSL-PCNA*$^{fLuc/+}$ model can be coupled to existing knock-in or knock-out mouse strains that apply the *Cre/loxP* system. Thus, it can be analyzed in the context of other mouse models and, therein, serve as reporter for cell proliferation *in vivo* in tumor development, inflammatory or developmental processes.

5.3. Development of a Versatile Screening Tool

Pancreatic cancer is a highly mortal disease and is mostly treated palliative as it is usually resistant to most conventional chemotherapies (Hingorani et al., 2003; Schneider et al., 2005; Chames et al., 2010). Hence, there is a tremendous need for the development of novel therapies. In drug screening two different approaches can be performed: biochemical assays or cell-based assays. In contrast to biochemical assays which employ isolated proteins, cell-based assays are aimed to identify drug candidates in a more physiological environment of a cell with intact regulatory networks and feedback control mechanisms (An and Tolliday, 2010). In common cell-based screening assays which apply bioluminescence imaging tumor cell lines are transiently or stably transfected with *fLuc* under control of a constitutive active promoter. In contrast, in our system mPCNA^{fLuc} cells express *fLuc* from the endogenous, proliferation-dependent *PCNA* locus. Thus, they offer a tool which enables, without any modification, direct access to proliferation state within the cell as a response to treatment. If desired, an additional reporter, e.g. *Renilla luciferase*, a *fLuc* mutant with a shifted emission wave length or a fluorescent protein, can be introduced into the cells by transfection or transduction for internal normalization or to address a different question within the same cell.

In this thesis, I present a versatile cell-based screening tool for identification and validation of novel drug targets. Murine PDAC of the genetically defined Kras^{G12D}-dependent mouse model served as a source for mPCNA^{fLuc} cell lines. I report that luciferase signal of isolated mPCNA^{fLuc} cells correlated exactly with cell number *in vitro* and tumor volume of subcutaneously transplanted mPCNA^{fLuc} cells *in vivo*. Furthermore, I was able to show that luciferase signal correlates with cell viability when treated with an inhibitor. By treatment with the PI3-kinase inhibitor LY294002 the luciferase signal was reduced, but upon LY294002 removal it increased up to level of controls. This clearly demonstrates that - in this system - it is possible to

distinguish between cytotoxic and cytostatic compounds in an easy-to-access way. Thus, mPCNA^{fLuc} cell lines provide a reproducible and reliable basis for the development of a screening platform for novel therapeutics.

PDAC is usually characterized by intratumoral heterogeneity (Hezel et al., 2006). Hence, mPCNA^{fLuc} cell lines isolated of PDAC resemble this heterogeneity as dispersed tumor cells, but not a clonal cell line was used. Furthermore, cell lines from different tumors can contain different genetic alterations. A large panel of mPCNA^{fLuc} cells with a multitude of genetic backgrounds offers an opportunity to assess overall treatment response and resistance mechanisms. I was able to report that mPCNA^{fLuc} cells used in experiments did not react uniformly to inhibitor treatment. Response differed in a time-dependent or drug-associated manner. Therefore, primary and also secondary resistance mechanisms can be investigated using this new model.

Although this approach was not further followed in this thesis, an advantage of the mPCNA^{fLuc} screening platform is that cell lines can be isolated from primary tumor, circulating tumor cells and metastasis of the same animal. This allows analysis of treatment response in primary tumor and corresponding metastasis via BLI.

Once a drug candidate is found, *in vivo* experiments are needed to validate results. Here, either the endogenous Kras^{G12D}-dependent, *LSL-PCNA$^{fLuc/+}$* PDAC model can be used or a subcutaneous or orthotopic transplantation model with mPCNA^{fLuc} cells. In contrast to most existing transplantation models, in which cancer cells need to be genetically modified before transplantation, mPCNA^{fLuc} cells can be transplanted without modification. As shown in preliminary results, orthotopic transplantation of mPCNA^{fLuc} cells can be applied for *in vivo* validation of drug candidates. Still, it is necessary to verify these results in larger cohorts.

In summary, mPCNA^{fLuc} cell lines offer a versatile screening tool which is reliable and reflects cellular proliferation state exactly. Assays are easy to perform and automatization is possible. mPCNA^{fLuc} cells mimic tumor heterogeneity and intertumoral variations and provide a unique possibility to access treatment response of primary tumor cells and corresponding metastasis via bioluminescence imaging.

5.4. Outlook

The understanding of PDAC development has advanced over last years, but it still leaves unanswered questions regarding the importance of Kras in tumor

maintenance. Furthermore, existing mouse models differ from the human disease as PDAC is an adult-onset disease in humans, but mouse models express the tumor-initiating *Kras*^{G12D} mutation already during embryonic development. In my thesis I present a new, tamoxifen-controllable mouse model, which is aimed to allow time- and dose-dependent modulation of Kras^{G12D} activity in the murine pancreas. I reported that KrasER^{T2} was not sufficient for tumorigenesis of PDAC in the absense of tamoxifen, even after introducing an additional Trp53 mutation. As we observed a stabilization and activation of KrasER^{T2} upon tamoxifen treatment, histological analysis of tamoxifen treated mice will clearify whether the stabilization and activation of KrasER^{T2} by tamoxifen leads to Kras activity levels which are sufficient for tumor initiation. Furthermore, investigation of different downstream targets of Kras *in vitro* and *in vivo* with and without tamoxifen treatment will identify Kras activated pathways, e.g. the Raf/MEK/Erk pathway, the PI3-kinase/Akt pathway, RALGDS and PLCε (Downward, 2003).

In order to monitor PDAC development and its response to targeted therapeutics, I evaluated a novel proliferation-dependent bioluminescence imaging mouse model, *LSL-PCNA*$^{fLuc/+}$. Although monitoring of PDAC development seems to be limited by location of the pancreas and the presence of dark fur in our model, the *LSL-PCNA*$^{fLuc/+}$ mouse model could be of great advantage in other mouse models that apply the *Cre/loxP* system. Moreover, when *LSL-PCNA*$^{fLuc/+}$ is crossed into *Cre/loxP* dependent tumor models, it is possible to generate screening platforms for testing of novel drugs, as described in this thesis.

First results indicate that orthotopic transplantation of mPCNA^{fLuc} cell lines enables monitoring of therapy response *in vivo*. These results have to be verified by transplantation of various cell lines and by treatment with several inhibitors. Additionally, the *LSL-PCNA*$^{fLuc/+}$ strain could be interbred with mice of bright fur color or, alternatively, be shaved to improve bioluminescence imaging results of PDAC development. Once this is achieved, treatment response can be monitored in the endogenous system. This would be of great benefit, as the endogenous system resembles the human disease more accurately than the transplantation model as mice have an intact immune system.

Furthermore, using a large panel of different isolated mPCNA^{fLuc} cell lines, it is possible to screen for novel drugs which act independently of the genetic alterations and which inhibit growth in both primary tumor and metastasis.

Last but not least, it would be of great interest to translate these results into other (tumor) models. The *LSL-PCNA*$^{fLuc/+}$ mouse offers a unique and universally applicable tool for cancer research and for the surveillance of developmental processes, tissue regeneration and inflammatory processes by bioluminescence imaging *in vivo*. Along the line, as shown within this thesis, it can serve as a source for *fLuc* expressing (tumor) cell lines which allow efficient, quick and inexpensive screening for novel drug targets along with the possibility to directly assess *in vivo* effects of drug candidates.

6 Summary

Pancreatic cancer is among the leading causes of cancer related death with an extremely poor five-year survival rate. Mouse models have opened a window to dissect the complex process of pancreatic ductal adenocarcinoma (PDAC) development. Although our knowledge has tremendously increased, treatment is mostly restricted to palliative care and new therapy strategies are desperately needed.

We set out to analyze the influence of adult-onset of *Kras*^{G12D} expression and the impact of Kras on tumor maintenance. We report the generation and characterization of a mouse strain, wherein *Kras*^{G12D} was fused to a mutated ligand binding domain of the estrogen receptor (KrasER^{T2}) and knocked into the murine *Rosa26* locus. Expression is silenced by a 5' transcriptional stop element flanked by *loxP* sites. *In vitro* experiments showed a dose-dependent shuttling of KrasER^{T2} into the nucleus upon 4-hydroxytamoxifen treatment. KrasER^{T2} was expressed in a gene-dose-dependent manner in *Ptf1a*$^{Cre/+}$*;LSL-Rosa26*^{KE} mice and was detected via Ras activation assay and Western blotting. Tamoxifen treatment lead to stabilization and activation of KrasER^{T2} *in vitro* and *in vivo*. As *Ptf1a*$^{Cre/+}$*;LSL-Rosa26*^{KE} mice failed to develop PanINs or PDAC in the absence of tamoxifen, it remains to be determined whether stabilization and activation of KrasER^{T2} by tamoxifen treatment is sufficient to induce tumorigenesis.

To monitor the impact of Kras^{G12D} at certain stages of PDAC development *in vivo*, we established the *LSL-PCNA*$^{fLuc/+}$ reporter mouse strain. *LSL-PCNA*$^{fLuc/+}$ mice carry *firefly luciferase* (*fLuc*) with a 5' floxed transcriptional stop element under control of the *proliferating cell nuclear antigen* (*PCNA)* promoter. The model was interbred with the genetically defined Kras^{G12D}-dependent PDAC model. *In vivo* bioluminescence imaging (BLI) displayed proliferative activity in the pancreas upon tissue-specific Cre recombination. Luciferase activity in mPCNA^{fLuc} cell lines, isolated from PDAC, correlated exactly with cell viability and cell number *in vitro* and tumor volume *in vivo*. Dose-dependent inhibition of proliferation was visualized by BLI in a cell-based screening assay with inhibitors of different signaling pathways and results were verified in an orthotopic transplantation model.

Thus, the LSL-PCNA$^{fLuc/+}$ reporter is a versatile tool for *in vivo* imaging of proliferation in *Cre/loxP* based models and enables the development of cell-based screening platforms with the ability to perform direct *in vivo* validation of drug candidates in

orthotopic transplantation models and genetically engineered endogenous mouse models.

7 Zusammenfassung

Mit einer extrem geringen Überlebensrate gehört das Pankreaskarzinom zu den führenden tumorassoziierten Todesursachen. Obwohl in den letzten Jahren das Wissen über die Entstehung des duktalen Pankreasadenokarzinoms immens gestiegen ist, bleiben noch Fragen offen. Darüber hinaus fehlen effiziente Therapeutika, die eine Behandlung über die palliative Versorgung hinaus ermöglichen.

Im Rahmen dieser Arbeit sollte der Einfluss der $Kras^{G12D}$ Expression in adulten Tieren sowie die $Kras^{G12D}$ Abhängigkeit etablierter Tumore analysiert werden. Generiert und charakterisiert wurde eine Mauslinie, in welcher ein Fusionsprotein aus $Kras^{G12D}$ und der mutierten Ligandenbindedomäne des humanen Östrogenrezeptors ($KrasER^{T2}$) durch homologe Rekombination in den murinen *Rosa26* Lokus eingebracht wurde. Durch eine 5' gelegene gefloxte Transkriptionsstopkassette wurde die Expression von $KrasER^{T2}$ verhindert. *In vitro* Versuche zeigten, dass $KrasER^{T2}$ durch die Zugabe von 4-Hydroxytamoxifen dosisabhängig in den Zellkern transportiert wird. $KrasER^{T2}$ wurde im Pankreas von $Ptf1a^{Cre/+};LSL\text{-}Rosa26^{KE}$ Mäusen gendosisabhängig exprimiert und konnte mit Ras-Aktivitätsassay und Western Blot nachgewiesen werden. Die Behandlung mit Tamoxifen führte *in vitro* und *in vivo* zu einer Stabilisierung und Aktivierung von $KrasER^{T2}$. Da $Ptf1a^{Cre/+};LSL\text{-}Rosa26^{KE}$ Mäuse ohne Tamoxifenbehandlung keine PanINs oder PDAC entwickelten, sollte des Weiteren untersucht werden, ob eine Stabilisierung des $KrasER^{T2}$ durch Tamoxifenbehandlung ausreichend ist, um die Tumorigenese zu initiieren.

Um den Einfluss von $Kras^{G12D}$ auf die PDAC Entstehung *in vivo* zu monitoren, etablierten wir die $LSL\text{-}PCNA^{fLuc/+}$ Reportermaus. In dieser Mauslinie wurde die *firefly luciferase* (*fLuc*) mit einem gefloxten 5' Transkriptionsstopelement (LSL) durch homologe Rekombination in den *proliferating cell nuclear antigen* (*PCNA)* Lokus eingebracht. Das Modell wurde mit dem genetisch definierten $Kras^{G12D}$ -abhängigen PDAC Modell verkreuzt. Nach Rekombination zeigten *in vivo* Biolumineszenzaufnahmen (BLI) eine pankreasspezifische Proliferation. Die Luciferaseaktivität isolierter Zellen ($mPCNA^{fLuc}$) korrelierte exakt mit der Zellzahl und -viabilität *in vitro* und mit dem Tumorvolumen *in vivo*. Eine dosisabhängige Inhibition der Proliferation durch verschieden Therapeutika wurde in einer zellbasierten Screeningplattform via BLI gezeigt und im orthotopen Transplantationsmodell

bestätigt. Das Model ermöglich es, den Effekt neuer Therapeutika auf die Proliferation der Tumoren *in vivo* zu untersuchen.

Die *LSL-PCNA*$^{fLuc/+}$ Reportermaus bietet somit ein vielseitiges Werkzeug für die *in vivo* Bildgebung von Proliferation in *Cre/loxP* basierten Mausmodellen und ermöglicht die Entwicklung zellbasierter Screeningplattformen für neue Therapeutika mit der Möglichkeit, potentielle Kandidaten direkt *in vivo* zu validieren.

8 Acknowledgements

First of all, I want to thank everyone who supported my PhD research and me during the last few years.

I want to thank Prof. Dr. Roland Schmid for offering the opportunity to do my PhD research in his department at the Klinikum rechts der Isar.

For taking over my external PhD supervision, I want to sincerely thank Prof. Dr. Angelika Schnieke. I also want to thank Prof. Dr. Angelika Schnieke for her strong support and the scientific discussion and input, which helped me very much.

Above all, I want to thank PD Dr. Dieter Saur for offering this extremely interesting topic. I want to thank him for giving me the opportunity to do my PhD research in his group. While working in his lab he supported me in any possible way and our scientific discussions were always fruitful. I learned a lot for my PhD thesis and for my scientific life.

For scientific discussion and input I want to thank Barbara Seidler. For excellent technical support I want to thank Uschi Götz, Kornelia Fritsch, Marco Göbel and Miriam Schiller. I also want to thank the animal keepers for taking good care of my animals.

I want to thank the whole Saur lab, Schneider lab and Vogelmann lab for the great working atmosphere over the years. For helpful scientific discussion and warm words I want to especially thank Mariel Paul, Anne Gohlke, Annika Henrich, Petra Fritsche, Sylvia Steininger and Viktoria Doll.

For reading this manuscript I want to thank Mariel Paul, Silke Huber and Petra Fritsche.

I want to thank my whole family, Florian's family and all of my friends, especially Eva, Mariel, Moni und Silke, for their support and their belief in my work and me. Your encouraging words pushed me forward in quite a few occasions.

By heart, I want to thank Florian Annetzberger for being at my side, for supporting me and for finding the right words at the right times to keep me going on. Without understanding a word of what I was talking/writing about, you helped me a great deal in successfully finishing this thesis. Thank you so much!

9 Declaration

Hiermit erkläre ich, dass ich die vorliegende Doktorarbeit selbständig angefertigt habe. Es wurden nur die in der Arbeit ausdrücklich benannten Quellen und Hilfsmittel benutzt. Wörtlich oder sinngemäß übernommenes Gedankengut habe ich als solches kenntlich gemacht.

_____ _____

Ort, Datum Unterschrift

10 References

Aguirre, A. J., N. Bardeesy, M. Sinha, L. Lopez, D. A. Tuveson, J. Horner, M. S. Redston and R. A. DePinho (2003). "Activated Kras and Ink4a/Arf deficiency cooperate to produce metastatic pancreatic ductal adenocarcinoma." Genes Dev **17**: 3112-26.

An, W. F. and N. Tolliday (2010). "Cell-based assays for high-throughput screening." Molecular biotechnology **45**(2): 180-6.

Angst, E., M. Chen, M. Mojadidi, O. J. Hines, H. A. Reber and G. Eibl (2010). "Bioluminescence imaging of angiogenesis in a murine orthotopic pancreatic cancer model." Mol Imaging Biol **12**(6): 570-5.

Arnold, M. A. and M. Goggins (2001). "BRCA2 and predisposition to pancreatic and other cancers." Exp. Rev. Mol. Med. **14**: 1-10.

Bar-Sagi, D. (2001). "A Ras by any other name." Molecular and cellular biology **21**(5): 1441-3.

Barbacid, M. (1987). "ras genes." Annual review of biochemistry **56**: 779-827.

Bardeesy, N., K. H. Cheng, J. H. Berger, G. C. Chu, J. Pahler, P. Olson, A. F. Hezel, J. Horner, G. Y. Lauwers, D. Hanahan and R. A. DePinho (2006). "Smad4 is dispensable for normal pancreas development yet critical in progression and tumor biology of pancreas cancer." Genes Dev **20**: 3130-46.

Bardeesy, N. and R. A. DePinho (2002). "Pancreatic cancer biology and genetics." Nat Rev Cancer **2**: 897-909.

Bondar, V. M., B. Sweeney-Gotsch, M. Andreeff, G. B. Mills and D. J. McConkey (2002). "Inhibition of the phosphatidylinositol 3'-kinase-AKT pathway induces apoptosis in pancreatic carcinoma cells in vitro and in vivo." Molecular cancer therapeutics **1**(12): 989-97.

Boschman, C. R., S. Stryker, J. K. Reddy and M. S. Rao (1994). "Expression of p53 protein in precursor lesions and adenocarcinoma of human pancreas." The American journal of pathology **145**(6): 1291-5.

Brembeck, F. H., F. S. Schreiber, T. B. Deramaudt, L. Craig, B. Rhoades, G. Swain, P. Grippo, D. A. Stoffers, D. G. Silberg and A. K. Rustgi (2003). "The mutant K-ras oncogene causes pancreatic periductal lymphocytic infiltration and gastric mucous neck cell hyperplasia in transgenic mice." Cancer research **63**(9): 2005-9.

Burnette, W. N. (1981). ""Western blotting": electrophoretic transfer of proteins from sodium dodecyl sulfate--polyacrylamide gels to unmodified nitrocellulose and radiographic detection with antibody and radioiodinated protein A." Analytical biochemistry **112**(2): 195-203.

Buschow, C., J. Charo, K. Anders, C. Loddenkemper, A. Jukica, W. Alsamah, C. Perez, G. Willimsky and T. Blankenstein (2010). "In vivo imaging of an inducible oncogenic tumor antigen visualizes tumor progression and predicts CTL tolerance." J Immunol **184**: 2930-8.

Celis, J. E., P. Madsen, A. Celis, H. V. Nielsen and B. Gesser (1987). "Cyclin (PCNA, auxiliary protein of DNA polymerase delta) is a central component of the pathway(s) leading to DNA replication and cell division." FEBS Lett **220**: 1-7.

Chames, P., B. Kerfelec and D. Baty (2010). "Therapeutic antibodies for the treatment of pancreatic cancer." TheScientificWorldJournal **10**: 1107-20.

Contag, C. H. (2007). "In vivo pathology: seeing with molecular specificity and cellular resolution in the living body." Annual review of pathology **2**: 277-305.

Contag, C. H. and M. H. Bachmann (2002). "Advances in in vivo bioluminescence imaging of gene expression." Annu Rev Biomed Eng **4**: 235-60.

Contag, C. H. and B. D. Ross (2002). "It's not just about anatomy: in vivo bioluminescence imaging as an eyepiece into biology." Journal of magnetic resonance imaging : JMRI **16**(4): 378-87.

Curtis, A., K. Calabro, J. R. Galarneau, I. J. Bigio and T. Krucker (2010). "Temporal Variations of Skin Pigmentation in C57Bl/6 Mice Affect Optical Bioluminescence Quantitation." Molecular imaging and biology : MIB : the official publication of the Academy of Molecular Imaging: Epub ahead of print.

Danielian, P. S., D. Muccino, D. H. Rowitch, S. K. Michael and A. P. McMahon (1998). "Modification of gene activity in mouse embryos in utero by a tamoxifen-inducible form of Cre recombinase." Curr Biol **8**: 1323-6.

De Vita, G., L. Bauer, V. M. da Costa, M. De Felice, M. G. Baratta, M. De Menna and R. Di Lauro (2005). "Dose-dependent inhibition of thyroid differentiation by RAS oncogenes." Mol Endocrinol **19**(1): 76-89.

Dothager, R. S., K. Flentie, B. Moss, M. H. Pan, A. Kesarwala and D. Piwnica-Worms (2009). "Advances in bioluminescence imaging of live animal models." Curr Opin Biotechnol **20**(1): 45-53.

Downward, J. (2003). "Targeting RAS signalling pathways in cancer therapy." Nat Rev Cancer **3**: 11-22.

Duffy, J. P., G. Eibl, H. A. Reber and O. J. Hines (2003). "Influence of hypoxia and neoangiogenesis on the growth of pancreatic cancer." Molecular cancer **2**: 12.

Edinger, M., T. J. Sweeney, A. A. Tucker, A. B. Olomu, R. S. Negrin and C. H. Contag (1999). "Noninvasive assessment of tumor cell proliferation in animal models." Neoplasia **1**(4): 303-10.

Eisenberg, S., K. Giehl, Y. I. Henis and M. Ehrlich (2008). "Differential interference of chlorpromazine with the membrane interactions of oncogenic K-Ras and its effects on cell growth." J Biol Chem **283**: 27279-88.

Feil, R., J. Brocard, B. Mascrez, M. LeMeur, D. Metzger and P. Chambon (1996). "Ligand-activated site-specific recombination in mice." Proceedings of the National Academy of Sciences of the United States of America **93**(20): 10887-90.

Feldmann, A. M. and D. McNamara (2000). "Myocarditis." N Engl J Med **343**(19): 1388-1398.

Fisher, G. H., S. Orsulic, E. Holland, W. P. Hively, Y. Li, B. C. Lewis, B. O. Williams and H. E. Varmus (1999). "Development of a flexible and specific gene delivery system for production of murine tumor models." Oncogene **18**(38): 5253-60.

Ghaneh, P., E. Costello and J. P. Neoptolemos (2007). "Biology and management of pancreatic cancer." Gut **56**: 1134-52.

Gidekel Friedlander, S. Y., G. C. Chu, E. L. Snyder, N. Girnius, G. Dibelius, D. Crowley, E. Vasile, R. A. DePinho and T. Jacks (2009). "Context-dependent transformation of adult pancreatic cells by oncogenic K-Ras." Cancer Cell **16**: 379-89.

Greulich, H. and R. L. Erikson (1998). "An analysis of Mek1 signaling in cell proliferation and transformation." J Biol Chem **273**(21): 13280-8.

Grippo, P. J., P. S. Nowlin, M. J. Demeure, D. S. Longnecker and E. P. Sandgren (2003). "Preinvasive pancreatic neoplasia of ductal phenotype induced by acinar cell targeting of mutant Kras in transgenic mice." Cancer research **63**(9): 2016-9.

Gross, S. and D. Piwnica-Worms (2005). "Spying on cancer: molecular imaging in vivo with genetically encoded reporters." Cancer Cell **7**: 5-15.

Guerra, C., A. J. Schuhmacher, M. Canamero, P. J. Grippo, L. Verdaguer, L. Perez-Gallego, P. Dubus, E. P. Sandgren and M. Barbacid (2007). "Chronic pancreatitis is essential for induction of pancreatic ductal adenocarcinoma by K-Ras oncogenes in adult mice." Cancer Cell **11**: 291-302.

Guz, Y., M. R. Montminy, R. Stein, J. Leonard, L. W. Gamer, C. V. Wright and G. Teitelman (1995). "Expression of murine STF-1, a putative insulin gene transcription factor, in beta cells of pancreas, duodenal epithelium and pancreatic exocrine and endocrine progenitors during ontogeny." Development **121**(1): 11-8.

Hancock, J. F., H. Paterson and C. J. Marshall (1990). "A polybasic domain or palmitoylation is required in addition to the CAAX motif to localize p21ras to the plasma membrane." Cell **63**: 133-9.

Hawes, J. J. and K. M. Reilly (2010). "Bioluminescent approaches for measuring tumor growth in a mouse model of neurofibromatosis." Toxicol Pathol **38**: 123-30.

Hezel, A. F., A. C. Kimmelman, B. Z. Stanger, N. Bardeesy and R. A. Depinho (2006). "Genetics and biology of pancreatic ductal adenocarcinoma." Genes Dev **20**: 1218-49.

Hingorani, S. R., E. F. Petricoin, A. Maitra, V. Rajapakse, C. King, M. A. Jacobetz, S. Ross, T. P. Conrads, T. D. Veenstra, B. A. Hitt, Y. Kawaguchi, D. Johann, L. A. Liotta, H. C. Crawford, M. E. Putt, T. Jacks, C. V. Wright, R. H. Hruban, A. M. Lowy and D. A. Tuveson (2003). "Preinvasive and invasive ductal pancreatic cancer and its early detection in the mouse." Cancer Cell **4**: 437-50.

Hingorani, S. R., L. Wang, A. S. Multani, C. Combs, T. B. Deramaudt, R. H. Hruban, A. K. Rustgi, S. Chang and D. A. Tuveson (2005). "Trp53R172H and KrasG12D cooperate to promote chromosomal instability and widely metastatic pancreatic ductal adenocarcinoma in mice." Cancer Cell **7**: 469-83.

Hruban, R. H., N. V. Adsay, J. Albores-Saavedra, C. Compton, E. S. Garrett, S. N. Goodman, S. E. Kern, D. S. Klimstra, G. Kloppel, D. S. Longnecker, J. Luttges and G. J. Offerhaus (2001). "Pancreatic intraepithelial neoplasia: a new nomenclature and classification system for pancreatic duct lesions." The American journal of surgical pathology **25**(5): 579-86.

Hruban, R. H., M. Goggins, J. Parsons and S. E. Kern (2000). "Progression model for pancreatic cancer." Clinical cancer research : an official journal of the American Association for Cancer Research **6**(8): 2969-72.

Hsieh, C. L., Z. Xie, Z. Y. Liu, J. E. Green, W. D. Martin, M. W. Datta, F. Yeung, D. Pan and L. W. Chung (2005). "A luciferase transgenic mouse model: visualization of prostate development and its androgen responsiveness in live animals." J Mol Endocrinol **35**: 293-304.

Ijichi, H., A. Chytil, A. E. Gorska, M. E. Aakre, Y. Fujitani, S. Fujitani, C. V. Wright and H. L. Moses (2006). "Aggressive pancreatic ductal adenocarcinoma in mice caused by pancreas-specific blockade of transforming growth factor-beta signaling in cooperation with active Kras expression." Genes Dev **20**: 3147-60.

Iseki, H., T. C. Ko, X. Y. Xue, A. Seapan and C. M. Townsend, Jr. (1998). "A novel strategy for inhibiting growth of human pancreatic cancer cells by blocking cyclin-dependent kinase activity." J Gastrointest Surg **2**: 36-43.

Jackson, E. L., N. Willis, K. Mercer, R. T. Bronson, D. Crowley, R. Montoya, T. Jacks and D. A. Tuveson (2001). "Analysis of lung tumor initiation and progression

using conditional expression of oncogenic K-ras." Genes & development **15**(24): 3243-8.

Jemal, A., R. Siegel, J. Xu and E. Ward (2010). "Cancer statistics, 2010." CA Cancer J Clin **60**: 277-300.

Jenkins, D. E., Y. S. Hornig, Y. Oei, J. Dusich and T. Purchio (2005). "Bioluminescent human breast cancer cell lines that permit rapid and sensitive in vivo detection of mammary tumors and multiple metastases in immune deficient mice." Breast Cancer Res **7**: R444-54.

Jenkins, D. E., Y. Oei, Y. S. Hornig, S. F. Yu, J. Dusich, T. Purchio and P. R. Contag (2003). "Bioluminescent imaging (BLI) to improve and refine traditional murine models of tumor growth and metastasis." Clinical & experimental metastasis **20**(8): 733-44.

Jurk, M. (1998), F. Lottspeich, H. Zorbas. Bioanalytik.1.Auflage, pp 626-628. Heidelberg, Berin, Spektrum, Akademischer Verlag.

Kawaguchi, Y., B. Cooper, M. Gannon, M. Ray, R. J. MacDonald and C. V. Wright (2002). "The role of the transcriptional regulator Ptf1a in converting intestinal to pancreatic progenitors." Nat Genet **32**: 128-34.

Kim, J. B., K. Urban, E. Cochran, S. Lee, A. Ang, B. Rice, A. Bata, K. Campbell, R. Coffee, A. Gorodinsky, Z. Lu, H. Zhou, T. K. Kishimoto and P. Lassota (2010). "Non-invasive detection of a small number of bioluminescent cancer cells in vivo." PloS one **5**(2): e9364.

Klerk, C. P., R. M. Overmeer, T. M. Niers, H. H. Versteeg, D. J. Richel, T. Buckle, C. J. Van Noorden and O. van Tellingen (2007). "Validity of bioluminescence measurements for noninvasive in vivo imaging of tumor load in small animals." Biotechniques **43**: 7-13, 30.

Kojima, K., S. M. Vickers, N. V. Adsay, N. C. Jhala, H. G. Kim, T. R. Schoeb, W. E. Grizzle and C. A. Klug (2007). "Inactivation of Smad4 accelerates Kras(G12D)-mediated pancreatic neoplasia." Cancer Res **67**: 8121-30.

Le Tourneau, C., E. Raymond and S. Faivre (2007). "Sunitinib: a novel tyrosine kinase inhibitor. A brief review of its therapeutic potential in the treatment of renal carcinoma and gastrointestinal stromal tumors (GIST)." Ther Clin Risk Manag **3**(2): 341-8.

Leach, S. D. (2004). "Mouse models of pancreatic cancer: the fur is finally flying!" Cancer Cell **5**(1): 7-11.

Leipner, C., K. Grün, I. Schneider, B. Glück, H. H. Sigusch and A. Stelzner (2004). "Coxsackievirus B3- induced myocarditis: differences in the immune response of C57BL/6 and Balb/c mice." Med Microbiol Immunol **193**: 141-147.

Lemmen, J. G., R. J. Arends, A. L. van Boxtel, P. T. van der Saag and B. van der Burg (2004). "Tissue- and time-dependent estrogen receptor activation in estrogen reporter mice." Journal of molecular endocrinology **32**(3): 689-701.

Leone, D. P., S. Genoud, S. Atanasoski, R. Grausenburger, P. Berger, D. Metzger, W. B. Macklin, P. Chambon and U. Suter (2003). "Tamoxifen-inducible glia-specific Cre mice for somatic mutagenesis in oligodendrocytes and Schwann cells." Mol Cell Neurosci **22**: 430-40.

Lin, J. W., A. V. Biankin, M. E. Horb, B. Ghosh, N. B. Prasad, N. S. Yee, M. A. Pack and S. D. Leach (2004). "Differential requirement for ptf1a in endocrine and exocrine lineages of developing zebrafish pancreas." Developmental biology **274**(2): 491-503.

Lu, Y. Y., D. D. Jing, M. Xu, K. Wu and X. P. Wang (2008). "Anti-tumor activity of erlotinib in the BxPC-3 pancreatic cancer cell line." World journal of gastroenterology : WJG **14**(35): 5403-11.

Lyons, S. K., R. Meuwissen, P. Krimpenfort and A. Berns (2003). "The generation of a conditional reporter that enables bioluminescence imaging of Cre/loxP-dependent tumorigenesis in mice." Cancer research **63**(21): 7042-6.

Maitra, A., N. V. Adsay, P. Argani, C. Iacobuzio-Donahue, A. De Marzo, J. L. Cameron, C. J. Yeo and R. H. Hruban (2003). "Multicomponent analysis of the pancreatic adenocarcinoma progression model using a pancreatic intraepithelial neoplasia tissue microarray." Modern pathology : an official journal of the United States and Canadian Academy of Pathology, Inc **16**(9): 902-12.

Maitra, A. and R. H. Hruban (2008). "Pancreatic cancer." Annual review of pathology **3**: 157-88.

Masamune, A., K. Kikuta, T. Watanabe, K. Satoh, M. Hirota and T. Shimosegawa (2008). "Hypoxia stimulates pancreatic stellate cells to induce fibrosis and angiogenesis in pancreatic cancer." Am J Physiol Gastrointest Liver Physiol **295**: G709-17.

Mayr, U., A. von Werder, B. Seidler, W. Reindl, M. Bajbouj, R. M. Schmid, G. Schneider and D. Saur (2008). "RCAS-mediated retroviral gene delivery: a versatile tool for the study of gene function in a mouse model of pancreatic cancer." Human gene therapy **19**(9): 896-906.

Milewski, W. M., S. J. Duguay, S. J. Chan and D. F. Steiner (1998). "Conservation of PDX-1 structure, function, and expression in zebrafish." Endocrinology **139**(3): 1440-9.

Miller, C. P., R. E. McGehee, Jr. and J. F. Habener (1994). "IDX-1: a new homeodomain transcription factor expressed in rat pancreatic islets and duodenum that transactivates the somatostatin gene." The EMBO journal **13**(5): 1145-56.

Miretti, S., I. Roato, R. Taulli, C. Ponzetto, M. Cilli, M. Olivero, M. F. Di Renzo, L. Godio, A. Albini, P. Buracco and R. Ferracini (2008). "A mouse model of pulmonary metastasis from spontaneous osteosarcoma monitored in vivo by Luciferase imaging." PloS one **3**(3): e1828.

Mosmann, T. (1983). "Rapid colorimetric assay for cellular growth and survival: application to proliferation and cytotoxicity assays." J Immunol Methods **65**: 55-63.

Nakhai, H., S. Sel, J. Favor, L. Mendoza-Torres, F. Paulsen, G. I. Duncker and R. M. Schmid (2007). "Ptf1a is essential for the differentiation of GABAergic and glycinergic amacrine cells and horizontal cells in the mouse retina." Development **134**: 1151-60.

Neoptolemos, J. P., D. D. Stocken, H. Friess, C. Bassi, J. A. Dunn, H. Hickey, H. Beger, L. Fernandez-Cruz, C. Dervenis, F. Lacaine, M. Falconi, P. Pederzoli, A. Pap, D. Spooner, D. J. Kerr and M. W. Buchler (2004). "A randomized trial of chemoradiotherapy and chemotherapy after resection of pancreatic cancer." N Engl J Med **350**(12): 1200-10.

O'Gorman, S., N. A. Dagenais, M. Qian and Y. Marchuk (1997). "Protamine-Cre recombinase transgenes efficiently recombine target sequences in the male germ line of mice, but not in embryonic stem cells." Proceedings of the National Academy of Sciences of the United States of America **94**(26): 14602-7.

Offield, M. F., T. L. Jetton, P. A. Labosky, M. Ray, R. W. Stein, M. A. Magnuson, B. L. Hogan and C. V. Wright (1996). "PDX-1 is required for pancreatic outgrowth and differentiation of the rostral duodenum." Development **122**(3): 983-95.

Ohlsson, H., K. Karlsson and T. Edlund (1993). "IPF1, a homeodomain-containing transactivator of the insulin gene." The EMBO journal **12**(11): 4251-9.

Prescher, J. A. and C. H. Contag (2010). "Guided by the light: visualizing biomolecular processes in living animals with bioluminescence." Curr Opin Chem Biol **14**: 80-89.

Raynaud, F. I., S. Eccles, P. A. Clarke, A. Hayes, B. Nutley, S. Alix, A. Henley, F. Di-Stefano, Z. Ahmad, S. Guillard, L. M. Bjerke, L. Kelland, M. Valenti, L. Patterson, S. Gowan, A. de Haven Brandon, M. Hayakawa, H. Kaizawa, T. Koizumi, T. Ohishi, S. Patel, N. Saghir, P. Parker, M. Waterfield and P. Workman (2007). "Pharmacologic characterization of a potent inhibitor of class I phosphatidylinositide 3-kinases." Cancer Res **67**: 5840-50.

Rehemtulla, A., L. D. Stegman, S. J. Cardozo, S. Gupta, D. E. Hall, C. H. Contag and B. D. Ross (2000). "Rapid and quantitative assessment of cancer treatment response using in vivo bioluminescence imaging." Neoplasia **2**(6): 491-5.

Rose, N. R. and S. L. Hill (1996). "The pathogenesis of postinfectious myocarditis." Clin Immunol Immunopathol **80**(3): S92-S99.

Rozenblum, E., M. Schutte, M. Goggins, S. A. Hahn, S. Panzer, M. Zahurak, S. N. Goodman, T. A. Sohn, R. H. Hruban, C. J. Yeo and S. E. Kern (1997). "Tumor-suppressive pathways in pancreatic carcinoma." Cancer research **57**(9): 1731-4.

Sadikot, R. T. and T. S. Blackwell (2005). "Bioluminescence imaging." Proc Am Thorac Soc **2**: 537-40, 511-2.

Safran, M., W. Y. Kim, A. L. Kung, J. W. Horner, R. A. DePinho and W. G. Kaelin, Jr. (2003). "Mouse reporter strain for noninvasive bioluminescent imaging of cells that have undergone Cre-mediated recombination." Molecular imaging : official journal of the Society for Molecular Imaging **2**(4): 297-302.

Samuels, M. L., M. J. Weber, J. M. Bishop and M. McMahon (1993). "Conditional transformation of cells and rapid activation of the mitogen-activated protein kinase cascade by an estradiol-dependent human raf-1 protein kinase." Mol Cell Biol **13**(10): 6241-52.

Sato, A., B. Klaunberg and R. Tolwani (2004). "In vivo bioluminescence imaging." Comparative medicine **54**(6): 631-4.

Saur, D., B. Seidler, G. Schneider, H. Algul, R. Beck, R. Senekowitsch-Schmidtke, M. Schwaiger and R. M. Schmid (2005). "CXCR4 expression increases liver and lung metastasis in a mouse model of pancreatic cancer." Gastroenterology **129**: 1237-50.

Schneider, G., J. T. Siveke, F. Eckel and R. M. Schmid (2005). "Pancreatic cancer: basic and clinical aspects." Gastroenterology **128**(6): 1606-25.

Seidler, B., A. Schmidt, U. Mayr, H. Nakhai, R. M. Schmid, G. Schneider and D. Saur (2008). "A Cre-loxP-based mouse model for conditional somatic gene expression and knockdown in vivo by using avian retroviral vectors." Proc Natl Acad Sci U S A **105**: 10137-42.

Southern, E. M. (1975). "Detection of specific sequences among DNA fragments separated by gel electrophoresis." Journal of Molecular Biology **98**(3): 503-517.

Spibey, C. A., P. Jackson and K. Herick (2001). "A unique charge-coupled device/xenon arc lamp based imaging system for the accurate detection and quantitation of multicolour fluorescence." Electrophoresis **22**: 829-36.

Stephen J. Taylor, R. J. R., David Shalloway (2001). "Nonradioactive Determination of RAs-GTP levels Using Activated Ras Interaction Assay." Methods Enzymology **333**: 333-342.

Tao, W., J. P. Davide, M. Cai, G. J. Zhang, V. J. South, A. Matter, B. Ng, Y. Zhang and L. Sepp-Lorenzino (2010). "Noninvasive Imaging of Lipid Nanoparticle-Mediated Systemic Delivery of Small-Interfering RNA to the Liver." Molecular Therapy **18**(9): 1657-1666.

Taylor, S. J., R. J. Resnick and D. Shalloway (2001). "Nonradioactive Determination of RAs-GTP levels Using Activated Ras Interaction Assay." Methods Enzymology **333**: 333-342.

Travali, S., D. H. Ku, M. G. Rizzo, L. Ottavio, R. Baserga and B. Calabretta (1989). "Structure of the human gene for the proliferating cell nuclear antigen." The Journal of biological chemistry **264**(13): 7466-72.

Uhrbom, L., E. Nerio and E. C. Holland (2004). "Dissecting tumor maintenance requirements using bioluminescence imaging of cell proliferation in a mouse glioma model." Nat Med **10**: 1257-60.

Vlahos, C. J., W. F. Matter, K. Y. Hui and R. F. Brown (1994). "A specific inhibitor of phosphatidylinositol 3-kinase, 2-(4-morpholinyl)-8-phenyl-4H-1-benzopyran-4-one (LY294002)." The Journal of biological chemistry **269**(7): 5241-8.

von Burstin, J., S. Eser, B. Seidler, A. Meining, M. Bajbouj, J. Mages, R. Lang, A. J. Kind, A. E. Schnieke, R. M. Schmid, G. Schneider and D. Saur (2008). "Highly sensitive detection of early-stage pancreatic cancer by multimodal near-infrared molecular imaging in living mice." International journal of cancer. Journal international du cancer **123**(9): 2138-47.

Vooijs, M., J. Jonkers, S. Lyons and A. Berns (2002). "Noninvasive imaging of spontaneous retinoblastoma pathway-dependent tumors in mice." Cancer research **62**(6): 1862-7.

Wetterwald, A., G. van der Pluijm, I. Que, B. Sijmons, J. Buijs, M. Karperien, C. W. Lowik, E. Gautschi, G. N. Thalmann and M. G. Cecchini (2002). "Optical imaging of cancer metastasis to bone marrow: a mouse model of minimal residual disease." The American journal of pathology **160**(3): 1143-53.

Wilentz, R. E., C. A. Iacobuzio-Donahue, P. Argani, D. M. McCarthy, J. L. Parsons, C. J. Yeo, S. E. Kern and R. H. Hruban (2000). "Loss of expression of Dpc4 in pancreatic intraepithelial neoplasia: evidence that DPC4 inactivation occurs late in neoplastic progression." Cancer research **60**(7): 2002-6.

Woolfenden, S., H. Zhu and A. Charest (2009). "A Cre/LoxP conditional luciferase reporter transgenic mouse for bioluminescence monitoring of tumorigenesis." Genesis **47**(10): 659-66.

Zambrowicz, B. P., A. Imamoto, S. Fiering, L. A. Herzenberg, W. G. Kerr and P. Soriano (1997). "Disruption of overlapping transcripts in the ROSA beta geo 26 gene trap strain leads to widespread expression of beta-galactosidase in mouse embryos and hematopoietic cells." Proceedings of the National Academy of Sciences of the United States of America **94**(8): 3789-94.

Zhang, N., S. Lyons, E. Lim and P. Lassota (2009). "A spontaneous acinar cell carcinoma model for monitoring progression of pancreatic lesions and response to treatment through noninvasive bioluminescence imaging." Clin Cancer Res **15**: 4915-24.

Zhao, H., T. C. Doyle, O. Coquoz, F. Kalish, B. W. Rice and C. H. Contag (2005). "Emission spectra of bioluminescent reporters and interaction with mammalian

tissue determine the sensitivity of detection in vivo." Journal of biomedical optics **10**(4): 41210.